UNIVERSITY OF VERONA

DEPARTMENT OF BIOTECHNOLOGY

GRADUATE SCHOOL OF

NATURAL SCIENCES AND ENGINEERING

DOCTORAL PROGRAM IN

BIOTECHNOLOGY

CYCLE: XXXIV

Novel Roles of Cullin-RING Ligases in Cell Signalling and Implications in Health and Disease

S.S.D. (Disciplinary Sector) BIO/11

Coordinator: Prof. Matteo Ballottari **Tutor: Prof.** Daniele Guardavaccaro

Signature: **Signature:**

PhD candidate: Onireti Jacob Olaleye

Signature:

Novel Roles of Cullin-RING Ligases in Cell Signalling and Implications in Health and Disease

Onireti Jacob Olaleye

Ph.D. thesis

Verona, 05 July 2022

ISBN:

University of Verona

Summary

Cullin-RING ligases (CRLs) play fundamental functions in key physiological and pathological processes. To identify novel roles of CRLs in cell signalling and their implication in health and diseases, we performed two separate studies:

In study 1, we analysed genomic databases to identify CRLs that are hypermutated in cancer. We found that the CRL substrate receptors FBXO24 and DCAF12L2 are hypermutated at critical domains that are necessary for the proper structure/function of the $CRL1^{FBXO24}$ and $CRL4^{DCAF12L2}$ complexes, respectively. We showed that the FBXO24(T65P) mutation within the F-box domain as found in cancer disrupts the $CRL1^{FBXO24}$ complex by blocking the binding of FBXO24 to SKP1. Similarly, we found that DCAF12L2 is hypermutated in cancer at the amino acids sequence positions 334, 335, and 337 within the WD40 repeats that mediate substrate binding. Our affinity purification coupled with mass spectrometry analysis identified MEKK4 and the WDR11 complex as two independent substrates of $CRL4^{DCAF12L2}$. Moreover, the DCAF12L2(P334L), (R335C), and (R335H) mutations block DCAF12L2 binding to MEKK4 and the WDR11 complex. We also showed that FAM91A1, a component of the WDR11 complex, is ubiquitylated by $CRL4^{DCAF12L2}$ and proposed that the ubiquitylation of FAM91A1 might be critical in regulating the stability and function of the WDR11 complex.

In study 2, we employed a proteomic approach to identify CRL3 complexes activated at the cellular membrane. Our mass spectrometry analysis identified $CRL3^{KLHL12}$ as a ubiquitin ligase that mediates the ubiquitylation of Lunapark, an endoplasmic reticulum (ER) shaping protein. We show that Lunapark interacts with mechanistic target of rapamycin complex1 (mTORC1) and that the ubiquitylation of Lunapark regulates mTORC1 activation. In addition, we show that the inhibition of Lunapark ubiquitylation leads to neurodevelopmental defects.

Table of Contents

1.Acknowledgments

The successful completion of this PhD is the result of help and kind support from many quarters, not only from people that have been involved in the projects but also those that have been part of my journey for many years with whom I have shared priceless moments and life experiences.

My profound gratitude to my supervisor **Prof. Daniele Guardavaccaro,** for accepting me and giving me the opportunity to pursue my PhD in his lab. Thanks, Prof. for your kind support, your wealth of knowledge and wisdom have always been there for me, I appreciate your advice and fatherly guidance. Despite your busy schedules, you take time out to grant me audience whenever I come knocking at your office, indeed I am highly grateful.

My most sincere thanks to all members of the group with whom I have spent most of my time these few years: **Angela Lauriola, Matteo Santucci, Juliana Haydee Enrique Steinberg, Mohsen Hajisadeghian,** and to the former and current students in the lab: **Sofia Munari, Richard Pozzetto, Francesco Ghirotto, Samanta Comincioli, Francesca Taddei, Giovanni Giglio, Anna Pianazzola.**

I am highly grateful to **Angela Lauriola,** for her valuable help right from when I started the PhD, you've been my tutor and I've learned quite a lot from you. I am particularly inspired by your activeness and creativity. Thanks to **Matteo Santucci** for your kind support, advice, and active contribution to the DCAF12L2 project, it was a memorable experience working with you. A special thanks to the "Queen of Western Blot" **Juliana Haydee Enrique Steinberg,** thanks for teaching me those amazing techniques of fast and good western blot analysis.

I can't talk about my PhD experience without acknowledging wonderful friends and colleagues that were ever and always there for me, I so much appreciate: **Mohsen Hajisadeghian** and **Samaneh Najafi,** you are both amazing and you mean so much to me than friends and colleagues. You surround me and support me as your very own brother, you embraced me so dearly and make me have the experience of a home away from home here in Verona, thanks for your kind support, advice, and encouragement. Part of the indelible moments of the PhD is the teamwork with Mohsen, it was a memorable experience working with you and

spending the days and workspace with you in the same lab. I am particularly thrilled by your high level of understanding, kindness, and depth of insight, thank you so much Mohsen, I really learnt a lot from you.

Thanks to our lab neighbours: **Prof. Massimiliano Perduca** and **Prof. Stefano Capaldi**, I've observed and learned a lot from you these few years and personally I appreciate the way you relate with your PhD students and other students. Thanks, **Stefano** for your kind and prompt response whenever I come knocking at your office. To **Salvatore Gaglio, Francesca Parolini, and Elham Ataie Kachoie** thanks for your kind support and for keeping up the nice atmosphere in the lab.

This PhD journey could not have been possible were it not for my highly esteemed family. Thanks, **Mum and Dad** for bringing me up, supporting and loving me so dearly, thanks for your tireless prayers and for the moral discipline and trainings, from early childhood you've taught and built us up to understand the power and wisdom embedded in meekness, in being prudent, diligent and the great value in service (Mat.23:11-12), thanks Mum and Dad for truly exemplifying the standard. My heartfelt thanks to my siblings: I owe the success of this PhD journey to your kind advice, encouragement, and tireless support dear brother **Oladoye Onireti (Baba D), Olayinka Onireti, Stephen Onireti, Gideon Onireti,** thanks for keeping up with weekend calls and for your keen interest in my progress. Thanks, aunty **Tolu** and dear sister **Olaronke Onireti** for your tremendous support. To you all, I am highly grateful. A special thank to my very dear brother Dr. Ayowadeji Abona, thanks for always being there for me, I could recall those wonderful old days in University of Jos, those memorable times of brainstorming and thoughtful discussions, the house in Lagos and the time I was working at Dabitos International school Lagos with the many demands and commitment wow! all thanks to God that changes time and season.

I am very grateful to my dear friends, **Reuben Olayinka Olaniyi, Abdulrasheed Adio, Gizella Aboagye, Solomon Lawrence, Felix Neumann, Sharath Tippur** especially to you **Reuben Olayinka Olaniyi**, thanks for always being there, we've come a long way, from those days in Baptist Academy, University of Jos, and till this very day, you've remained my ever-present friend, a brother, and a bosom

friend, indeed, I'm highly grateful. Thank you **Reuben** for your strong support in pushing through the journey this far. To dear **Federica**, thanks for your kind support, prayers, and encouragement, I appreciate you, dear.

All thanks to my dear aunty and Pastor, **Mrs. Bolatito Braithwaite**, and to all the members of **RCCG Uppsala Sweden** as well as the Pastor of **RCCG Verona Italy**, **Mr Leonard Odighizuwa** and his entire family, thanks for your prayers, and kind support. How could I thank all these people without giving thanks to the Most High God, the writer of my life's journey, my sustainer, and my defender, Thank You Lord, for in all You've made all things work together for my good and my advantage according to Your divine plan and purpose.

2.Background

2.1 Ubiquitylation in cell signalling

Ubiquitylation is a post-translational modification essential in virtually all cells signalling networks. A vast variety of stimuli and upstream signalling networks induce ubiquitylation of cell surface receptors, cytoplasmic and nuclear proteins thereby controlling the signal transduction steps leading to specific cellular responses (Haglund & Dikic, 2005). The E3 ubiquitin ligases are core functional components of ubiquitylation process. Cullin-RING ligases (CRLs) represent the largest family of E3 ubiquitin ligases with a broad array of characterised functions, some of which include regulation of cell cycle progression, signal transduction, and transcription (Cui et al., 2016).

Although CRLs have been extensively studied, the function and regulation mechanisms of many members of the CRLs family are still unknown. Genetic studies have predicted that some human diseases such as cancer could be linked to the aberrant function or mutation of unknown CRLs (Kim et al., 2018) (Fujita et al., 2013), this is in addition to computational, and genomic screening studies that have also predicted that several components of CRLs, particularly, the substrate receptors, are often mutated in cancers (Bailey et al., 2020; Koboldt et al., 2012).

Interestingly, recent studies by Meyer-Schaller et al. have shown that CRL3 complexes are formed at cellular membranes where CUL3 is recruited and activated at the membrane (Meyer-Schaller et al., 2009), yet these CRL3 ligases have not been identified and the substrates and functions of these CRL3 complexes as well as their implication in health and diseases remain unclear.

This thesis describes novel roles of CRLs in cell signalling and their implication in human diseases. The thesis consists of two sections: studies 1 and 2.

Study 1

This section identifies CRLs that are hypermutated in human cancer, assess their roles in cell signalling pathways and their implication in the pathogenesis of cancer.

Study 2

This section identifies new CRL3 complexes formed at cellular membranes, characterize the specific substrates, and investigates the implication of these membrane-bound CRLs in human health and diseases. This part of the thesis is based on the following paper:

Laurensia Yuniati, Angela Lauriola, Manouk Gerritsen, Susana Abreu, Eric Ni, Chiara Tesoriero, Jacob O. Onireti, Teck Yew Low, Albert J.R. Heck, Andrea Vettori, Timothy Cardozo, and Daniele Guardavaccaro. Ubiquitylation of the ER-Shaping Protein Lunapark via the $CRL3^{KLHL12}$ Ubiquitin Ligase Complex. *Cell Reports*. **31,** 107664 (2020)

3. Aims of the thesis

In this thesis, we explore novel roles of Cullin-RING ligases (CRLs) in cell signalling and their implication in health and diseases.

Study 1 explores the effect of CRLs mutations in cell signalling and their implication in the pathogenesis of cancer by:

1. Performing comprehensive genomic screening of all the approximately 700 E3 ligases encoded by the human genome to identify CRLs that are hypermutated in human cancer.
2. Identifying the substrates of CRLs found to be hypermutated in human cancer.
3. Characterising the molecular mechanisms regulating substrate ubiquitylation and assessing its biological significance.
4. Investigating the implication and how the CRL mutations found in cancer contribute to the pathogenesis of the disease in human.

Study 2 focuses on identifying the set of CRL3 complexes formed at cellular membranes and exploring their roles in cell signalling as well as their implication to human disease, this was done by:

1. Using affinity purification and mass spectrometry to identify the CRL3 complexes that are recruited and activated at cellular membranes.
2. Characterising the molecular mechanisms of substrate ubiquitylation mediated by membrane-bound CRL3s.
3. Investigating the regulatory mechanisms of substrate recruitment and ubiquitylation.
4. Investigating the biological significance of substrate ubiquitylation mediated by membrane-linked CRL3.
5. Assessing the implication of deregulated ubiquitylation by membrane-linked CRL3s in diseases.

Study I

NOVEL ROLES OF CRL4 LIGASES IN CELL SIGNALLING AND THEIR IMPLICATIONS IN THE PATHOGENESIS OF CANCER

4. Abstract

To investigate the novel roles of CRLs in cell signalling and their implication in pathogenesis of cancer, we screened CRLs to identified those that are mutated in cancer as well as identified the substrates of these CRLs. We assessed how the mutations found in cancer affect the function of the CRL complex and the possible contribution to cancer development.

By genomic database analysis we found that the CRL substrate receptors FBXO24 and DCAF12L2 are hypermutated in cancer at critical domains necessary for the proper structure/function of the $CRL1^{FBXO24}$ and $CRL4^{DCAF12L2}$ complexes, respectively. We demonstrated by mass spectrometry screening and immunoblotting that the most frequent mutation of FBXO24 on the F-box domain disrupts the $CRL1^{FBXO24}$ complex by blocking the binding to SKP1.

In addition, our genomic screening analysis shows that DCAF12L2 is hypermutated on the WD40 repeats and the hotspots of these mutations in cancer are the amino acid residues at sequence position 334, 335, and 337. By proteomic screening and western blot analysis, we identified MEKK4 and a *trans* Golgi network complex known as the WDR11 complex as two independent substrates of the $CRL4^{DCAF12L2}$ complex. The WDR11 complex facilitate vesicular trafficking in cells. Immunoprecipitation and western blot analysis showed that DCAF12L2 mutations [(P334L), (R335C), and (R335H)] block its interaction with the WDR11 complex and MEKK4. In addition, we show that $CRL4^{DCAF12L2}$ binds the WDR11 complex to mediate the ubiquitylation of FAM91A1, a component of the WDR11 complex and propose that $CRL4^{DCAF12L2}$ mediated ubiquitylation of FAM91A1 might be critical to regulate the stability and function of the WDR11 complex.

5. Introduction

5.1 The ubiquitin-proteasome system

Protein homeostasis is one of the dynamic cellular processes critical for cell function and health. The master regulator of protein homeostasis is the ubiquitin-proteasome system (UPS), which is an interconnected network of two dependent systems, i.e., the ubiquitin system and the proteasome system. The ubiquitin system involves the activity of specific enzymes that ubiquitylate or deubiquitylate targeted proteins (Zheng et al., 2016), the ubiquitylated proteins are recognised and degraded by the core multicomponent proteolytic complex of the UPS, the proteasome (Meyer-Schwesinger, 2019) (Ciechanover & Schwartz, 1998).

Ubiquitylation is an enzymatic process that involves the covalent conjugation of ubiquitin to lysine residues of a protein (Meyer-Schwesinger, 2019), It is a versatile post-translational modification that controls protein levels in cells and modulates virtually all cellular processes (Fouad et al., 2019). Cellular processes regulated via ubiquitin-dependent degradation include gene transcription, translation, endocytosis, cell cycle, DNA repair, gene expression, receptor activity as well as the subcellular localization of proteins (Sun & Chen, 2004). In addition, ubiquitylation plays a role in regulating membrane trafficking as well as the development, activation, and differentiation of T cells to effect efficient adaptive immune responses to pathogens (Hu & Sun, 2016).

5.1.1 The ubiquitylation cascade

Ubiquitylation is a sequential enzymatic process that involves the covalent linkage of ubiquitin to a protein through a process mediated by the E1 ubiquitin-activating enzymes, the E2 ubiquitin-conjugating enzymes and the E3 ubiquitin ligases,these enzymes, respectively activate, conjugate and ligate ubiquitin to a substrate protein **(Figure 1A)** (Hershko & Ciechanover, 1998, 2003). The human genome encodes 2 distinct E1 ubiquitin-activating enzymes, approximately 40 E2 ubiquitin-conjugating enzymes and over 700 E3 ubiquitin ligases (Weller et al., 2014). E1 ubiquitin-activating enzymes activate ubiquitin forming a covalent thioester bond between their catalytic cysteine and the di-glycine motif at the ubiquitin C-terminal.

During the activation, ubiquitin first forms a ubiquitin-adenylate intermediate complex then, following a nucleophilic attack by an active site cysteine thiol, it forms a C-terminal thioester complex with the E1 activating enzyme and remains attached to the enzyme (Buetow & Huang, 2016). Subsequently, the E1 activating enzyme transfers the activated ubiquitin through its di-glycine motif to the catalytic cysteine of an E2 conjugating enzyme thereby forming an E2-ubiquitin thioester complex **(Figure 1B).** The E3 ligase then catalyses the condensation of the ubiquitin thioester with lysine side-chain ε-amines in the substrate, promoting the formation of an isopeptide bond between the C-terminal of ubiquitin and the ε-amino group of a lysine side chain or free N-terminal amino group of the substrate (Metzger et al., 2012) (Buetow & Huang, 2016). However, in the case of HECT family E3 ubiquitin ligases, they have an active site cysteine, which forms an intermediate thioester bond with ubiquitin before it is finally link to the substrate (Qian et al., 2020).

Additional ubiquitin monomers can be added to the ubiquitin moiety conjugated to the substrate protein through successive rounds of E3-catalysed reactions to produce substrates with polyubiquitin chains linked through one of the seven lysine residues (K6, K11, K27, K29, K33, K48, and K63) or N-terminal methionine of ubiquitin (Komander & Rape, 2012) (Ohtake et al., 2018). Besides, diverse forms of polyubiquitin chains with different linkages can be formed through the regulatory process of specific E2s/E3s and deubiquitinase enzymes. Linkage-specific ubiquitin-binding proteins recognise diverse polyubiquitin chain linkages and specify their distinct function in cells, the diverse functional specificity of different polyubiquitin chains is known as the ubiquitin code (Komander & Rape, 2012).

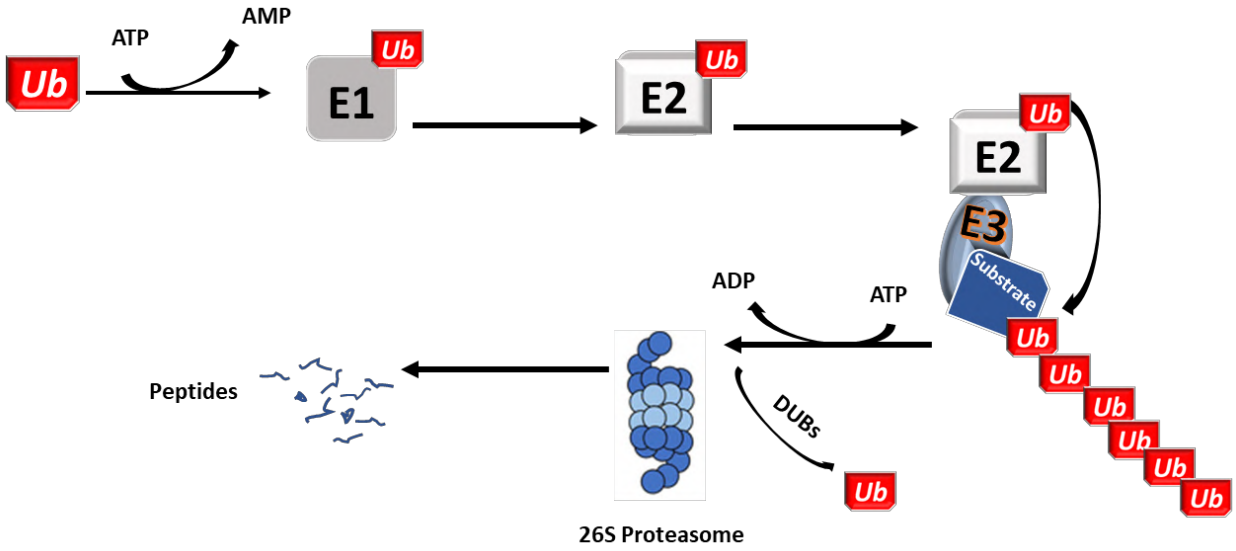

Figure 1. Schematic representation of the ubiquitin-proteasome system

Generally, ubiquitin can form eight different linkage types, using one of seven internal lysine residues which are K6, K11, K27, K29, K33, K48, K63, or methionine at position 1 (M1). In mammalian cells, the K48 and K63 linkages account for approximately 80% of the total ubiquitin linkages (Ohtake et al., 2018) (Yau & Rape, 2016). The K48-linked polyubiquitin chain specifically targets the protein substrate to the 26S proteasome for degradation. But on few occasions, other ubiquitin linkages such as K11 or K29 linked chains, as well as multiple monoubiquitylations, could also function in proteasomal targeting signals (Yau & Rape, 2016). The K63-linked chains regulate processes such as inflammatory signal transduction, DNA repair, endocytosis, and selective autophagy (Pontrelli et al., 2019).

The polyubiquitin chains can be homogeneous, consisting of one type of linkage, or heterogeneous, consisting of more than one type of linkage. Ubiquitylation patterns can also follow a branched-chain linkage, consisting of different linkages such as two degradative linkages, K11/K48 or K29/K48, that promote proteasomal degradation (Meyer & Rape, 2014) (Liu et al., 2017)(Ohtake et al., 2018).

5.2 E3 ubiquitin ligases

E3 ubiquitin ligases specifically catalyse the covalent attachment of ubiquitin to protein substrates in the cell. The human genome encodes approximately 700 E3 ubiquitin ligases. Generally, all E3 ligases have an E2-ubiquitin-binding domain hence, they are classified into three classes based on the structure of this domain and their ubiquitin transfer mechanism. Based on this classification, we have the RING (Really Interesting New Gene) E3 ligases, the HECT (Homologous to E6AP C-terminal) E3 ligases and the RBR (RING-between-RING) E3 ligases (Buetow & Huang, 2016).

The RING E3 ligases represent the largest class of the E3 ligases, they contain the RING domain that binds directly to the E2 conjugating enzyme to facilitate the transfer of ubiquitin from the E2-ubiquitin thioester complex to the substrate (Deshaies RJ et al., 2009). The HECT and the RBR E3 ligases contain a catalytic cysteine that accepts ubiquitin from the E2 ubiquitin thioester complex to form an E3-ubiquitin thioester intermediate and then directly transfers the ubiquitin to the substrate (Pickart & Eddins, 2004).

The Cullin-RING ligases (CRLs) are the largest family within the RING E3 ligase class, they are multi-subunit complexes comprising of a RING finger protein, a Cullin (CUL) protein, an adaptor protein, and a substrate receptor protein **(Schematic representation on the last page of this introduction section)**. The human genome encodes six classical and two atypical Cullin proteins. The classical Cullin is characterized by a Cullin homology (CH) domain in the carboxyl (C)-terminal, and they include CUL1, CUL2, CUL3, CUL4A, CUL4B, and CUL5. The two atypical cullins are CUL7 and CUL9 which bear additional homology domains such as the DOC1 (destruction of cyclin B) (Z. Chen et al., 2015).

The cullin proteins have a rigid, N-terminal stalk that is comprised of three repeats of a five-helix bundle (cullin repeat (CR)1–3) and a C-terminal globular domain (Petroski & Deshaies, 2005). The cullins serve as the central scaffold on which the multi-subunit CRL ubiquitin ligase complexes are assembled. The CUL links the RING box protein Rbx1 or Rbx2, (also known as the Regulator of cullins 1 (ROC1)

or ROC2, respectively) to the adaptor protein (Fouad et al., 2019). The adaptor protein binds to the N-terminal CR1 region while the RING box protein binds to the C-terminal globular domain. The RING component is active in recruiting ubiquitin-loaded E2 ubiquitin-conjugating enzymes to the CRL complex to facilitate substrate ubiquitylation (Sarikas et al., 2011). The adaptor proteins contain a domain that interacts with a range of variable substrate recruitment subunits (substrate receptors) specific to a particular cullin class (Fouad et al., 2019; Petroski & Deshaies, 2005). The substrate receptors determine the specificity of a CRL for targeted protein degradation (Zhou et al., 2020). The human genome encodes approximately 400 different substrate receptors hence the CRLs are very flexible at ubiquitylating numerous substrates (Petroski & Deshaies, 2005).

Cullin-RING ligases (CRLs) have been implicated in the pathogenesis of many developmental and neurodevelopmental diseases as well as in tumorigenesis. For instance, dysregulation of Cullins, especially the classical Cullins, have been linked to tumorigenesis through multiple cellular processes that include the obstruction of cell cycle progression, disrupted DNA damage repair, alteration in the ubiquitylation of oncoproteins, as well as increase in the ubiquitin-dependent degradation of tumor suppressors (Z. Chen et al., 2015).

5.2.1 Cullin 1-RING E3 ligases (CRL1)

Cullin-RING ubiquitin ligase 1 complexes (CRL1s), also known as the Skp1–CUL1–F-box protein complex (SCF), is a multi-subunit RING finger-type ubiquitin ligase (Nakagawa et al., 2020). These group of E3 ligases consist of the S-phase kinase-associated protein 1 (Skp1), cullin 1 (CUL1), the RING finger protein RBX1 (RING box protein 1; also known as regulator of Cullins 1(ROC1)), and the variable F-box proteins (Frescas & Pagano, 2008). The CUL1 protein serves as a scaffold and connects Skp1 with RBX1. Skp1 binds to CUL1 and plays a crucial role in identifying and binding the F-box protein. RBX1 is characterised by the presence of a Zinc-binding domain known as the RING Finger domain, which binds the E2-ubiquitin conjugated complex to facilitates the transfer of ubiquitin to the lysine residues of the target protein (Zheng et al., 2002). The F-box protein determines the

specificity of the SCF complex as it recognises and recruits the specific substrate (Zheng et al., 2002).

5.2.1.1 The F-box proteins

F-box proteins are the substrate receptors of CRL1 E3 ligase complexes. This family of proteins was named after the presence of the F-box motif in mammalian cyclin F protein and they are evolutionally conserved in eukaryotes with at least about 38 F-box proteins encoded in the human genome (Kipreos & Pagano, 2000). F-box proteins contain two main functional domains: the N-terminal F-box motif and various C-terminal domains that recognise and bind to specific substrates. The F-box motif is a 40-amino acid residues domain at the N-terminal of F-box proteins, this domain links the F-box proteins to the SCF complex by binding directly with the adaptor protein Skp1 (Chang et al., 1996). Depending on the motifs at the C-terminal, F-box proteins are classified into three major subfamilies which are: (1) FBXWs containing WD repeats, (2) FBXLs containing leucine-rich repeats (LRR), and (3) FBXOs containing other various domains (Ho et al., 2006). The F-box proteins Skp2, β-Trcp, and FBW7 target substrates that control cell proliferation in the mammalian system (Ho et al., 2006). FBW7 controls cell cycle progression by mediating the degradation of cyclin E during the G1 phase of the cell cycle (Koepp et al., 2001; Strohmaier et al., 2001), Skp2 on the other hand regulates the S phase entry and other phases of the cell cycle by targeting p27 for ubiquitylation and degradation (Nakayama et al., 2004).

Several studies including patient-based data from The Cancer Genome Atlas (TCGA) have shown that aberrant expression and/or function of F-box proteins have pathogenic roles in cancer (Hoadley et al., 2018). According to Wang et al., the dysregulation of F-box protein-mediated proteolysis leads to malignancies in human (Z. Wang et al., 2014). Skp2 has been reported to be overexpressed in several human tumor samples including lymphoma, prostate cancer, colorectal cancer, melanoma, nasopharyngeal carcinoma, pancreatic cancer, and breast carcinoma (Z. Wang et al., 2014). In addition, several studies have identified FBXW7 as a tumor-suppressor that promotes the degradation of various oncoproteins (Welcker & Clurman, 2008). Besides, the overexpression of FBXO11

in diffuse large B cell lymphoma (DLBCL) has been found to inhibit cell growth and induce cell death by target BCL-6 for ubiquitylation and degradation (Duan et al., 2012)(Welcker & Clurman, 2008). It has been shown that FBXO31 is downregulated in human breast cancer and hepatocellular carcinoma cell line (Huang et al., 2010)(Kumar et al., 2005).

5.2.1.1.1 F-box only protein 24 (FBXO24)

FBXO24 is a poorly characterised F-box protein within the FBXO subfamily. Studies have shown that FBXO24 binds to PRMT6 precisely at the 270 to 275 amino acid residues sequence position to cause polyubiquitination of lysine at the 369-sequence position of PRMT6 (Chen et al., 2020). Besides the overexpression of FBXO24 has been reported to inhibit cell proliferation, migration, and invasion in H1299 cells (Chen et al., 2020). Exome sequencing studies have revealed FBXO24 as a new candidate of diffuse gastric cancer susceptibility genes (Donner et al., 2015) and preliminary studies by Chen et al., have also shown that FBXO24 might have role in tumorigenesis (Chen et al., 2015).

5.2.2 Cullin 3-RING E3 ligases (CRL3)

Cullin-RING ubiquitin ligase 3 complexes (CRL3s) are members of the Cullin-RING superfamily type of E3 ligases. They are composed of a Cullin 3 (CUL3) scaffold protein, a RING-finger protein (RBX1) and a substrate adaptor protein with Bric-a-brac/Tramtrack/Broad (BTB) domain. The substrate adaptor protein recognises and recruits the substrate to the CRL3 complex, the CUL3 protein serves as a scaffold to connect the substrate adaptors and RBX1 (Xiang et al., 2021). Members of the large family of BTB-domain proteins have been identified as substrate-specific adaptors of CUL3-based E3 complexes (Krek, 2003).

5.2.2.1 The BTB proteins

This family of proteins contains the BTB domain (also known as the POZ domain) and a variety of functional roles have been linked to this domain, this includes transcription repression, cytoskeleton regulation, dimerization, and protein ubiquitination (Furukawa & Xiong, 2005; Kobayashi et al., 2004). The BTB domain is a versatile protein-protein interaction motif and is typically found as a

single copy in proteins that contain only one or two other types of domains, and this defines the BTB-zinc finger (BTB-ZF), BTB-BACK-kelch (BBK), voltage-gated potassium channel T1 (T1-Kv), MATH-BTB, BTB-NPH3 and BTB-BACK-PHR (BBP) families of proteins, among others (Stogios et al., 2005). The BTB domain is present near the N-terminus of a fraction of zinc finger proteins and in proteins that contain the Kelch motif and a family of pox virus proteins. In CRL3, the BTB proteins associate directly with CUL3 through their BTB domain. A typical BTB protein is the Kelch-like proteins (KLHLs) family proteins, this family of proteins is known to serve as substrate adaptor proteins of the CRL3 complexes, they exert biological function dependent of the CRL3 complex in many cellular processes (Xiang et al., 2021).

5.2.2.2 The Kelch-like proteins (KLHLs)

These are BTB proteins encoded by 42 Kelch-like gene family members (KLHLs), they formed a prominent class of substrate adaptors of the CRL3 complexes. Structurally, they are composed of a BTB/POZ domain, a BACK domain, and a five to six kelch repeats domain (Kelch motifs). The BTB/POZ domain facilitates protein binding, while the Kelch motifs form β-propellers (Dhanoa et al., 2013). The Kelch gene superfamily of proteins are subdivided into five groups: (1) N-propeller, C-dimer proteins, (2) N-propeller proteins, (3) propeller proteins, (4) N-dimer, C-propeller proteins, and (5) C-propeller proteins. KLHL family members belong to the N-dimer, C-propeller subclass of Kelch gene proteins (Adams et al., 2000). The Kelch motif of the KLHLs differ from each other and it is the main part of the protein for substrate specificity and binding in CUL3-based E3 ubiquitin ligases (Dhanoa et al., 2013). For instance, KLHL6 specifically targets cyclin-dependent kinase 2 (CDK2) for degradation and contributes to the differentiation process of acute myeloid leukemia (AML) (Ying et al., 2018). KLHL24 targets Keratin 14 for degradation, an essential process for maintaining the integrity of human skin (Lin et al., 2016).

5.2.2.2 .1 The Kelch-like protein 14 (KLHL14)

KLHL14 belongs to the Kelch gene family. It is also known as printor (protein interactor of torsinA) as it selectively binds to the ATP-free form of torsinA (Giles et al., 2009). TorsinA is a member of the AAA-ATPase family of chaperones with multiple functions in the cell (Granata & Warner, 2010). KLHL14 promotes the development of ovarian cancer by regulating signalling pathways such as mTOR, WNT, and TGF-beta and it may be a target for ovarian cancer detection and treatment (Z. Chen et al., 2020). KLHL14 has been reported as a novel tumor suppressor that associates with the endoplasmic reticulum-associated protein degradation (ERAD) machinery. It mediates the ubiquitylation of B cell receptor (BCR) subunits and decreases the stability of immature BCR glycoforms in the endoplasmic reticulum, thereby reducing BCR levels (Choi et al., 2020). KLHL14 gene acquires frequent inactivating mutations in DLBCL, often in ABC tumors of the MCD genetic subtype and in PCNSL (Schmitz et al., 2018; Young et al., 2019). KLHL14 is highly expressed in immune tissues, especially in B cells (Li et al., 2018).

5.2.3 Cullin 4-RING E3 ligases (CRL4)

Cullin 4-RING E3 ligases (CRL4s) are composed of one of the two homologous scaffolds: Cullin 4A (CUL4A) or Cullin 4B (CUL4B). CUL4A and CUL4B bind to the damaged DNA binding protein 1 (DDB1) adaptor protein through their N-terminal and through their C-terminal, they bind to the catalytic subunit RING-finger protein RBX1 (Jackson & Xiong, 2009). CUL4A and CUL4B share about 82% amino acid sequence identity yet each scaffold targets a unique set of substrates. The major difference between the two scaffolds is the extended N-terminal of CUL4B with an additional nuclear localization signal (NLS) (149 amino acids longer) that controls its nucleus localization and has an essential role in nuclear protein ubiquitylation and degradation while CUL4A is predominantly cytoplasmic and controls the ubiquitylation and degradation of cytoplasmic proteins (Zhuan Zhou et al., 2020). The DDB1 adaptor protein contains three WD40 repeats (BPA, BPB, and BPC) and acts to bridge the scaffold CUL4A or CUL4B to the DCAFs (DDB1 and Cul4 Associated Factor) substrate recognition receptors using

a WDXR motif within the substrate recruitment factors (Jin et al., 2006) (Hannah & Zhou 2015; Sang et al., 2015).

CRL4 plays an important role in early embryonic development as well as tissue or organogenesis (Zhuan Zhou et al., 2020). Several substrates of CRL4 have been implicated in germ cell apoptosis and defection and some known substrates of CRL4 include TET1, p53, and CDT1 (Natarajan and Takeda, 2017; Bulatov and Ciulli 2015; Liu et al., 2018). CRL4 regulates protein homeostasis in the hematopoietic lineage by ubiquitylating the homeodomain transcription factors (HOX) and targeting them for proteasomal degradation (Zhang et al., 2003) (Pineault et al., 2002). CRL4 regulates the nervous system and other organ systems such as the liver, skin, and pancreas (Zjuan Zhou et al., 2020).

CUL4A is overexpressed in many human cancers including breast cancer, squamous cell carcinoma, adrenocortical carcinoma, childhood medulloblastoma, prostate cancer, and hepatocellular carcinoma, and is associated with poor prognosis in node-negative breast cancer (Wang et al., 2014) (Yasui et al., 2002) (Caiguo Zhang et al., 2018). In malignancies, the canonical Wnt signalling pathway upregulates the CUL4 mRNA level and subsequently leads to CUL4A protein accumulation (Miranda-Carboni et al., 2008). In multiple human cancer specimens, such as lung carcinoma, including lung cancer (Jia et al., 2017), gastric carcinoma (Gong et al., 2017), colon cancer, as well as breast cancer, abnormal accumulation of CUL4A protein has been detected (Wang et al., 2013). Likewise, CUL4B has been reported to be aberrantly expressed in a broad set of malignancies such as colorectal cancer (He et al., 2018), lung cancer, and pancreatic cancer (Zhang et al., 2018).

5.2.3.1 The DDB1- and CUL4-associated factor (DCAF) proteins

The DDB1- and CUL4-associated factor (DCAF) proteins act as substrate recognition components of CRL4 E3 ubiquitin ligase complexes, recruiting diverse proteins for ubiquitylation (Jackson & Xiong, 2009)(He et al., 2006). DCAF proteins belong to the subfamily of the WD40-repeat containing (WDR) proteins that contain four or more repeats of 40 - 60 amino acids stretch that end in tryptophan (W) aspartate (D) dipeptides (Lee & Zhou, 2007). These sets of proteins

are highly abundant and well conserved, they play critical roles in diverse cellular processes including signal transduction, transcription regulation, DNA damage response, histone modification, cell cycle control, protein degradation, and apoptosis (Xu & Min, 2011).

Four or more WD40-repeats fold around a central axis to form a structure known as the β propeller (Lee & Zhou, 2007). One unique feature of the DCAFs is the presence of a relatively conserved WDXR motif, found in the short linker peptide connecting two β strands within the WD40 repeat (Lee & Zhou, 2007). This conserved WDXR motifs in the DCAFs proteins is the main motif that binds DCAFs to the Damaged DNA Binding protein 1 (DDB1) adaptor protein in the CRL4 complex.

5.2.3.1.1 DDB1 and CUL4-associated factor 12 like protein 2 (DCAF12L2)

DCAF12L2 (DDB1 and CUL4 associated factor 12 like protein 2) is a WD40-repeat (WDR) containing protein and a member of the DCAF proteins. DCAF12L2 is one of the retrocopies of the DCAF12 parental gene (Szcześniak et al., 2011). While the parental gene DCAF12 is present in vertebrate and insect genomes, the retrocopies are found only in placental mammals. The second retrocopy DCAF12L1 is known to have emerged as a result of the tandem duplication of DCAF12L2 which is located next to the DCAF12L1 gene on chromosome X (Szcześniak et al., 2011). The parental gene DCAF12, located on chromosome 9, is widely expressed with the highest expression in the testis and trachea. It has been reported by Szcześniak et al, that the retrogene DCAF12L1 is expressed only in the kidney and testis while the second retrogene, DCAF12L2, has been reported to be expressed in the eye and testis.

5.3. The WD repeat-containing protein 11 (WDR11) complex

The WDR11 complex is a stable complex localized at the *trans*-Golgi network (TGN). It is composed of FAM91A1, C17orf75 and the WDR11 proteins (Navarro Negredo et al., 2018) **(Schematic representation on the last page of this introduction section)**. The complex acts along with TBC1D23 to facilitate the golgin-mediated capture of vesicles generated using the adaptor protein-1 complex

(AP-1), which transports cargo between the *trans*-Golgi network and endosomes (Navarro Negredo et al., 2018). The complex was reported to play a vital role in vesicular trafficking, most precisely within the endosome-to TGN trafficking (Navarro Negredo et al., 2018). WDR11 (WD repeat-containing protein 11) is a member of the WD repeat-containing protein family. The WDR11 gene is located on chromosome 10 and encodes a 1,224-amino acid polypeptide with a calculated molecular mass of 137 kDa. The WDR11 protein contains 6 putative WD40 repeats, a predicted transmembrane region, and a tyrosine kinase phosphorylation site, the protein is ubiquitously expressed in human tissues and highly conserved in vertebrates (Chernova et al., 2001).

It has been shown that WDR11 modulates the Hedgehog (Hh) signalling pathway by regulating the proteolytic processing of GLI3. In addition, it interacts with the transcription factor EMX1 to induce the downstream Hh pathway gene expression and gonadotrophin-releasing hormone production (Kim et al., 2018). EMX1 is a homeodomain transcription factor involved in the development of olfactory neurons, and according to Kim et al., missense alterations reduce or abolish its interaction with WDR11 (Kim et al., 2010).

Besides, disruption of WDR11 expression and function in the Hh signalling pathway has been implicated in human developmental genetic disorders defined by delayed puberty and infertility known as congenital hypogonadotropic hypogonadism (CHH) and Kallmann syndrome (KS) (Kim et al., 2018). In addition, a missense mutation in the WDR11 gene has been implicated in severe growth retardation, ventricular septal defect, and coloboma symptoms (Sutani et al., 2020). WDR11 has been reported to be inactivated in glioblastoma cells and it has been suggested to be a candidate tumor suppressor gene involved in tumorigenesis of glial and other tumors (Jönsson et al., 2007)(Katoh & Katoh, 2003). WDR11 is localized to the *trans*-Golgi network (TGN), where it interacts with herpes simplex virus (HSV) protein ICP0 to promote viral assembly and/or secondary envelopment (Taylor & Mossman, 2015).

The FAM91A1 (Family with Sequence Similarity 91, Member A1) gene encodes an 838 amino acid polypeptide with a calculated molecular mass of 94 kDa. FAM91A1 is a component of the WDR11 complex that acts along with TBC1D23

to facilitate the golgin-mediated capture of vesicles generated using AP-1 (Navarro Negredo et al., 2018). FAM91A1 and WDR11 are essential for the proper localization of the WDR11 complex in cells. The disruption of FAM91A1 affects the stability of other components of the complex both WDR11 and C17orf75 (Navarro Negredo et al., 2018). In general, FAM91A1 is a poorly characterized protein, and the biological function of the protein is largely unknown. However, according to Zhang et al., the FAM91A1 gene is involved in mouse embryonic stem cell pluripotency maintenance (Zhang et al., 2016).

C17orf75 (chromosome 17 open reading frame 75,) also known as NJMU-R1, is a 396 amino acid protein that is encoded by a gene located on chromosome 17. It is the third component of the WDR11 complex involved in intracellular protein transport and vesicle tethering to Golgi. It has been reported that C17orf75 is upregulated in retinoblastoma (Chakraborty et al., 2010). In addition, the C17orf75 gene is upregulated in squamous cell carcinomas (Chakraborty et al., 2010).

5.4 Mitogen-activated protein kinase kinase kinase 4 (MAP3K4)

MAP3K4, also known as MEKK4 or MTK1 or MAPKKK4, is a Ser/Thr protein kinase, it is a mitogen-activated protein kinase kinase kinase that regulates the activity of its downstream mitogen-activated kinases, p38, and c-Jun N-terminal kinase (JNK). MEKK4 has a C-terminal kinase catalytic domain, which is approximately 55% homologous to the catalytic domains of MEKKs 1, 2, and 3 (Gerwins et al., 1997). Similarly, the N-terminal of MEKK4 contains an autoinhibitory domain that interacts with the C-terminal kinase domain, this interaction inhibits MEKK4 kinase activity and prevents substrate binding (Mita et al., 2002). MEKK4 phosphorylates and activates an intermediate protein kinase (MKK) (MKK3, MKK4, MKK6, and/or MKK7). The activated protein kinase subsequently phosphorylates and activates another MAP kinase (such as the JNK or p38) thereby triggering a corresponding cellular response through the phosphorylation of numerous proteins including transcription factors (Bacher et al., 2021)(Gerwins et al., 1997). Environmental stresses such as osmotic shock, UV irradiation, wound stress, and inflammatory factors trigger MEKK4 activation thereby leading to the subsequent phosphorylation and activation of the CSBP2 and

JNK MAPK pathways. Two isoforms of MEKK4, α and β have been reported in humans and mice. The human isoform α contains 49 amino acids (1175–1223) not found in the β isoform while the mouse isoform α contains 52 amino acids insertion (1162–1213) not found in the β isoform(Bacher et al., 2021). The interactions of MEKK4 with other proteins control its dimerization and activation. For instance, the binding of GSK3β to MEKK4 blocks MEKK4 dimerization and prevents its activation, thereby inhibiting MEKK4 stimulation of the JNK and p38 MAPK pathway (Abell et al., 2007a). MEKK4 promotes IL-21 expression in malignant T cells, and it's been linked with associated increased in the progression of cutaneous T cell lymphoma (Fredholm et al., 2016). MEKK4 activation of Jun N-terminal kinase (JNK) mediates fibroblast growth factor 4 (FGF4) maintenance of trophoblast stem (TS) cells in an undifferentiated state (Abell & Johnson, 2005) (Abell et al., 2009).

MEKK4 has been identified as a critical signalling molecule during cardiovascular development. The kinase activity of MEKK4 is essential to support epithelial-mesenchymal transformation (EMT) in the embryonic heart (Stevens et al., 2006). MEKK4 is strongly expressed in the developing neuroepithelium. Studies have shown that MEKK4 is require for human epidermal growth factor receptor 2/3 (HER2/HER3)-heregulin beta1 (HRG) induced cell migration in MCF-7 breast cancer cells (Sollome et al., 2014). Gadd45 mediated MEKK4 activation promotes muscle fiber atrophy (Ebert et al., 2020). In humans, it has been reported that loss of function mutations of the MKK4 gene are found in approximately 5% of tumors from a variety of tissues, suggesting it may have a tumor suppression function (Whitmarsh & Davis, 2007).

6.Table of the list of proteins studied with a brief description of the structures and biological functions

Protein	Domains		Biological Functions
DDB1- and CUL4-associated factor 12-like protein 2 **(DCAF12L2)**	**7 WD40 repeats** WD repeats are minimally conserved regions of approximately 40 amino acids typically bracketed by Gly-His and Trp-Asp (GH-WD)	The WD40 repeats facilitate the formation of heterotrimeric or multi-protein complexes.	Members of this family served as a substrate-recognition component of a CRL3 E3 ubiquitin-ligase complex.

F-box only protein 24 **(FBXO24)**	**F-box domain** Regulator of Chromosome Condensation 1 **(RCC1)** repeats	The F-box motif mediates protein-protein interaction. The F-box motif connects F-box protein to Skp1 in CRL1 E3 ligase complexes. The RCC1 repeats consist of 7 homologous repeats of 51–68 amino acid residues, which fold to form a 7-bladed β-propeller fold. The β-propeller fold mediates substrate binding in CRL1 E3 ligase complexes	It is involved in a variety of processes, such as polyubiquitination, transcription elongation, centromere binding and translational repression.
FAM91A1	The domains are disordered and poorly characterized.	According to uniport.org, Sequence 339-369 are polar residue	FAM91A1 is a component of the WDR11 complex, the complex acts together with TBC1D23 to facilitate the golgin-mediated capture of vesicles generated using AP-1in cells.
C17orf75 (also known as **Njmu-R1**)	Poorly characterized protein		It is also a component of the

			WDR11 complex, the complex acts together with TBC1D23 to facilitate the golgin-mediated capture of vesicles generated using AP-1in cells and may have a role in spermatogenesis.
WD repeat-containing protein 11**(WDR11)**	Contained 9 WD repeats (also known as WD 40 repeats)	The WD repeat is a conserved domain of about 40 amino acids in length with a central conserved Trp-Asp motif. The WD repeats typically form a four stranded anti-parallel β sheet or blade, the blades fold to form a bladed β-propeller structure. In general, the WD repeats mediate in protein-protein interactions.	WDR11 is involved in the proteolytic processing of GLI3 and interacts with the transcription factor EMX1 in the induction of downstream Hedgehog (Hh) pathway gene expression as well as in the production of gonadotropin-releasing hormone. It is a major part of the WDR11 complex.
Mitogen-activated protein kinase kinase kinase 4 (**MAP3K4**)	Autoinhibitory domain at the N-terminal.	The autoinhibitory domain is located at the N-terminal, this domain interacts with	MEKK4 is a stress-induced protein kinase. It specifically

also known as **MEKK4**	Kinase domain at the C-terminal, between sequence position 1343-1601.	the C-terminal kinase domain and this interaction inhibits MEKK4 kinase activity and prevents substrate binding.	phosphorylates and activates MAP2K4 and MAP2K6, it also activates the CSBP2, P38 and JNK MAPK pathways.
Kelch-like protein 14 **(KLHL14)** also known as Printor	**BTB domain:** between sequence position 33-151 **BACK domain:** between sequence position 210- 279 **6 Kelch repeats:** between sequence position 323-620	The BTB domain is a versatile protein-protein interaction motif. BTB domain is present near the N-terminus of a fraction of zinc finger proteins and in proteins that contain the Kelch motif. In CRL3, the BTB domain mediates the binding of the substrate adaptor CUL3. The Kelch motifs form β-propeller structure and confer substrate specificity and binding in CUL3-based E3 ubiquitin ligases.	KLHL14 selectively binds to the ATP-free form of torsinA. It mediates the ubiquitylation of B cell receptor (BCR) subunits and decreases the stability of immature BCR glycoforms in the endoplasmic reticulum, thereby reducing BCR levels. KLHL14 promotes the development of ovarian cancer by regulating signalling pathways such as mTOR, WNT, and TGF-

			beta and it may be a target for ovarian cancer detection and treatment.

7. Schematic representation of the Cullin-RING E3 ligase (CRLs) complexes and the WDR11 complex

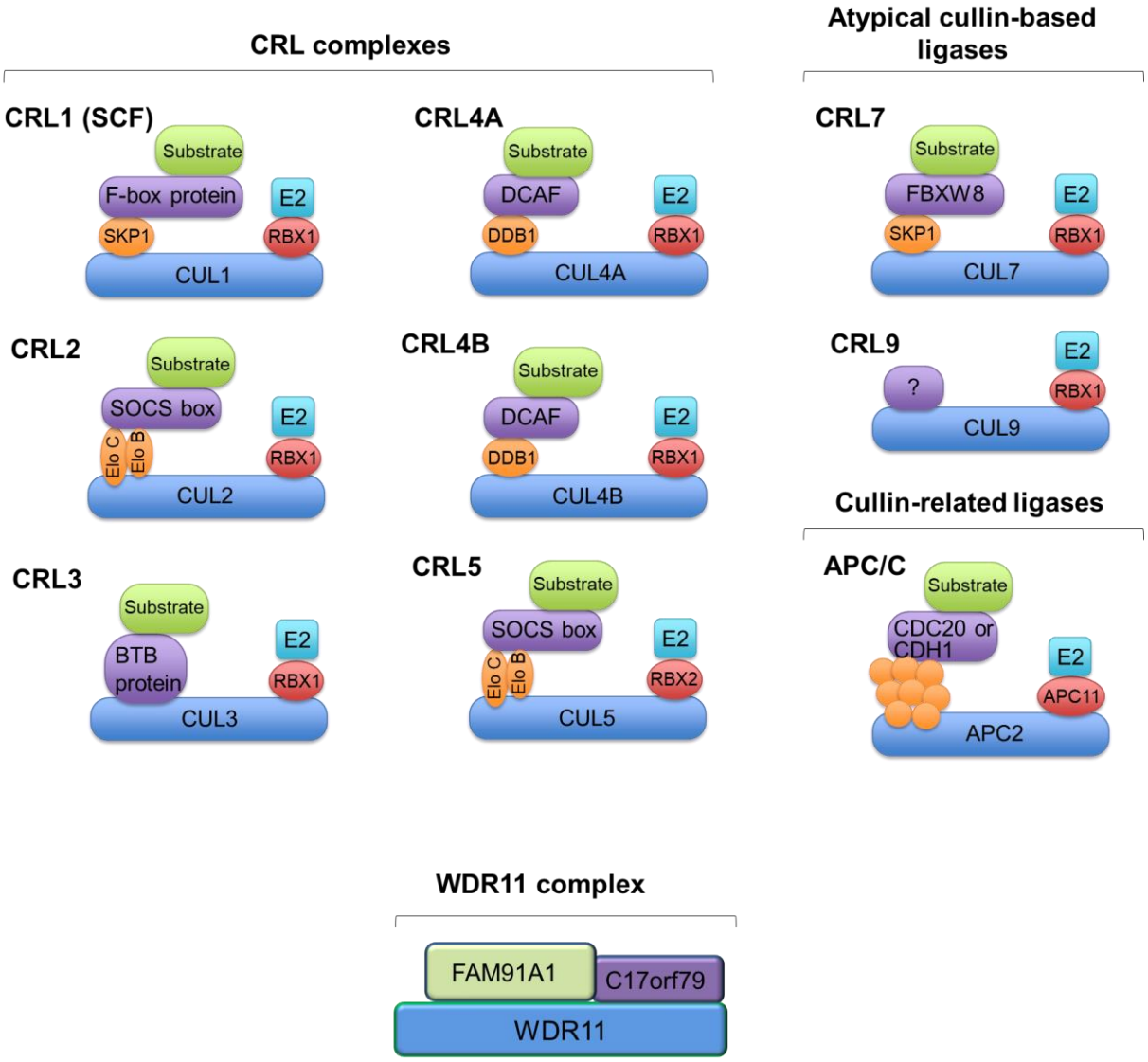

8. Results

8.1 Analysis of genomic databases to identify hypermutated E3 ubiquitin ligases in cancer

To gain new insight on the roles of E3 ligases in the pathogenesis of human cancers, we used the COSMIC database and performed a comprehensive genomic database mining analysis of the approximately 700 E3 ubiquitin ligase genes encoded in the human genome, to identify those that are mutated in cancer. COSMIC (Catalogue of Somatic Mutations in Cancer) is a database that includes genome-wide screen data of over 37,000 genomes samples across many human cancer types **(https://cancer.sanger.ac.uk/cosmic).** In particular, we focused on those E3 ligases displaying abundant mutations within known functional domains. Among these E3 ligases, we shortlisted FBXO24, KLHL14, and DCAF12L2, substrate receptor subunits of CRL1, CRL3, and CRL4 ubiquitin ligases complexes, respectively. As shown in figure 2, these E3 ligases were found with significant hypermutations, with most of the mutations occurring in the F-box domain, the Kelch motif, the BTB domains, and the WD-repeat, respectively **(Figure 2: A, B, C, and D).** Other E3 ligases found mutated are the PDZRN4 and the RNF111 with several mutations across the protein full length **(Figure 2: E, and F).**

8.1.1 Mutations of FBXO24 in human cancer

To screen for mutation of FBXO24 in human cancer, 40678 unique human cancer patient samples were screened for possible mutations in cancer, 585 unique samples were found with mutations in the FBXO24 gene (COSMIC database). Genomic analysis of FBXO24 shows that the gene is hypermutated in cancer **(Figure 2B and Figure 3B).** The hotspot of FBXO24 mutations in cancer was found at the 65 amino acid sequence position within the critical F-box domain (Winston et al., 1999). The mutation at this position leads to missense substitution of the amino acid from threonine to proline (T65P) **(Figure 3B).**

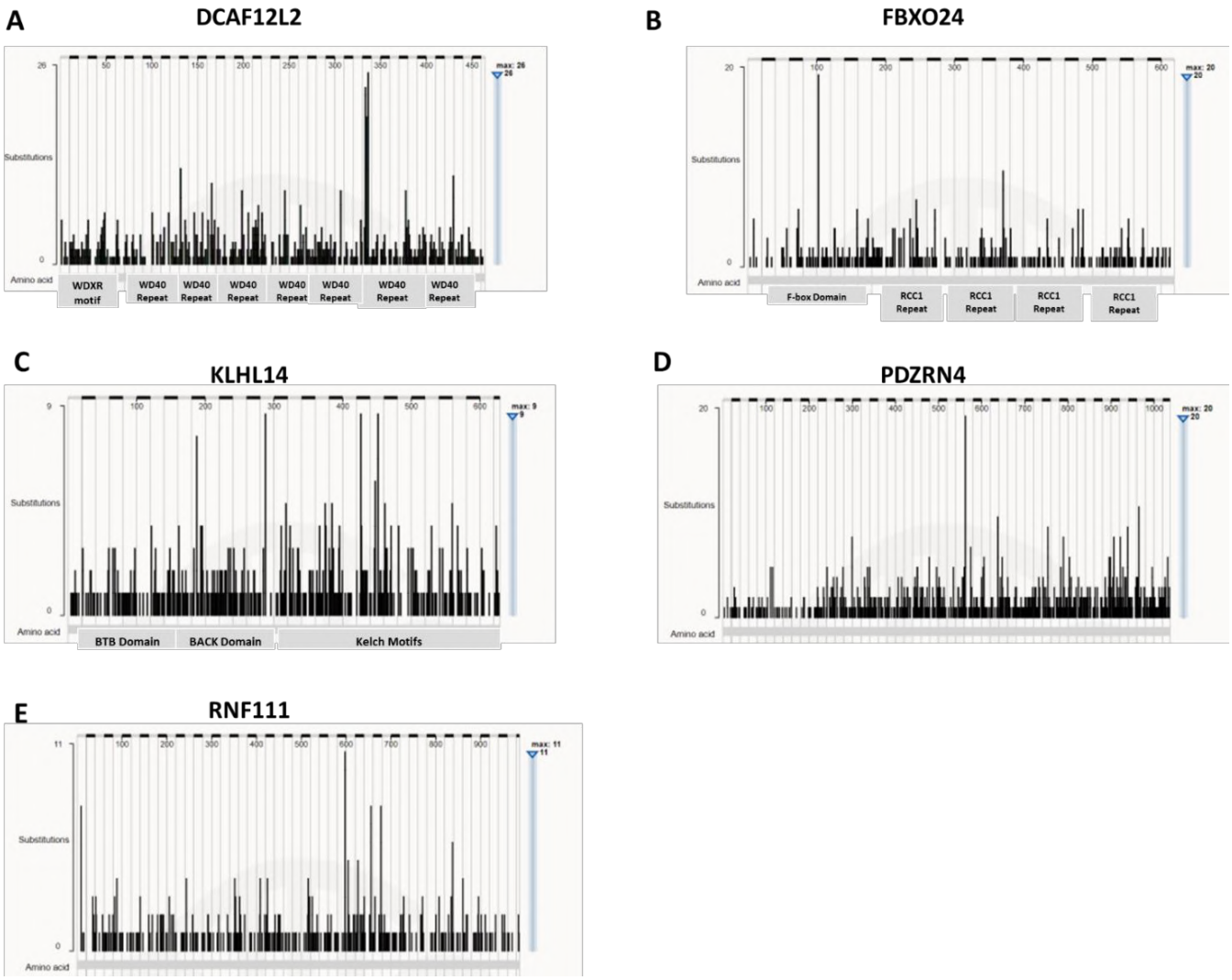

Figure 2. Gene view histograms represent graphical views of mutations across the genes DCAF12L2 **(A)**, FBXO24 **(B),** KLHL14 **(C),** PDZRN4 **(D),** and RNF111 **(E)**. These mutations are displayed at the amino acid level across the full length of each gene.

8.1.1.1 Distribution of FBXO24 mutations in human cancer

A comprehensive screening of FBXO24 mutations in human cancer shows that FBXO24 is mutated in adenocarcinoma, carcinoma, lymphoid neoplasm, and malignant melanoma. These are typically found in the large intestine, endometrium, liver, lung, stomach, skin, hematopoietic and lymphoid. Of note, the most frequent mutation of FBXO24, i.e. T65P, is found in squamous cell carcinoma of the aerodigestive tract **(Figure 4F).**

8.1.2 Mutations of DCAF12L2 in human cancer

Among the 39729 unique human cancer patient samples screened for possible mutations in cancer, 785 unique samples were found with mutations in the DCAF12L2 gene (COSMIC database). Interestingly, the highest incidence of DCAF12L2 mutations occurred within the WD40 repeats domain. DCAF12L2 is composed of seven WD40 repeats **(uniprot.org)** and these WD40 repeats domain is critical for the substrate binding ability of the $CRL4^{DCAF12L2}$ complex. By performing further genomic analysis, we found the highest incidence of DCAF12L2 mutations in human cancer at the amino acid sequence positions: 334, where proline changes to lysine (P334L); 335, where arginine changes to cysteine or histidine (R335C or R335H); and at the 337 amino acid sequence where arginine changes to cysteine or histidine (R337C or R337H) (COSMIC database) **(Figure 3A).** Also, it's important to note that at the 334 amino acid sequence position, there cases of silent mutations with no significant change in the amino acid.

8.1.2.1 Distribution of DCAF12L2 mutations in human cancer

Next, we characterize the tissue distribution of DCAF12L2 in human cancer. Many DCAF12L2 mutations were found in adenocarcinoma, carcinoma, and metaplastic carcinoma of the large intestine, colon, liver, prostate, stomach, and breast **(Figure 4: A, B, C, and D).** The DCAF12L2(P334L) mutation is frequent in the large intestine, stomach, prostate, lungs, and endometrium **(Figure 4A).** The DCAF12L2(R335C) mutation is frequent in the liver, while the top tissue found with DCAF12L2(R335H) mutation is the large intestine **(Figure 4B and 4C).** The DCAF12L2(R337H) mutation is found in the large intestine, colon, prostate, and breast **(Figure 4D).**

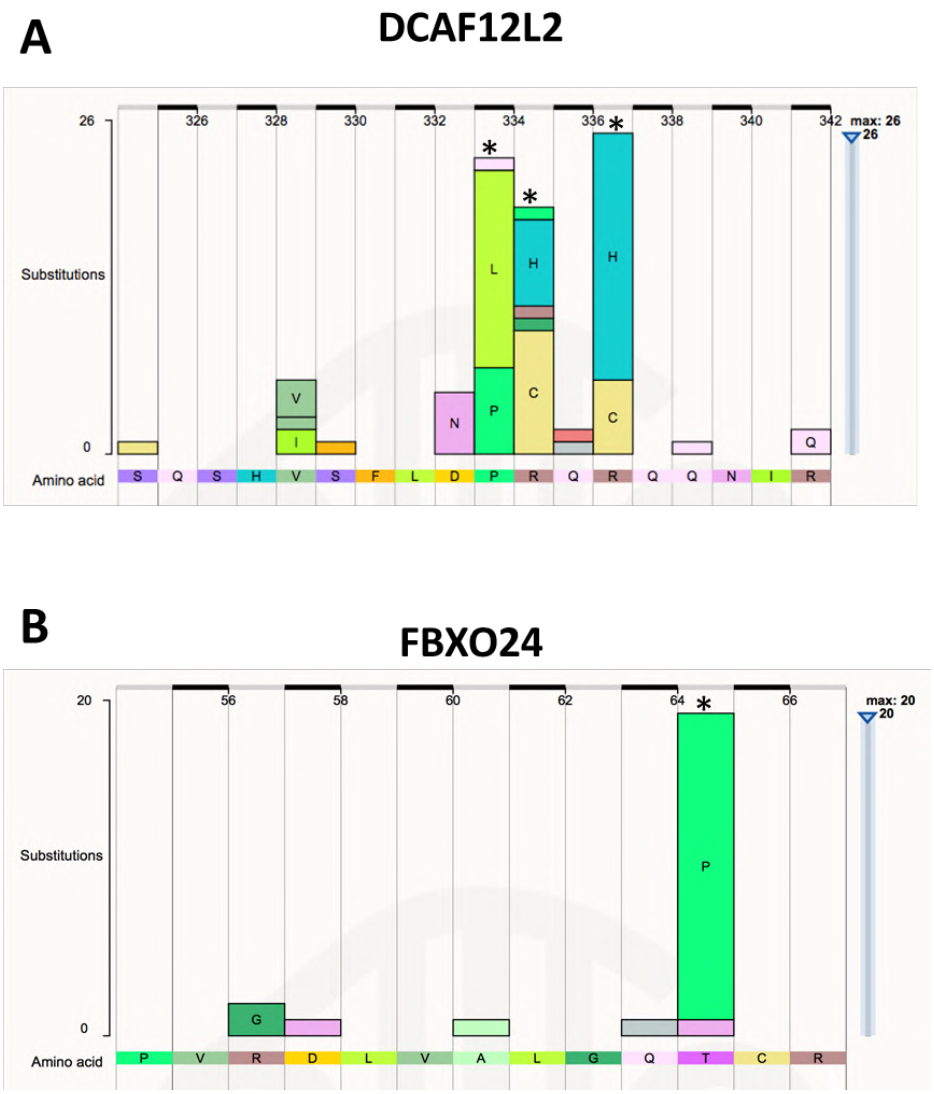

Figure 3. Mutations of DCAF12L2 and FBXO24 in Human Cancer

(A) Details of amino acid substitution at the DCAF12L2 mutation hotspots in cancer at sequence positions: 334, 335, and 337 within the WD40 domain.

(B) Details of amino acid substitution at the hotspot of FBXO24 mutation in cancer at the 65th sequence position within the F-box domain.

***: Mutation Hotspot**

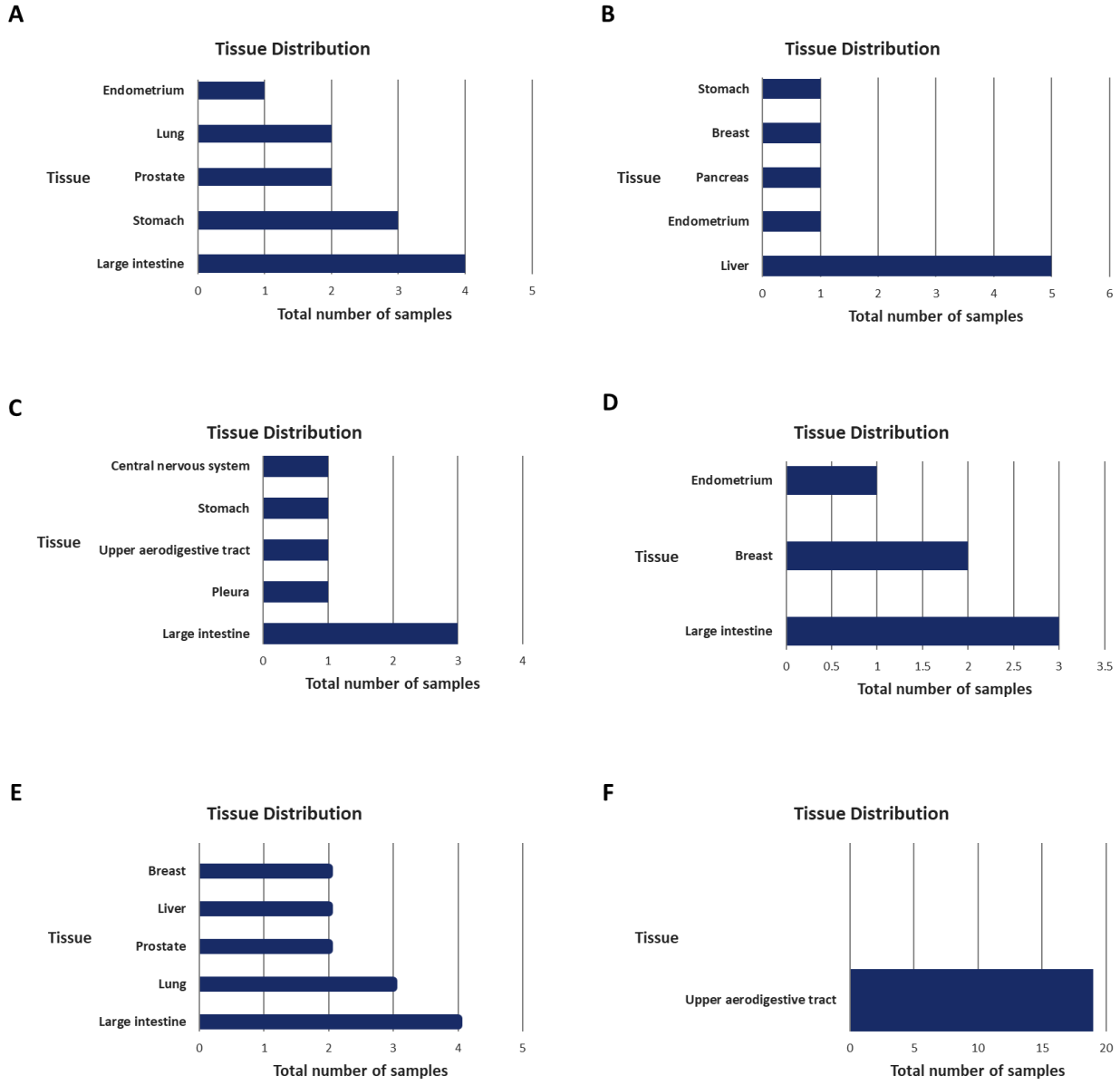

Figure 4. Tissue Distribution of DCAF12L2 and FBXO24 Mutations in Human Cancer

(A) Tissue distribution of DCAF12L2 mutation: DCAF12L2 (P334L) found in cancer.

(B) Tissue distribution of DCAF12L2 mutation: DCAF12L2 (R335C) found in cancer

(C) Tissue distribution of DCAF12L2 mutation: DCAF12L2 (R335H) found in cancer.

(D) Tissue distribution of DCAF12L2 mutation: DCAF12L2 (R337C) found in cancer.

(E) Tissue distribution of DCAF12L2 mutation: DCAF12L2 (R337H) found in cancer.

(F) Tissue distribution of FBXO24 mutation: FBXO24 (T65P) found in cancer.

8.2 The FBXO24 mutation found in cancer prevents its interaction with SKP1

To identify the substrates of $CRL1^{FBXO24}$, we obtained clone constructs of wild-type FBXO24 tagged with FLAG-FLAG-HA-HA-tag and by performing site-directed mutagenesis, we obtained the FBXO24(T65P) mutant with FLAG-FLAG-HA-HA-tagged. These clone constructs were generated for mass spectrometry screening of FBXO24 substrates. However, since our genomic data screening revealed the F-box domain as the hotspot of FBXO24 mutation in cancer, prior to the mass spectrometry analysis, we decided to perform immunoprecipitation analysis to check the interaction of the FLAG-FLAG-HA-HA-tagged FBXO24 wild type or the FLAG-FLAG-HA-HA-tagged FBXO24(T65P) mutant with endogenous SKP1 in HEK293T cells. We expressed FLAG-FLAG-HA-HA-tagged FBXO24 wild-type or FLAG-FLAG-HA-HA-tagged FBXO24(T65P) mutant in HEK293T cells and performed anti-FLAG immunoprecipitation to pull down the FBXO24 proteins. The immunoprecipitation and western blot analysis shows that the FBXO24(T65P) mutation found in cancer blocks the interaction of FBXO24 with Skp1 and CUL1 **(Figure 5C).**

8.3 Proteomic screen to identify $CRL1^{FBXO24}$ substrates

Subsequently, we performed mass spectrometry analysis of FBXO24 wild type and FBXO24(T65P) mutant by expressing FLAG-FLAG-HA-HA-tagged FBXO24 wild-type or FLAG-FLAG-HA-HA-tagged FBXO24(T65P) mutant in HEK293T cells and performed affinity-purification (AP) followed by mass spectrometry analysis **(Figure 5A).** From the mass spectrometry screening, we recovered 5 peptides of Skp1 and 6 peptides of CUL1 in the FBXO24(T65P) mutant as compared 14 peptides of Skp1 and 38 peptides of CUL1 found in the FBXO24 wild type **(Figure 5B).** The mass spectrometry results further confirmed our previous anti-FLAG immunoprecipitation analysis of FBXO24 and show that indeed the FBXO24(T65P) mutation found in cancer blocks FBXO24 binding with Skp1 and CUL1 **(Figure 5C).**

A

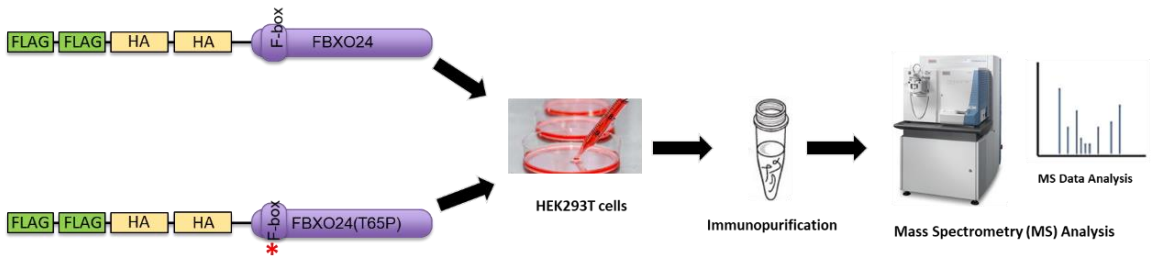

B

Accession	Description	Number of peptides after AP-MS EV	FBXO24	FBXO24(T65P)	Gene Symbol
O75426	F-box only protein 24 OS=Homo sapiens OX=9606 GN= FBXO24 PE=1 SV=2	11	39	35	FBXO24
Q13616	Cullin-1 OS=Homo sapiens OX=9606 GN= CUL1 PE=1 SV=2	0	38	6	CUL1
P63208	S-phase kinase-associated protein 1 OS=Homo sapiens OX=9606 GN= SKP1 PE=1 SV=2	1	14	5	SKP1
Q6UXM1	Leucine-rich repeats and immunoglobulin-like domains protein 3 OS=Homo sapiens OX=9606 GN= LRIG3 PE=2 SV=1	0	10	11	LRIG3
Q9NXX6	Non-structural maintenance of chromosomes element 4 homolog A OS=Homo sapiens OX=9606 GN= NSMCE4A PE=1 SV=2	0	4	6	NSMCE4A
Q70CQ2	Ubiquitin carboxyl-terminal hydrolase 34 OS=Homo sapiens OX=9606 GN= USP34 PE=1 SV=2	0	5	10	USP34
P17028	Zinc finger protein 24 OS=Homo sapiens OX=9606 GN= ZNF24 PE=1 SV=4	0	3	5	ZNF24

C

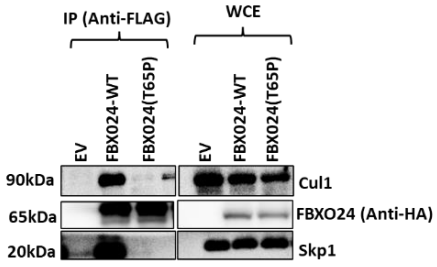

Figure 5. Proteomic Analysis of FBXO24 Substrates

(A) Schematic representation of AP-MS of FBXO24 WT and FBXO24(T65P).

(B) List of peptides obtained by AP-MS of Empty Vector (EV), FBXO24 WT and FBXO24(T65P) mutant.

(C) Immunoprecipitation (IP) of FLAG-FLAG-HA-HA-tagged FBXO24 WT and the FLAG-FLAG-HA-HA-tagged FBXO24(T65P) mutant to validate the interaction with endogenous Skp1. HEK293T cells were transfected with either an empty vector (EV) or FLAG-FLAG-HA-HA-tagged FBXO24 WT or FLAG-FLAG-HA-HA-tagged FBXO24(T65P) mutant. MG132 was added 5 hours before harvesting the cells. The whole-cell extract (WCE) was subjected to anti-FLAG IP and immunoblotted as indicated.

8.4 Proteomic screen to identify CRL4^{DCAF12L2} substrates

To identify the substrates of CRL4^{DCAF12L2}, we expressed wild-type FLAG-FLAG-HA-HA-tagged DCAF12L2 in HEK293T cells and performed affinity-purification (AP) followed by mass spectrometry (MS) analysis **(Figure 6A).** We found peptides derived from the CRL subunits CUL4A (16 peptides), CUL4B (27 peptides), and DDB1 (53 peptides). In addition, we recovered unique peptides corresponding to FAM91A1 (17 peptides), C17orf75 (11 peptides), WDR11 (27 peptides), and MEKK4 (21 peptides) **(Figure 6B).** FAM91A1, C17orf75, and WDR11 are known to form a complex known as the WDR11 complex (Navarro Negredo et al., 2018), while MEKK4 is a protein kinase involved in the mitogen-activated protein (MAP) kinase transduction cascade (Abell, Granger, & Johnson, 2007; Abell & Johnson, 2005).

8.4.1 DCAF12L2 interacts with the WDR11 complex and MEKK4

To validate the mass spectrometry results, we expressed in cells FLAG-FLAG-HA-HA tagged wild type DCAF12L2 in HEK293T cell, we treated the cells with MG132 to block protein degradation, 5 hours after treatment the cells were collected, lysed and the whole cell extracts were subjected to anti-FLAG immunoprecipitation and western blot analysis. Anti-FLAG immunoprecipitation of DCAF12L2, coimmunoprecipitates with endogenous CUL4 thereby confirming that DCAF12L2 is part of a CRL4 ubiquitin ligase complex **(Figure 6C).** In addition, DCAF12L2 coimmunoprecipitates with endogenous FAM91A1, C17orf75, WDR11, and MEKK4 thus validating the mass spectrometry result **(Figure 6C).**

8.5 The DCAF12L2 mutations found in cancer prevent its interaction with the WDR11 complex and MEKK4

DCAF12L2 is composed of 7 repeats of WD40 repeats. The peaks of mutation with the highest incident of mutation of DCAF12L2 found in cancer occur on the 6th WD40 repeat and the mutated amino acids sequence are in positions 334, 335, and 337. To assess the effect of these mutations and the link to cancer pathogenesis, we generated DCAF12L2 mutants with the corresponding mutations found in cancer

on the amino acids sequence position 334, or 335 or 337 (P334L, R335H, R335C, R337C, R337H) **(Figure 3A).** Next, we tested the interaction of these mutants with endogenous FAM91A1, C17orf75, WDR11, and MEKK4. Interestingly, the P334L, R335C, and R335H mutants found in cancer did not coimmunoprecipitate with FAM91A1, C17orf75, WDR11, and MEKK4. However, the R337C and R337H mutations do not have any detectable effect on DCAF12L2 binding to FAM91A1, C17orf75, WDR11 and MEKK4 **(Figure 6C).**

A

B

Accession	Description	Number of peptides after AP-MS		
		Empty Vector (EV)	DCAF12L2	Gene Symbol
Q16531	DNA damage-binding protein 1 OS=Homo sapiens OX=9606 GN=DDB1 PE=1 SV=1	4	53	DDB1
Q5VW00	DDB1- and CUL4-associated factor 12-like protein 2 OS=Homo sapiens OX=9606 GN=DCAF12L2 PE=2 SV=1	7	30	DCAF12L2
Q9BZH6	WD repeat-containing protein 11 OS=Homo sapiens OX=9606 GN=WDR11 PE=1 SV=1	0	27	WDR11
Q13620	Cullin-4B OS=Homo sapiens OX=9606 GN=CUL4B PE=1 SV=4	0	27	CUL4B
Q658Y4	Protein FAM91A1 OS=Homo sapiens OX=9606 GN=FAM91A1 PE=1 SV=3	0	17	FAM91A1
F5H538	Mitogen-activated protein kinase kinase kinase 4 OS=Homo sapiens OX=9606 GN=MAP3K4 PE=1 SV=1	0	21	MEKK4
Q9HAS0	Protein Njmu-R1 OS=Homo sapiens OX=9606 GN=C17orf75 PE=1 SV=2	0	11	C17orf75
Q13619	Cullin-4A OS=Homo sapiens OX=9606 GN=CUL4A PE=1 SV=3	0	16	CUL4A
Q5T447	E3 ubiquitin-protein ligase HECTD3 OS=Homo sapiens OX=9606 GN=HECTD3 PE=1 SV=1	0	12	HECTD3

C

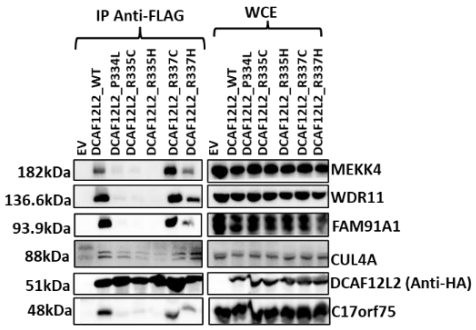

Figure 6. Proteomic Analysis of DCAF12L2 Substrates

(A) Schematic representation of AP-Mass Spectrometry of DCAF12L2_wild type. **(B)** List of peptides recovered from the AP-MS of DCAF12L2. **(C)** Immunoprecipitation (IP) of FLAG-FLAG-HA-HA-tagged DCAF12L2(WT) and FLAG-FLAG-HA-HA-tagged DCAF12L2 mutants (P334L), (R335C), (R335H), (R337C), and (R337H). HEK293T cells were transfected with either an empty vector (EV), or FLAG-FLAG-HA-HA-tagged DCAF12L2(WT) or FLAG-FLAG-HA-HA-tagged DCAF12L2 mutants (P334L), or (R335C), or (R335H), or (R337C), or (R337H). MG132 was added 5 hours before harvesting. Whole-cell extract (WCE) were subjected to anti-FLAG IP and immunoblotted as indicated.

8.6 $CRL4^{DCAF12L2}$ mediates the ubiquitylation of FAM91A1, a component of the WDR11 complex.

Among the proteins identified in the mass spectrometry analysis of DCAF12L2, we found the DDB1, CUL4A and CUL4B, which are known subunits of a CRL4 E3 complex **(Figure 6B).** Thus, we thought that DCAF12L2 could be a specific substrate recognition protein within the CRL4 complex that recognises and recruits substrate proteins for ubiquitylation. To determine whether DCAF12L2 mediates the ubiquitylation of any of the three components of the WDR11 complex (FAM91A1, C17orf75 and WDR11), we performed *in vivo* ubiquitylation assays in HEK293T cells. HEK293T cells were transfected with HA-tagged FAM91A1 or HA-tagged WDR11 and MYC-tagged ubiquitin, with or without FLAG-tagged

DCAF12L2. The whole-cell extract (WCE) was subjected to anti-MYC IP and immunoblotted with anti-HA to detect ubiquitylated WDR11 or FAM91A1. As shown in **Figure 7A**, ectopic expression of DCAF12L2 promotes the ubiquitylation of FAM91A1 whereas WDR11 shows no sign of ubiquitylation both in the presence and absence of DCAF12L2 **(Figure 7B).**

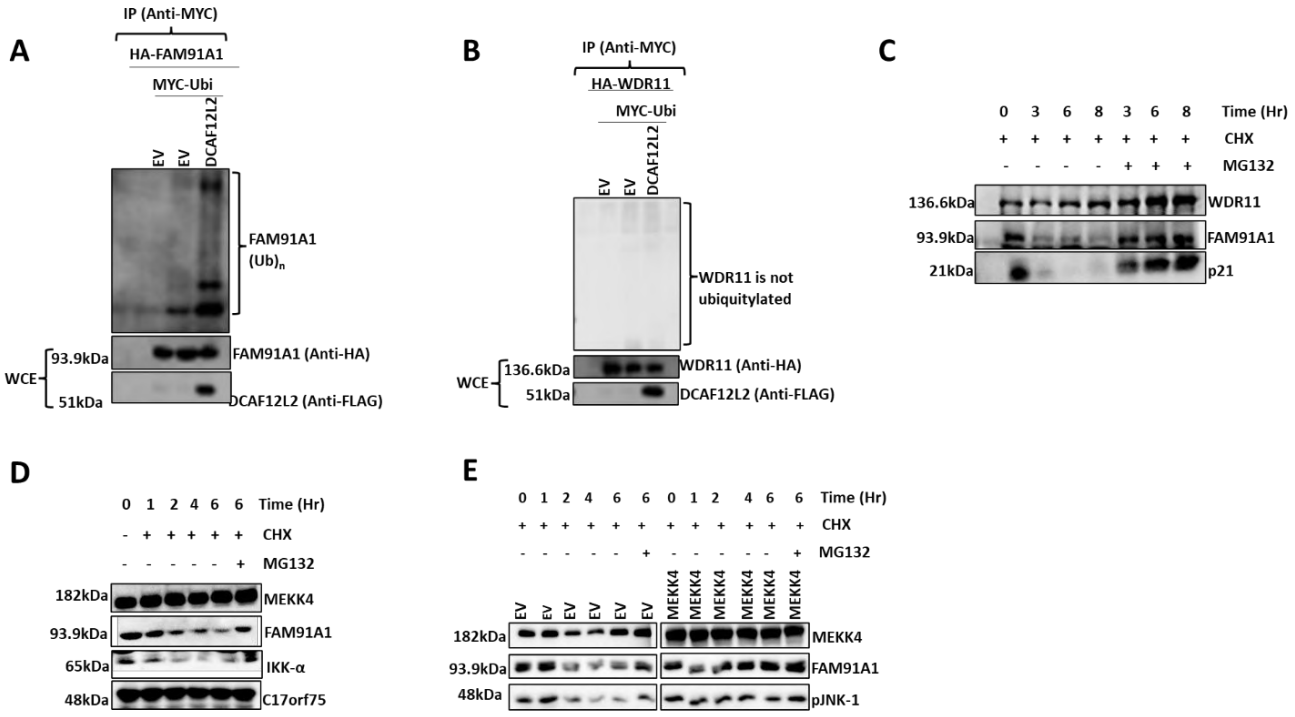

Figure 7. CRL4^{DCAF12L2} mediates the ubiquitylation of FAM91A1, a component of the WDR11 complex.

(A) HEK293T cells were transfected with HA-tagged FAM91A1 and MYC-tagged ubiquitin, with or without FLAG-tagged DCAF12L2. The whole-cell extract (WCE) was subjected to anti-MYC IP and immunoblotted with anti-HA to detect ubiquitylated FAM91A1. **(B)** Same as in **(A)** except that HA-tagged WDR11 was used. **(C)** Cycloheximide chase assay of FAM91A1 and WDR11, where global protein synthesis is blocked using the translation elongation inhibitor cycloheximide in the presence or not of the proteasome inhibitor MG132**,** p21 is a CRL target and it was used as a positive control. **(D)** Time course stability studies of FAM91A1 C17orf75, and MEKK4 in the presence of cycloheximide or both cycloheximide and MG132 treatment. IKK-α was used as a positive control to monitor protein stability **(E)** Stability study of FAM91A1 when MEKK4 was overexpressed in HEK293T cells treated with cycloheximide only or with cycloheximide and MG132 treatment, here pJNK-1 serves as a control positive to compare and monitor MEKK4 activity in empty vectors cells and cells expressing MEKK4.

9. Biological significance of CRL4^{DCAF12L2} mediated ubiquitylation

Next, we explored the biological significance of CRL4^{DCAF12L2} ubiquitin ligase mediated ubiquitylation. First, we reasoned that DCAF12L2 might target its substrates for proteasomal degradation. Hence, we performed stability analysis of FAM91A1, C17orf75, WDR11 and MEKK4. To that aim, we treated cells with cycloheximide (CHX) to block *de novo* protein synthesis with or without MG132 to block proteasomal degradation. As shown in **Figures 7; C and D**, FAM91A1 shows significant degradation which was reversed by treatment with the proteasome inhibitor MG132. The CRL target p21 was used as a positive control to monitor CRL targeted degradation while the IKK-α was used as a positive control to monitor protein stability.

9.1 MEKK4 promotes the stability of FAM91A1

Phosphorylation is a common post-translational modification of the substrate that regulates its interaction with the CRL and consequently its ubiquitylation and degradation (Dhiani & Mehellou, 2020)(Hunter, 2007). Thus, the protein kinase MEKK4, which was one of the proteins found in the affinity purification of DCAF12L2, might be involved in the regulation of DCAF12L2 mediated ubiquitylation of FAM91A1. To test this hypothesis, we assessed the effect of MEKK4 ectopic expression on the stability of endogenous FAM91A1 in HEK293T cells. As shown in **Figure 7E**, overexpression of MEKK4 promotes the stability of FAM91A1 in HEK293T cells. To monitor MEKK4 activity, pJNK-1 was used a control to compare and monitor MEKK4 activity in empty vectors and in cells expressing MEKK4.

9.2 The CRL4^{DCAF12L2} ubiquitin ligase mediates MEKK4 ubiquitylation

To test whether MEKK4 is a substrate of the CRL4^{DCAF12L2} ubiquitin ligase, we performed an *in vivo* ubiquitylation assay upon ectopic expression of MEKK4 in HEK293T cells. HEK293T cells were transfected with HA-tagged MEKK4 and MYC-tagged ubiquitin or MYC-tagged ubiquitin K-less that cannot be ubiquitylated, with or without FLAG-tagged DCAF12L2. The whole-cell extract (WCE) was subjected to anti-MYC immunoprecipitation and then analysed by

immunoblotting with an anti-HA antibody to detect ubiquitylated MEKK4. As shown in **Figure 8A**, ectopic expression of DCAF12L2 promotes MEKK4 ubiquitylation.

9.3 The WDR11 complex and MEKK4 are two independent substrates of $CRL4^{DCAF12L2}$

It has been reported that the WDR11 complex is a *trans*-Golgi network-associated stable complex that facilitates vesicular trafficking in cells (Navarro Negredo et al., 2018) and interestingly, MEKK4 is localized in Golgi-associated vesicles. This suggests that MEKK4 could also be involved in vesicular trafficking in cells. Thus, we thought that $CRL4^{DCAF12L2}$ mediated ubiquitylation of MEKK4 might be linked to the WDR11 complex. To investigate whether MEKK4 and the WDR11 complex are two independent substrates of $CRL4^{DCAF12L2}$ ligase, we expressed HA-FAM91A1 or HA-C17orf75 or HA-WDR11 in HEK293T cells and subject the whole-cell extract (WCE) to anti-HA IP. Our main goal was to check if FAM91A1, C17orf75 or WDR11 would interact with endogenous MEKK4. As shown in **Figure 8B**, neither FAM91A1 C17orf75 nor WDR11 interacts with endogenous MEKK4.

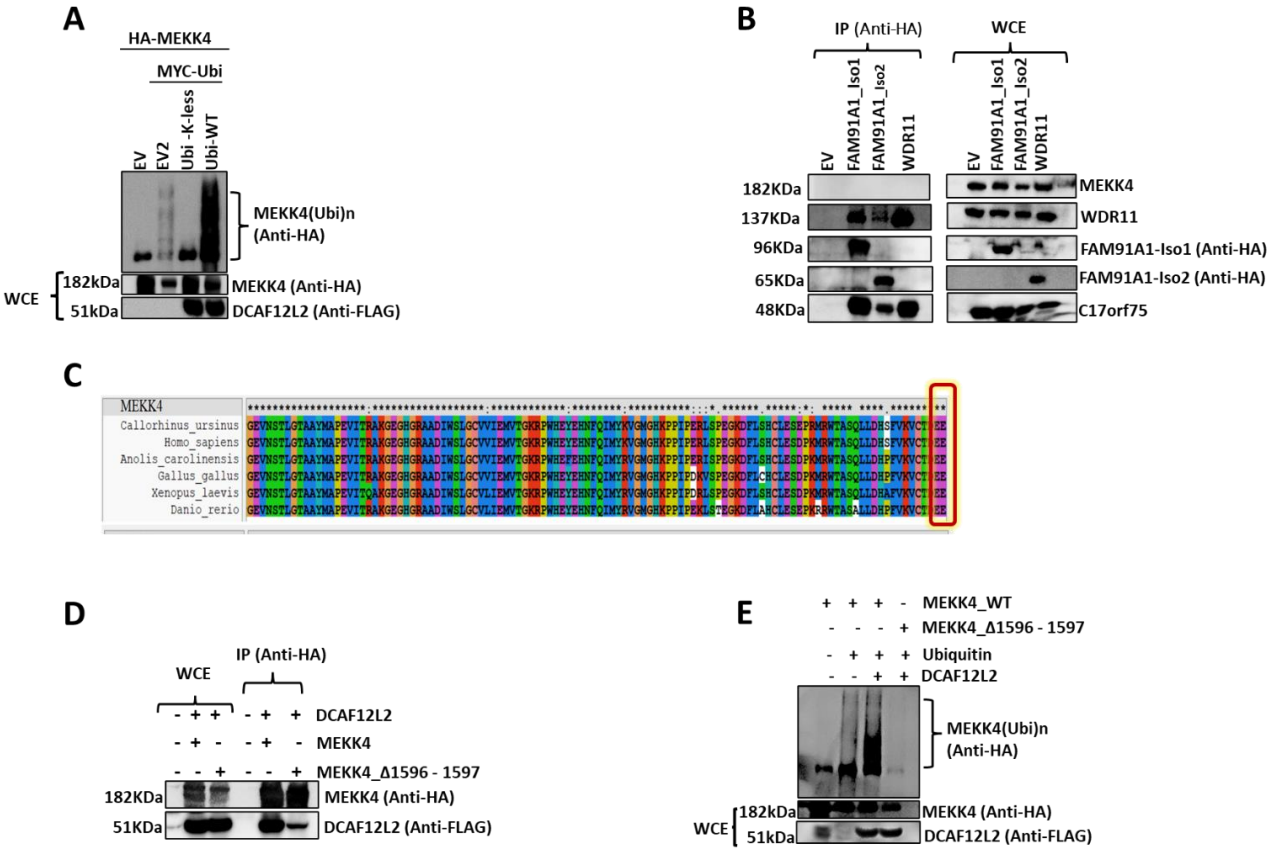

Figure 8. The CRL4^{DCAF12L2} ubiquitin ligase mediates the ubiquitylation of MEKK4

(A) HEK293T cells were transfected with HA-tagged MEKK4 and MYC-tagged ubiquitin or MYC-tagged ubiquitin K-less that cannot be ubiquitylated, with or without FLAG-tagged DCAF12L2. The whole-cell extract (WCE) was subjected to anti-MYC IP and immunoblotted with anti-HA to detect ubiquitylated MEKK4. **(B)** Immunoprecipitation (IP) of FAM91A1 and WDR11. HEK293T cells were transfected with either an empty vector (EV), HA-tagged FAM91A1_Iso1 or HA-tagged FAM91A1_Iso2, or HA-tagged WDR11. The whole-cell extract (WCE) was subjected to anti-HA IP and immunoblotted as indicated. **(C)** Multiple sequence alignment of MEKK4 C-terminus from the indicated species. **(D)** Immunoprecipitation (IP) of MEKK4 and MEKK4-Δ1596-1597 mutant. HEK293T cells were co-transfected with either an empty vector (EV), or FLAG-tagged DCAF12l2 and HA-tagged MEKK4, or HA-tagged MEKK4Δ1596-1597. The whole-cell extract (WCE) was subjected to anti-HA IP and immunoblotted with anti-FLAG antibody to detect DCAF12L2. The deletion of the C-terminal ends di-glutamic acids (EE) residues in MEKK4-Δ1596-1597 mutant affects its binding to DCAF12L2.

(E) HEK293T cells were transfected with HA-tagged MEKK4, or HA-tagged MEKK4Δ1596-1597, MYC-tagged ubiquitin, with or without FLAG-tagged DCAF12L2. The whole-cell extract (WCE) was subjected to anti-MYC IP and immunoblotted with anti-HA to detect ubiquitylated MEKK4.

9.4 DCAF12L2 recognises and targets the C-terminal di-glutamic acid (EE) motif as degron

The identification of the substrate recognition degrons in the protein substrates is critical to comprehend the underlying mechanism of E3 ligase/substrate binding. Previous studies by Koren et al. have demonstrated that DCAF12, a mammalian paralog of DCAF12L2, specifically recognises and targets the C-terminal di-glutamic acid (EE) motif as substrate degradation degron (Koren et al., 2018). Interestingly, human MEKK4 ends with the C-terminal di-glutamic acid (EE) motif and this EE C-terminal motif is found to be evolutionary conserved **(Figure 8C)**. Hence, we speculated that perhaps the EE C-terminal motif could be the signalling degron for DCAF12L2/MEEK4 binding. To test this hypothesis, we generated a MEKK4-Δ1596-1597 mutant in which the C-terminal EE amino acid residues were deleted. We co-transfected HA-tagged MEKK4 WT or HA-tagged MEKK4-Δ1596-1597 mutant with FLAG-tagged DCAF12L2 in HEK293T cells and subject the whole-cell extract (WCE) to anti-HA IP then immunoblotted with anti-FLAG antibodies to detect DCAF12L2 binding **(Figure 8D)**. The deletion of the C-terminal ends di-glutamic acids (EE) motif in MEKK4-Δ1596-1597 mutant affects its binding to DCAF12L2.

Subsequently, we assessed the requirement of the C-terminal di-glutamic acids (EE) motif in DCAF12L2 mediated ubiquitylation assay of MEKK4, we co-transfected HEK292T cells with HA-tagged MEKK4 or HA-tagged MEKK4-Δ1596-1597 and MYC-tagged ubiquitin, with or without FLAG-tagged DCAF12L2. The whole-cell extract (WCE) was subjected to anti-MYC IP and then we immunoblotted with anti-HA antibody to detect MEKK4 ubiquitylation. As shown in **Figure 8E**, the deletion of the C-terminal ends di-glutamic acids (EE) residues prevents the ubiquitylation of MEKK4.

10. Discussion

In our genomic database screening of E3 ligase mutations in human cancer, we found several CRL substrate receptors that are hypermutated in cancer. In this study, we focused on DCAF12L2, and FBXO24 which are substrate receptors subunit of $CRL4^{DCAF12L2}$ and $CRL1^{FBXO24}$ complexes respectively. By performing comprehensive analysis on the mutations of FBXO24 in cancer, we found the mutation hotspot within the F-box domain, precisely on the amino acid residue 65 where threonine changed to proline (T65P) **(Figure 3B)**. As part of our major findings, we show that this FBXO24 (T65P) mutation strongly impacts the formation of the $CRL1^{FBXO24}$ (SCF^{FBXO24}) complex by preventing the binding of FBXO24 to Skp1 thereby blocking the recruitment of the FBXO24 protein needed to form the $CRL1^{FBXO24}$ complex **(Figure 5C)**. Unfortunately, we could not identify the specific substrates of the $CRL1^{FBXO24}$ complex. Our ability to successfully identify the substrates of the $CRL1^{FBXO24}$ complex is paramount for detailed understanding of how the mutation of FBXO24 found in cancer contributes to the pathogenesis of head and neck cancers in which the FBXO24(T65P) mutations were found.

Similarly, we performed comprehensive analysis of DCAF12L2 mutations found in cancer and found several mutations spanning across the whole WD-40 repeats domains **(Figure 2A)**. This WD-40 repeats domain is critical in $CRL4^{DCAF12L2}$ complex ubiquitylation function, it is this domain that enables DCAF12L2 to recognise and bind to the substrates (Xu & Min, 2011). The hotspots of mutation of DCAF12L2 in cancer were found within the WD-40 repeats domain with the amino acid residues at sequence positions: 334, 335, and 337. However, it is unclear why these amino acid residues at sequence positions: 334, 335, and 337 **(Figure 3A)** are hotspots of mutation of DCAF12L2 in cancer. Considering the chemical properties of the amino acid substitutions found in cancer at these sequence positions, there are indications that the mutation of proline to lysine (P334L), or arginine to cysteine or histidine at positions 335 and 337 would likely disrupt the conformation of the β-propeller structure in DCAF12L2 and consequently affect the function of DCAF12L2 in the $CRL4^{DCAF12L2}$ complex.

Proteomic screening of DCAF12L2 revealed the presence of peptides of CUL4A (16 peptides) and CUL4B (27 peptides) **(Figure 6B)**. With CUL4A being predominantly cytoplasmic and CUL4B specifically localized within the nucleus (Zhou et al., 2020), the co-immunoprecipitation of CUL4A and CUL4B in DCAF12L2 proteomic screening suggests that the $CRL4^{DCAF12L2}$ complex might be involved in mediating the ubiquitylation of cytoplasmic and nuclear substrates. Besides, sequence analysis of DCAF12L2 amino acids sequence mapped the presence of nuclear localization signal (NLS) (GSRKRKAPAV) sequence near the N-terminal of DCAF12L2, which indicates the presence of DCAF12L2 in the nucleus thus confirming the targeting and ubiquitylation nuclear substrates by the $CRL4B^{DCAF12L2}$ complex.

Among the protein substrates found enriched in the proteomic analysis of DCAF12L2, the WD repeat-containing protein 11 (WDR11) is the only protein that shuttles between the cytoplasm and the nucleus (Kim et al., 2018), while FAM91A1, C17orf75, and MEKK4 are strictly cytoplasmic. WDR11 itself does not contain a nuclear localization signal but contains a putative nuclear export signal such that it shuttles between the cytoplasm and the nucleus (Kim et al., 2018). Ubiquitylation assay shows that WDR11 is not the main component of the WDR11 complex targeted for ubiquitylation by the $CRL4^{DCAF12L2}$ complex. Hence, we speculated that WDR11 might shuttle between the cytoplasm and the nucleus to serve as a scaffold to mediate the binding of the $CRL4^{DCAF12L2}$ complex to the targeted cytoplasmic or nuclear substrates. Besides, according to Kim et al., in response to hedgehog (Hh) signalling, WDR11 undergoes intracellular trafficking from the cilium to the nucleus where it forms a complex with EMX1 and GLI3 to mediate the proteolytic degradation of GL13. However, it remains unknown the exact mechanism by which WDR11 regulates the proteolytic degradation of GLI3, but based on our findings, we speculate that the $CRL4B^{DCAF12L2}$ complex might be responsible for the ubiquitylation and proteolytic degradation of GLI3, this happens by binding to the EMX1-WDR11-GLI3 complex through the WDR11 protein that serves as scaffold protein to facilitate the targeting of GLI3 to the $CRL4B^{DCAF12L2}$ complex for ubiquitylation. This provides more details to the studies by Kim et al., where it was demonstrated that WDR11 is not the direct target of GLI3 but rather

it functions as a scaffolding protein to link GLI3 to an unknown target (Kim et al., 2018). To confirm our speculation, we would need to assess GLI3 stability and ubiquitylation in the presence of DCAF12L2 when Hh signalling are triggered in cells.

WDR11 forms a stable complex with FAM91A1 and C17orf75 in the cytoplasm precisely at the *trans*-Golgi network (TGN). This complex, known as the WDR11 complex, facilitates vesicular docking and trafficking in cells (Navarro Negredo et al., 2018). Nevertheless, the exact mechanism by which the WDR11 complex is stabilized and regulated to maintain its cellular function in vesicular docking and trafficking remains unclear. Although, it has been demonstrated by Navarro Negredo et al. that the disruption of FAM91A1 does affect the stability of the complex, thereby causing a dramatic change in the localization of WDR11 and C17orf75 from the *trans*-Golgi network (TGN) to a dispersed cytoplasmic distribution. The exact mechanism that could be responsible to triggers the disruption of FAM91A1 is unknown. Our studies have shown that the $CRL4^{DCAF12L2}$ complex mediates the ubiquitylation of FAM91A1 **(Figure 7A)**. Thus, we speculated that the ubiquitylation of FAM91A1 could be a critical mechanism involved in the assembling and dissociation of the WDR11 complex as well as in regulating its cellular functions in vesicular docking and trafficking.

Moreover, because of the *trans*-Golgi network (TGN) localization of the WDR11 complex, we reasoned that $CRL4A^{DCAF12L2}$ complex would likely be responsible in mediating the ubiquitylation of FAM91A1, with the WDR11 protein serving as scaffold protein to facilitate the binding of the WDR11 complex to the $CRL4A^{DCAF12L2}$ complex to target FAM91A1 for ubiquitylation. In general, from our studies, we found that WDR11 is not ubiquitylated thus, we reason perhaps that WDR11 would likely serves as scaffold protein that mediate the binding of cytoplasmic and nuclear substrates to the $CRL4^{DCAF12L2}$ complex. Which agrees with the studies by Neocleous et al. where WDR11 was proposed to be a scaffolding protein involved in multiple cellular processes, including cell cycle progression, signal transduction, apoptosis, and gene regulation (Neocleous et al., 2020), (Kim et al., 2018).

The reversibility and fast kinetics of phosphorylation is one dynamic way of regulating protein complexes. As reported by Nishi et al., phosphorylation at the binding interface of protein-protein interaction directly affects the binding energy and the stability of the protein complex (Nishi et al., 2011). Thus, we hypothesized that the phosphorylation by the protein kinase MEKK4 might be critical in the stability of the WDR11 complex. However, we observed from our binding studies that MEKK4 has no direct interaction with the components of WDR11 complex; FAM91A1, and WDR11 **(Figure 8B)**.

Crosstalk between phosphorylation and ubiquitination widely affects the interaction between the CUL-RING ligase receptors and the substrates (Chen et al., 2021; Ni et al., 2018). Interestingly, the stability studies of FAM91A1 in the presence of MEKK4, show that the overexpression of MEKK4 promotes the stability of endogenous FAM91A1 in HEK293T cells and one of the ways by which phosphorylation regulates protein ubiquitylation is by positively or negatively regulating the activity at the E3 ligase substrate receptor (Hunter, 2007). Here, we foresee the possibility of MEKK4 negatively regulating FAM91A1 ubiquitylation at the $CRL^{DCAF12L2}$ complex by phosphorylating DCAF12L2 thereby blocking the targeting of FAM91A1 by the $CRL^{DCAF12L2}$ complex. Perhaps this could be the reason why we found some phosphorylated peptides of DCAF12L2 in our mass spectrometry data.

MEKK4 is activated by environmental stresses such as osmotic shock, UV irradiation, wound stress, and inflammatory factors (Abell et al., 2007; Abell & Johnson, 2005). Hence, we proposed that the phosphorylation of DCAF12L2 by MEKK4 could serve as sort of an immediate response aimed at preventing FAM91A1 disruption, to foster the stability of the WDR11 complex in an event of sudden cell stress triggered by environmental or intracellular stress such as osmotic shock, UV irradiation, or DNA damage.

In general, in our studies, we found the crosstalk and interplay between phosphorylation and ubiquitylation working to regulate the WDR11 complex in respect to the interaction between the $CRL4^{DCAF12L2}$ complex and its WDR11 complex substrate, such that while the $CRL4^{DCAF12L2}$ complex mediated

ubiquitylation of FAM91A1 leads to the disruption of the WDR11 complex, the phosphorylation of DCAF12L2 in $CRL^{DCAF12L2}$ complex promotes the stability of the WDR11 complex.

Although our studies showed that MEKK4 and WDR11 complex are two independent substrates of the $CRL4^{DCAF12L2}$ complex, the biological significance of $CRL4^{DCAF12L2}$ mediated ubiquitylation of MEKK4 remains unclear. Here we proposed that MEKK4 ubiquitylation might also be involved in vesicular trafficking or could be another way by which the MEKK4 activity is regulated in cells. For comprehensive details on the biological significance of MEKK4 ubiquitylation, we would need to understand the interaction between DCAF12L2 and MEKK4 when MEKK4 activity is stimulated by environmental and intracellular stresses such as osmotic shock, UV irradiation, oxidative stress, or DNA damage (Canovas & Nebreda, 2021; Wagner & Nebreda, 2009).

Also, as demonstrated by Navarro Negredo et al., we might need to perform vesicle tethering assay for comprehensive details on the effect of $CRL4^{DCAF12L2}$ mediated ubiquitylation on the function of the WDR11 complex in vesicular capturing and trafficking. This would help to understand the consequence effect of DCAF12L2 mutations found in cancer on the function of the WDR11 complex in cells.

As stated, the WDR11 is a protein scaffold that facilitates the trafficking and processing of GLI3 in the nucleus, orchestrating the GLI3/EMX1 mediated transcriptional activation of Hh targeted genes (Kim et al., 2018). As a transcription factor, GLI3 must be tightly regulated and if the $CRL4^{DCAF12L2}$ complex binds WDR11 to target GLI3 for degradation as proposed then the mutation of DCAF12L2 as found in human cancer could block the WDR11 mediated proteolytic targeting of GLI3 by the $CRL4^{DCAF12L2}$ complex, which could disrupt the regulation in the expression of the Hh targeted genes leading to overexpression of the targeted gene proteins and cause tumorigenesis.

11. Conclusion and future perspectives

By genomic database analysis, we found that DCAF12L2 is hypermutated in cancer. By affinity purification and mass spectrometry analysis, we identified FAM91A1, C17orf75, WDR11 and MEKK4 as the substrates of DCAF12L2. The hotspots of mutation of DCAF12L2 in cancer are found on sequence positions 334, 335, and 337. The mutations at positions 334 and 335 blocked DCAF12L2 binding to FAM91A1, C17orf75, WDR11, and MEKK4. FAM91A1, C17orf75, and WDR11 formed a stable complex known as the WDR11 complex at the *trans*-Golgi network (TGN). $CRL4^{DCAF12L2}$ complex mediates the ubiquitylation of FAM91A1 which we proposed could be critical in regulating the WDR11 complex.

For more details on the role of $CRL4^{DCAF12L2}$ ubiquitin ligase mediated ubiquitylation on the WDR11 complex, as part of future work, it is important to assess the ubiquitylation of C17orf75 the third component of the WDR11 complex. *In vivo* ubiquitylation assay of $CRL4^{DCAF12L2}$ ubiquitin ligase mediated ubiquitylation of C17orf75 would be performed in HEK293T cells.

Furthermore, thorough studies on $CRL4^{DCAF12L2}$ ubiquitin ligase mediated ubiquitylation is necessary for details understanding of the biological significance of MEKK4 and WDR11 complex ubiquitylation. Here it would be paramount to assess the structure/function of the WDR11 complex when DCAF12L2 mediated ubiquitylation is blocked, this can be done by employing WDR11-knockout cells transduced with lentiviruses to express at physiological level, WDR11 wild type or truncated WDR11 mutant that can't bind to DCAF12L2 to facilitate the $CRL4^{DCAF12L2}$ ubiquitin ligase mediated ubiquitylation of FAM91A1 as shown in our findings. Besides, another approach could also be to study the stability of the WDR11 complex as well as its function in vesicular trafficking when DCAF12L2 mediated ubiquitylation is blocked, by employing FAM91A1-knockout cells transduced with lentiviruses to express at physiological level, FAM91A1 wild type or truncated FAM91A1 mutant that cannot be ubiquitylated by the $CRL4^{DCAF12L2}$ complex. This same approach can also be employed to investigate the role of $CRL4^{DCAF12L2}$ mediated ubiquitylation of MEKK4 found in our studies.

Also, for detailed understanding of the effect of mutation of DCAF12L2 found in cancer and the implication in the pathogenesis of cancer, it's important to assess the effect of DCAF12L2 (P334L), (R335C), and (R335H) mutants in $CRL4^{DCAF12L2}$ complex mediated ubiquitylation. DCAF12L2-knockout cells can be employed and transduced with lentiviruses to express DCAF12L2 wild type or the DCAF12L2 mutants found in cancer (P334L) or (R335C) or (R335H).

Moreover, to investigate the role of DCAF12L2 mediated ubiquitylation in health and the implication in the pathogenesis of cancer, it would be interesting to study the phenotypic changes associated with these mutations. Here we could employ the use of animal mode like the mice or zebrafish, with the zebrafish we can perform microinjection of one-cell stage zebrafish with mRNA encoding wild type DCAF12L2 or the DCAF12L2 (P334L) or (R335C) or (R335H) mutants and study the morphological changes as the embryo develops.

12. Materials and methods

DNA Constructs

Human DCAF12L2 and FBXO24 cDNAs were obtained from Dharmacon (catalog numbers MHS6278-213243600 and MHS6278-202804725 respectively), the cDNAs were PCR amplified and subcloned into pCDNA3 vector containing the FLAG-FLAG-HA-HA tag. The mutated versions of DCAF12L2 (P334L), (R335C) (R335H), (R337C), and (R337H) were obtained by site-directed mutagenesis according to the Invitrogen GENEART Site-Directed Mutagenesis System protocol, using the pCDNA3-FLAG-FLAG-HA-HA-DCAF12L2 wild type construct as template (Life Technologies). The same Site-Directed Mutagenesis System protocol was followed to generate the FBXO24(T65P) mutant using the pCDNA3-FLAG-FLAG-HA-HA-FBXO24 wild type clone construct as template.

Human FAM91A1 and WDR11 cDNAs were also obtained from Dharmacon (catalog numbers MHS6278-213246252 and MHS6278-202806240 respectively), the cDNAs were tagged with HA tag by PCR amplification and subcloned into pCDNA3 vector. Mouse MEKK4alpha wild type and MEKK4alpha kinase-dead (KD) mutant cloned into pCMV5 vectors containing the HA-tag were obtained from Addgene (plasmid #12188 and plasmid #116759 respectively). The truncated version of MEKK4alpha (Δ1596 – 1597) was obtained by site-directed mutagenesis according to the Invitrogen GENEART Site-Directed Mutagenesis System protocol using the pCMV5-MEKK4alpha wild type construct as templates. All plasmids were verified by sequencing.

Cell Culture

Cells were cultured at 37 ^{o}C and 5% CO_2. HEK293T cells were maintained in Dulbecco's modified Eagle's medium (DMEM) (Thermo Fisher Scientific) containing 10% fetal calf serum, 100 U/ml penicillin, and 100 µg/ml streptomycin. Transient DNA transfections were carried out using the polyethyleneimine (PEI) transfection reagent. Cells were treated with the following inhibitors: MG132 (Peptide Institute, 10 µM) and cycloheximide (Sigma-Aldrich, 100 µM).

Identification of DCAF12L2 substrates

HEK293T cells were transfected with pCDNA3-FLAG-FLAG-HA-HA-DCAF12L2, grown for 48 hours. The cells were treated with MG132 for 5 hours before collection. Cells were harvested and subsequently lysed in lysis buffer composed of 50 mM Tris-HCl (pH 7.5), 150 mM NaCl, 1 mM EDTA, and 0.5% NP-40 plus protease and phosphatase inhibitors. We performed double immunoprecipitation to immunopurified DCAF12L2, in the first step, DCAF12L2 was immunopurified with anti-FLAG agarose resin (Roche), incubating for 2 hours on a wheel at 4º C. The beads were washed, and proteins were eluted using RapiGest SF. The eluates were subsequently used in the second immunoprecipitation step with anti-HA incubating overnight on a wheel at 4º C. The final eluates were analysed by mass spectrometry at the Structural and Functional Proteomics platform of the Jacques Monod Institute, University of Paris Diderot.

Identification of FBXO24 substrates

HEK293T cells were transfected with pCDNA3-FLAG-FLAG-HA-HA-FBXO24 wild-type or pCDNA3-FLAG-FLAG-HA-HA-FBXO24 (T65P) mutant and grown for 48 hours. Cells were harvested and subsequently lysed in lysis buffer composed of 50 mM Tris-HCl (pH 7.5), 150 mM NaCl, 1 mM EDTA, and 0.5% NP-40 plus protease and phosphatase inhibitors. Double immunoprecipitation was used to immunopurified FBXO24. In the first step, FBXO24 was immunopurified with anti-FLAG agarose resin (Roche), incubating for 2 hours on a wheel at 4º C. The beads were washed, and proteins were eluted using RapiGest SF. The eluates were subsequently used in the second immunoprecipitation step with anti-HA incubating overnight on a wheel at 4º C. The final eluates were analysed by mass spectrometry at the Structural and Functional Proteomics platform of the Jacques Monod Institute, University of Paris Diderot.

Biochemical methods

Cells were rinsed twice with ice-cold PBS and lysed in Triton-X lysis buffer (50 mM Tris pH 7.5, 250 mM NaCl, 0.1% Triton X-100, 1 mM EDTA, 50 mM NaF,

protease and phosphatase inhibitors) by incubating for 30 minutes on ice, then centrifuged for 20 minutes at 4ºC. For ubiquitylation assay, cells were lysed in RIPA lysis buffer (10mM Tris-HCl, pH 8.0, 1mM EDTA, 0.5mM EGTA, 1% Triton X-100, 0.1% Sodium Deoxycholate, 0.1% SDS 140mM NaCl protease and phosphatase inhibitors).

For immunoprecipitation, the cell extracts were first precleared by incubation with protein A-Sepharose (Thermo Fisher Scientific) for 45 minutes at 4ºC to remove any nonspecific binding to the beads. The precleared extracts were incubated with the indicated primary antibodies for 3 hours at 4ºC this is followed by conjugation with protein G- or protein A-Sepharose beads for 45 minutes. The beads were washed 4 times with lysis buffer and the immunoprecipitated proteins were eluted in 5x Laemmli sample buffer [50mM Tris-HCl, pH 6,8, 2% (w/v) SDS, 5% (v/v), β-mercaptoethanol, 0,1% (w/v) bromophenol blue and 1% (v/v) glycerol]. The immunoprecipitated proteins in 5x Laemmli sample buffer were separated by SDS-polyacrylamide gel electrophoresis (SDS-PAGE) and transferred onto PVDF membranes (Merck-Millipore), followed by immunoblotting with the indicated antibodies.

Antibodies

The following antibodies were used in this study: anti-FAM91A1 rabbit polyclonal (Bethyl Laboratories, A301-588A-T), anti-WDR11 rabbit polyclonal (Bethyl Laboratories, A302-632A-T), anti-MEKK4 rabbit polyclonal (Bethyl Laboratories, A304-277A-T), anti-C17orf75 rabbit polyclonal (Gene Tex, GTX108779), anti-FLAG, rabbit polyclonal (Sigma-Aldrich, F7425), anti-FLAG, mouse monoclonal (Sigma-Aldrich, F7425), anti-HA, mouse monoclonal (Biolegend, 901514), anti-HA, rabbit monoclonal (Cell Signalling Technology, 3724), anti-β-actin, mouse monoclonal (Santa Cruz, sc-69879), anti-MYC, mouse monoclonal (Sigma-Aldrich, M5546).

References

Abell, A. N., Granger, D. A., & Johnson, G. L. (2007). MEKK4 stimulation of p38 and JNK activity is negatively regulated by GSK3beta. *The Journal of Biological Chemistry*, *282*(42), 30476–30484.

Abell, A. N., Granger, D. A., Johnson, N. L., Vincent-Jordan, N., Dibble, C. F., & Johnson, G. L. (2009). Trophoblast stem cell maintenance by fibroblast growth factor 4 requires MEKK4 activation of Jun N-terminal kinase. *Molecular and Cellular Biology*, *29*(10), 2748–2761.

Abell, A. N., & Johnson, G. L. (2005). MEKK4 is an effector of the embryonic TRAF4 for JNK activation. *Journal of Biological Chemistry*, *280*(43), 35793–35796.

Adams, J., Kelso, R., & Cooley, L. (2000). The kelch repeat superfamily of proteins: propellers of cell function. *Trends in Cell Biology*, *10*(1), 17–24.

Bacher, S., Stekman, H., Farah, C. M., Karger, A., Kracht, M., Lienhard Schmitz, M., & Schmitz, M. L. (2021). MEKK1-Dependent Activation of the CRL4 Complex Is Important for DNA Damage-Induced Degradation of p21 and DDB2 and Cell Survival. *Molecular and Cellular Biology Mcb.Asm.Org*, *41*, 81–102.

Bailey, M. H., Meyerson, W. U., Dursi, L. J., Wang, L. B., Dong, G., Liang, W. W., Weerasinghe, A., Li, S., Kelso, S., Akbani, R., Anur, P., Bailey, M. H., Buchanan, A., Chiotti, K., Covington, K., Creason, A., Ding, L., Ellrott, K., Fan, Y., … von Mering, C. (2020). Retrospective evaluation of whole exome and genome mutation calls in 746 cancer samples. *Nature Communications 2020 11:1*, *11*(1), 1–27.

Buetow, L., & Huang, D. T. (2016). Structural insights into the catalysis and regulation of E3 ubiquitin ligases. *Nature Reviews Molecular Cell Biology 2016 17:10*, *17*(10), 626–642.

Canovas, B., & Nebreda, A. R. (2021). Diversity and versatility of p38 kinase signalling in health and disease. *Nature Reviews. Molecular Cell Biology*, *22*(5), 1.

Chakraborty, S., Nagashri, M. N., Mohiyuddin, S. M. A., Gopinath, K. S., & Kumar, A. (2010). Gene expression profiling of oral squamous cell carcinoma by differential display rt-PCR and identification of tumor biomarkers. *Indian Journal of Surgical Oncology*, *1*(4), 284–293.

Chang, B., Partha, S., Hofmann, K., Lei, M., Goebl, M., Harper, J. W., & Elledge, S. J. (1996). SKP1 connects cell cycle regulators to the ubiquitin proteolysis machinery through a novel motif, the F-box. *Cell*, *86*(2), 263–274.

Chen, W., Gao, D., Xie, L., Wang, A., Zhao, H., Guo, C., Sun, Y., Nie, Y., Hong, A., & Xiong, S. (2020). SCF-FBXO24 regulates cell proliferation by mediating ubiquitination and degradation of PRMT6. *Biochemical and Biophysical Research Communications*, *530*(1), 75–81.

Chen, W., Xiong, S., Li, J., Li, X., Liu, Y., Zou, C., & Mallampalli, R. K. (2015). The ubiquitin E3 ligase SCF-FBXO24 recognizes deacetylated nucleoside diphosphate kinase A to enhance its degradation. *Molecular and Cellular Biology*, *35*(6), 1001–1013.

Chen, Y., Shao, X., Cao, J., Zhu, H., Yang, B., He, Q., & Ying, M. (2021). Phosphorylation regulates cullin-based ubiquitination in tumorigenesis. *Acta Pharmaceutica Sinica B*, *11*(2), 309–321.

Chen, Z., Sui, J., Zhang, F., & Zhang, C. (2015). Cullin family proteins and tumorigenesis: Genetic association and molecular mechanisms. *Journal of Cancer*, *6*(3), 233–242.

Chen, Z., Wu, M., & Liu, J. (2020). Kelch-like protein 14 promotes proliferation and migration of ovarian cancer cells. *International Journal of Clinical and Experimental Pathology*, *13*(12), 2950–2961.

Chernova, O. B., Hunyadi, A., Malaj, E., Pan, H., Crooks, C., Roe, B., & Cowell, J. K. (2001). A novel member of the WD-repeat gene family, WDR11, maps to the 10q26 region and is disrupted by a chromosome translocation in human glioblastoma cells. *Oncogene*, *20*(38), 5378–5392.

Choi, J., Phelan, J. D., Wright, G. W., Häupl, B., Huang, D. W., Shaffer, A. L., Young, R. M., Wang, Z., Zhao, H., Yu, X., Oellerich, T., & Staudt, L. M. (2020). Regulation of B cell receptor-dependent NF-κB signaling by the tumor suppressor KLHL14. *Proceedings of the National Academy of Sciences of the United States of America*, *117*(11), 6092–6102.

Ciechanover, A., & Schwartz, A. L. (1998). The ubiquitin-proteasome pathway: The complexity and myriad functions of proteins death. *Proceedings of the National Academy of Sciences*, *95*(6), 2727–2730.

Cui, D., Xiong, X., & Zhao, Y. (2016). Cullin-RING ligases in regulation of autophagy. *Cell Division 2016 11:1*, *11*(1), 1–14.

Dhanoa, B. S., Cogliati, T., Satish, A. G., Bruford, E. A., & Friedman, J. S. (2013). Update on the Kelch-like (KLHL) gene family. *Human Genomics*, *7*(1), 1–7.

Dhiani, B. A., & Mehellou, Y. (2020). The Cul4-DDB1-WDR3/WDR6 Complex Binds SPAK and OSR1 Kinases in a Phosphorylation-Dependent Manner. *Chembiochem : A European Journal of Chemical Biology*, *21*(5), 638–643.

Donner, I., Kiviluoto, T., Ristimäki, A., Aaltonen, L. A., & Vahteristo, P. (2015). Exome sequencing reveals three novel candidate predisposition genes for diffuse gastric cancer. *Familial Cancer*, *14*(2), 241–246.

Duan, S., Cermak, L., Pagan, J. K., Rossi, M., Martinengo, C., di Celle, P. F., Chapuy, B., Shipp, M., Chiarle, R., & Pagano, M. (2012). FBXO11 targets BCL6 for degradation and is inactivated in diffuse large B-cell lymphomas. *Nature*, *481*(7379), 90.

Ebert, S. M., Bullard, S. A., Basisty, N., Marcotte, G. R., Skopec, Z. P., Dierdorff, J. M., Al-Zougbi, A., Tomcheck, K. C., DeLau, A. D., Rathmacher, J. A., Bodine, S. C., Schilling, B., & Adams, C. M. (2020). Activating transcription factor 4 (ATF4) promotes skeletal muscle atrophy by forming a heterodimer with the transcriptional regulator C/EBPβ. *Journal of Biological Chemistry*, *295*(9), 2787–2803.

Fouad, S., Wells, O. S., Hill, M. A., & D'Angiolella, V. (2019). Cullin Ring Ubiquitin Ligases (CRLs) in Cancer: Responses to Ionizing Radiation (IR) Treatment. *Frontiers in Physiology*, *0*, 1144.

Fredholm, S., Litvinov, I. v., Mongan, N. P., Schiele, S., Willerslev-Olsen, A., Petersen, D. L., Krejsgaard, T., Sibbesen, N., Nastasi, C., Bonefeld, C. M., Persson, J. L., Straten, P. T., Andersen, M. H., Koralov, S. B., Wasik, M. M., Geisler, C., Sasseville, D., Woetmann, A., & Ødum, N. (2016). The Expression of IL-21 Is Promoted by MEKK4 in Malignant T Cells and Associated with Increased Progression Risk in Cutaneous T-Cell Lymphoma. *Journal of Investigative Dermatology*, *136*(4), 866–869.

Frescas, D., & Pagano, M. (2008). Deregulated proteolysis by the F-box proteins SKP2 and β-TrCP: tipping the scales of cancer. *Nature Reviews Cancer 2008 8:6*, *8*(6), 438–449.

Fujita, H., Iwabu, Y., Tokunaga, K., & Tanaka, Y. (2013). Membrane-associated RING-CH (MARCH) 8 mediates the ubiquitination and lysosomal degradation of the transferrin receptor. *Journal of Cell Science*.

Furukawa, M., & Xiong, Y. (2005). BTB Protein Keap1 Targets Antioxidant Transcription Factor Nrf2 for Ubiquitination by the Cullin 3-Roc1 Ligase. *Molecular and Cellular Biology*, *25*(1), 162–171.

Gerwins, P., Blank, J. L., & Johnson, G. L. (1997). Cloning of a novel mitogen-activated protein kinase kinase kinase, MEKK4, that selectively regulates the c-Jun amino terminal kinase pathway. *The Journal of Biological Chemistry*, *272*(13), 8288–8295.

Giles, L. M., Li, L., & Chin, L. S. (2009). Printor, a novel torsinA-interacting protein implicated in dystonia pathogenesis. *The Journal of Biological Chemistry*, *284*(32), 21765–21775.

Granata, A., & Warner, T. T. (2010). The role of torsinA in dystonia. *European Journal of Neurology*, *17 Suppl 1*(SUPPL. 1), 81–87.

Haglund, K., & Dikic, I. (2005). Ubiquitylation and cell signaling. *The EMBO Journal*, *24*(19), 3353.

He, Y. J., McCall, C. M., Hu, J., Zeng, Y., & Xiong, Y. (2006). DDB1 functions as a linker to recruit receptor WD40 proteins to CUL4–ROC1 ubiquitin ligases. *Genes & Development*, *20*(21), 2949.

Hershko, A., & Ciechanover, A. (1998). THE UBIQUITIN SYSTEM. *Annual Review of Biochemistry*, *67*(1), 425–479.

Hershko, A., & Ciechanover, A. (2003). THE UBIQUITIN SYSTEM. *Https://Doi.Org/10.1146/Annurev.Biochem.67.1.425*, *67*, 425–479.

HL, H., WL, Z., R, Z., B, Z., & WL, M. (2010). FBXO31 is down regulated and may function as a tumor suppressor in hepatocellular carcinoma. *Oncology Reports*, *24*(3).

Ho, M. S., Tsai, P. I., & Chien, C. T. (2006). F-box proteins: the key to protein degradation. *Journal of Biomedical Science*, *13*(2), 181–191.

Hoadley, K. A., Yau, C., Hinoue, T., Wolf, D. M., Lazar, A. J., Drill, E., Shen, R., Taylor, A. M., Cherniack, A. D., Thorsson, V., Akbani, R., Bowlby, R., Wong, C. K., Wiznerowicz, M., Sanchez-Vega, F., Robertson, A. G., Schneider, B. G., Lawrence, M. S., Noushmehr, H., Laird, P. W. (2018). Cell-of-Origin Patterns Dominate the Molecular Classification of 10,000 Tumors from 33 Types of Cancer. *Cell*, *173*(2), 291-304.e6.

Hu, H., & Sun, S.-C. (2016). Ubiquitin signaling in immune responses. *Cell Research 2016 26:4*, *26*(4), 457–483.

Huang, H.-L., Zheng, W.-L., Zhao, R., Zhang, B., & Ma, W.-L. (2010). FBXO31 is down-regulated and may function as a tumor suppressor in hepatocellular carcinoma. *Oncology Reports*, *24*(3), 715–720.

Hunter, T. (2007). The Age of Crosstalk: Phosphorylation, Ubiquitination, and Beyond. *Molecular Cell*, *28*(5), 730–738.

Jackson, S., & Xiong, Y. (2009). CRL4s: the CUL4-RING E3 ubiquitin ligases. *Trends in Biochemical Sciences*, *34*(11), 562–570.

Jönsson, G., Staaf, J., Olsson, E., Heidenblad, M., Vallon-Christersson, J., Osoegawa, K., de Jong, P., Oredsson, S., Ringnér, M., Höglund, M., & Borg, Å. (2007). High-resolution genomic profiles of breast cancer cell lines assessed by tiling BAC array comparative genomic hybridization. *Genes, Chromosomes and Cancer*, *46*(6), 543–558.

Katoh, M., & Katoh, M. (2003). Recombination cluster around FGFR2-WDR11-HTPAPL locus on human chromosome 10q26. *International Journal of Molecular Medicine*, *11*(5), 579–583.

Kim, H. G., Ahn, J. W., Kurth, I., Ullmann, R., Kim, H. T., Kulharya, A., Ha, K. S., Itokawa, Y., Meliciani, I., Wenzel, W., Lee, D., Rosenberger, G., Ozata, M., Bick, D. P., Sherins, R. J., Nagase, T., Tekin, M., Kim, S. H., Kim, C. H., … Layman, L. C. (2010). WDR11, a WD protein that interacts with transcription factor EMX1, is mutated in idiopathic hypogonadotropic hypogonadism and Kallmann syndrome. *American Journal of Human Genetics*, *87*(4), 465–479.

Kim, Y., Osborn, D. P., Lee, J., Araki, M., Araki, K., Mohun, T., Känsäkoski, J., Brandstack, N., Kim, H., Miralles, F., Kim, C., Brown, N. A., Kim, H., Martinez-Barbera, J. P., Ataliotis, P., Raivio, T., Layman, L. C., & Kim, S. (2018). WDR11-mediated Hedgehog signalling defects underlie a new ciliopathy related to Kallmann syndrome. *EMBO Reports*, *19*(2), 269–289.

Kipreos, E. T., & Pagano, M. (2000). The F-box protein family. *Genome Biology*, *1*(5), XIX–XX.

Kobayashi, A., Kang, M.-I., Okawa, H., Ohtsuji, M., Zenke, Y., Chiba, T., Igarashi, K., & Yamamoto, M. (2004). Oxidative Stress Sensor Keap1 Functions as an Adaptor for Cul3-Based E3 Ligase To Regulate Proteasomal Degradation of Nrf2. *Molecular and Cellular Biology*, *24*(16), 7130.

Koboldt, D. C., Zhang, Q., Larson, D. E., Shen, D., McLellan, M. D., Lin, L., Miller, C. A., Mardis, E. R., Ding, L., & Wilson, R. K. (2012). VarScan 2: Somatic mutation and copy number alteration discovery in cancer by exome sequencing. *Genome Res.*, *22*(3), 568–576.

Koepp, D. M., Schaefer, L. K., Ye, X., Keyomarsi, K., Chu, C., Harper, J. W., & Elledge, S. J. (2001). Phosphorylation-dependent ubiquitination of cyclin E by the SCFFbw7 ubiquitin ligase. *Science (New York, N.Y.)*, *294*(5540), 173–177.

Komander, D., & Rape, M. (2012). The ubiquitin code. *Annual Review of Biochemistry*, *81*, 203–229.

Koren, I., Timms, R. T., Kula, T., Xu, Q., Li, M. Z., & Elledge, S. J. (2018). The Eukaryotic Proteome Is Shaped by E3 Ubiquitin Ligases Targeting C-Terminal Degrons. *Cell*, *173*(7), 1622-1635.e14.

Krek, W. (2003). BTB proteins as henchmen of Cul3-based ubiquitin ligases. *Nature Cell Biology 2003 5:11*, *5*(11), 950–951.

Kumar, R., Neilsen, P. M., Crawford, J., McKirdy, R., Lee, J., Powell, J. A., Saif, Z., Martin, J. M., Lombaerts, M., Cornelisse, C. J., Cleton-Jansen, A. M., & Callen, D. F. (2005). FBXO31 is the chromosome 16q24.3 senescence gene, a candidate breast tumor suppressor, and a component of an SCF complex. *Cancer Research*, *65*(24), 11304–11313.

Lee, J., & Zhou, P. (2007). DCAFs, the Missing Link of the CUL4-DDB1 Ubiquitin Ligase. *Molecular Cell*, *26*(6), 775–780.

Lemmon, M. A., & Schlessinger, J. (2010). Cell signaling by receptor tyrosine kinases. *Cell*, *141*(7), 1117–1134.

Leth-Larsen, R., Lund, R., Hansen, H. v., Laenkholm, A. V., Tarin, D., Jensen, O. N., & Ditzel, H. J. (2009). Metastasis-related Plasma Membrane Proteins of Human Breast Cancer Cells Identified by Comparative Quantitative Mass Spectrometry. *Molecular & Cellular Proteomics : MCP*, *8*(6), 1436.

Li, S., Liu, J., Min, Q., Ikawa, T., Yasuda, S., Yang, Y., Wang, Y. Q., Tsubata, T., Zhao, Y., & Wang, J. Y. (2018). Kelch-like protein 14 promotes B-1a but suppresses B-1b cell development. *International Immunology*, *30*(7), 311–318.

Lin, C. Y., Lee, C. H., Chuang, Y. H., Lee, J. Y., Chiu, Y. Y., Wu Lee, Y. H., Jong, Y. J., Hwang, J. K., Huang, S. H., Chen, L. C., Wu, C. H., Tu, S. H., Ho, Y. S., & Yang, J. M. (2019). Membrane protein-regulated networks across human cancers. *Nature Communications 2019 10:1*, *10*(1), 1–17.

Lin, Z., Li, S., Feng, C., Yang, S., Wang, H., Ma, D., Zhang, J., Gou, M., Bu, D., Zhang, T., Kong, X., Wang, X., Sarig, O., Ren, Y., Dai, L., Liu, H., Zhang, J., Li, F., Hu, Y., … Tan, X. (2016). Stabilizing mutations of KLHL24 ubiquitin ligase cause loss of keratin 14 and human skin fragility. *Nature Genetics*, *48*(12), 1504–1516.

Liu, C., Liu, W., Ye, Y., & Li, W. (2017). Ufd2p synthesizes branched ubiquitin chains to promote the degradation of substrates modified with atypical chains. *Nature Communications 2017 8:1*, *8*(1), 1–15.

Metzger, M. B., Hristova, V. A., & Weissman, A. M. (2012). HECT and RING finger families of E3 ubiquitin ligases at a glance. *Journal of Cell Science*, *125*(Pt 3), 531–537.

Meyer, H. J., & Rape, M. (2014). Enhanced protein degradation by branched ubiquitin chains. *Cell*, *157*(4), 910–921.

Meyer-Schaller, N., Chou, Y. C., Sumara, I., Martin, D. D. O., Kurz, T., Katheder, N., Hofmann, K., Berthiaume, L. G., Sicheri, F., & Peter, M. (2009). The human Dcn1-like protein DCNL3 promotes Cul3 neddylation at membranes. *Proceedings of the National Academy of Sciences of the United States of America*, *106*(30), 12365–12370.

Meyer-Schwesinger, C. (2019). The ubiquitin–proteasome system in kidney physiology and disease. *Nature Reviews Nephrology 2019 15:7*, *15*(7), 393–411.

Mita, H., Tsutsui, J., Takekawa, M., Witten, E. A., & Saito, H. (2002). Regulation of MTK1/MEKK4 Kinase Activity by Its N-Terminal Autoinhibitory Domain and GADD45 Binding. *Molecular and Cellular Biology*, *22*(13), 4544.

Nakagawa, T., Nakayama, K., & Nakayama, K. I. (2020). Knockout Mouse Models Provide Insight into the Biological Functions of CRL1 Components. *Advances in Experimental Medicine and Biology*, *1217*, 147–171.

Nakayama, K., Nagahama, H., Minamishima, Y. A., Miyake, S., Ishida, N., Hatakeyama, S., Kitagawa, M., Iemura, S. ichiro, Natsume, T., & Nakayama, K. I. (2004). Skp2-mediated degradation of p27 regulates progression into mitosis. *Developmental Cell*, *6*(5), 661–672.

Navarro Negredo, P., Edgar, J. R., Manna, P. T., Antrobus, R., & Robinson, M. S. (2018). The WDR11 complex facilitates the tethering of AP-1-derived vesicles. *Nature Communications*, *9*(1).

Neocleous, V., Fanis, P., Toumba, M., Tanteles, G. A., Schiza, M., Cinarli, F., Nicolaides, N. C., Oulas, A., Spyrou, G. M., Mantzoros, C. S., Vlachakis, D., Skordis, N., & Phylactou, L. A. (2020). GnRH Deficient Patients with Congenital Hypogonadotropic Hypogonadism: Novel Genetic Findings in ANOS1, RNF216, WDR11, FGFR1, CHD7, and POLR3A Genes in a Case Series and Review of the Literature. *Frontiers in Endocrinology*, *11*, 626.

Ni, Z., He, J., Wu, Y., Hu, C., Dai, X., Yan, X., Li, B., Li, X., Xiong, H., Li, Y., Li, S., Xu, L., Li, Y., Lian, J., & He, F. (2018). AKT-mediated phosphorylation of ATG4B impairs mitochondrial activity and enhances the Warburg effect in hepatocellular carcinoma cells. *Autophagy*, *14*(4), 685–701.

Nishi, H., Hashimoto, K., & Panchenko, A. R. (2011). Phosphorylation in protein-protein binding: effect on stability and function. *Structure (London, England : 1993)*, *19*(12), 1807.

Petroski, M. D., & Deshaies, R. J. (2005). Function and regulation of cullin–RING ubiquitin ligases. *Nature Reviews Molecular Cell Biology 2005 6:1*, *6*(1), 9–20.

Pickart, C. M., & Eddins, M. J. (2004). Ubiquitin: structures, functions, mechanisms. *Biochimica et Biophysica Acta*, *1695*(1–3), 55–72.

Ohtake, F., Tsuchiya, H., Saeki, Y., & Tanaka, K. (2018). K63 ubiquitylation triggers proteasomal degradation by seeding branched ubiquitin chains. *Proceedings of the National Academy of Sciences*, *115*(7), E1401–E1408.

Petroski, M. D., & Deshaies, R. J. (2005). Function and regulation of cullin–RING ubiquitin ligases. *Nature Reviews Molecular Cell Biology 2005 6:1*, *6*(1), 9–20.

Pickart, C. M., & Eddins, M. J. (2004). Ubiquitin: structures, functions, mechanisms. *Biochimica et Biophysica Acta*, *1695*(1–3), 55–72.

Pontrelli, P., Conserva, F., & Gesualdo, L. (2019). The Role of Lysine 63-Linked Ubiquitylation in Health and Disease. *Ubiquitin Proteasome System - Current Insights into Mechanism Cellular Regulation and Disease*.

Qian, H., Zhang, Y., Wu, B., Wu, S., You, S., Zhang, N., & Sun, Y. (2020). Structure and Function of HECT E3 Ubiquitin Ligases and their Role in Oxidative Stress. *Journal of Translational Internal Medicine*, *8*(2), 71.

Sarikas, A., Hartmann, T., & Pan, Z. Q. (2011). The cullin protein family. *Genome Biology*, *12*(4), 1–12.

Schmitz, R., Wright, G. W., Huang, D. W., Johnson, C. A., Phelan, J. D., Wang, J. Q., Roulland, S., Kasbekar, M., Young, R. M., Shaffer, A. L., Hodson, D. J., Xiao, W., Yu, X., Yang, Y., Zhao, H., Xu, W., Liu, X., Zhou, B., Du, W., … Staudt, L. M. (2018). Genetics and Pathogenesis of Diffuse Large B-Cell Lymphoma. *New England Journal of Medicine*, *378*(15), 1396–1407.

Sollome, J. J., Thavathiru, E., Camenisch, T. D., & Vaillancourt, R. R. (2014). HER2/HER3 regulates extracellular acidification and cell migration through MTK1 (MEKK4). *Cellular Signalling*, *26*(1), 70–82.

Stevens, M. v., Parker, P., Vaillancourt, R. R., & Camenisch, T. D. (2006). MEKK4 regulates developmental EMT in the embryonic heart. *Developmental Dynamics : An Official Publication of the American Association of Anatomists*, *235*(10), 2761–2770.

Stogios, P. J., Downs, G. S., Jauhal, J. J. S., Nandra, S. K., & Privé, G. G. (2005). Sequence and structural analysis of BTB domain proteins. *Genome Biology*, *6*(10), 1–18.

Strohmaier, H., Spruck, C. H., Kaiser, P., Won, K. A., Sangfelt, O., & Reed, S. I. (2001). Human F-box protein hCdc4 targets cyclin E for proteolysis and is mutated in a breast cancer cell line. *Nature*, *413*(6853), 316–322.

Sun, L., & Chen, Z. J. (2004). The novel functions of ubiquitination in signaling. *Current Opinion in Cell Biology*, *16*(2), 119–126.

Sutani, A., Shima, H., Hijikata, A., Hosokawa, S., Katoh-Fukui, Y., Takasawa, K., Suzuki, E., Doi, S., Shirai, T., Morio, T., Fukami, M., & Kashimada, K. (2020). WDR11 is another causative gene for coloboma, cardiac anomaly and growth retardation in 10q26 deletion syndrome. *European Journal of Medical Genetics*, *63*(1), 103626.

Szcześniak, M. W., Ciomborowska, J., Nowak, W., Rogozin, I. B., & Makałowska, I. (2011). Primate and Rodent Specific Intron Gains and the Origin of Retrogenes with Splice Variants. *Molecular Biology and Evolution*, *28*(1), 33.

Taylor, K. E., & Mossman, K. L. (2015). Cellular Protein WDR11 Interacts with Specific Herpes Simplex Virus Proteins at the trans-Golgi Network To Promote Virus Replication. *Journal of Virology*, *89*(19), 9841.

Wagner, E. F., & Nebreda, Á. R. (2009). Signal integration by JNK and p38 MAPK pathways in cancer development. *Nature Reviews Cancer*, *9*(8), 537–549.

Wang, Y., Zhang, P., Liu, Z., Wang, Q., Wen, M., Wang, Y., Yuan, H., Mao, J. H., & Wei, G. (2014). CUL4A overexpression enhances lung tumor growth and sensitizes lung cancer cells to Erlotinib via transcriptional regulation of EGFR. *Molecular Cancer*, *13*(1), 1–13.

Wang, Z., Liu, P., Inuzuka, H., & Wei, W. (2014). Roles of F-box proteins in cancer. *Nature Reviews. Cancer*, *14*(4), 233.

Welcker, M., & Clurman, B. E. (2008). FBW7 ubiquitin ligase: a tumour suppressor at the crossroads of cell division, growth, and differentiation. *Nature Reviews Cancer 2008 8:2*, *8*(2), 83–93.

Weller, C. E., Pilkerton, M. E., & Chatterjee, C. (2014). Chemical strategies to understand the language of ubiquitin signaling. *Biopolymers*, *101*(2), 144.

Whitmarsh, A. J., & Davis, R. J. (2007). Role of mitogen-activated protein kinase kinase 4 in cancer. *Oncogene 2007 26:22*, *26*(22), 3172–3184.

Winston, J. T., Koepp, D. M., Cihui, Z., Elledge, S. J., & Harper, J. W. (1999). A family of mammalian F-box proteins. *Current Biology*, *9*(20), 1180-S3.

Xiang, S., Shi, X., Chen, P., Chen, Y., Bing, S., Jin, X., Cao, J., Wang, J., Yang, B., Shao, X., He, Q., & Ying, M. (2021). Targeting Cul3-scaffold E3 ligase complex via KLHL substrate adaptors for cancer therapy. *Pharmacological Research*, *169*, 105616.

Xu, C., & Min, J. (2011). Structure and function of WD40 domain proteins. *Protein & Cell*, *2*(3), 202.

Yau, R., & Rape, M. (2016). The increasing complexity of the ubiquitin code. *Nature Cell Biology 2016 18:6*, *18*(6), 579–586.

Ying, M., Shao, X., Jing, H., Liu, Y., Qi, X., Cao, J., Chen, Y., Xiang, S., Song, H., Hu, R., Wei, G., Yang, B., & He, Q. (2018). Ubiquitin-dependent degradation of CDK2 drives the therapeutic differentiation of AML by targeting PRDX2. *Blood*, *131*(24), 2698–2711.

Young, R. M., Phelan, J. D., Shaffer, A. L., Wright, G. W., Huang, D. W., Schmitz, R., Johnson, C., Oellerich, T., Wilson, W., & Staudt, L. M. (2019). Taming the Heterogeneity of Aggressive Lymphomas for Precision Therapy. *Https://Doi.Org/10.1146/Annurev-Cancerbio-030518-055734*, *3*(1), 429–455.

Zhang, J., Zhou, Y., Dai, Q. S., Zhu, S. C., Han, Y. H., Han, H. L., Zhao, B., Gao, R. R., & Zhang, J. (2016). AK048794 maintains the mouse embryonic stem cell pluripotency by functioning as an miRNA sponge for miR-592. *The Biochemical Journal*, *473*(20), 3639–3654.

Zheng, N., Schulman, B. A., Song, L., Miller, J. J., Jeffrey, P. D., Wang, P., Chu, C., Koepp, D. M., Elledge, S. J., Pagano, M., Conaway, R. C., Conaway, J. W., Harper, J. W., & Pavletich, N. P. (2002a). Structure of the Cul1-Rbx1-Skp1-F boxSkp2 SCF ubiquitin ligase complex. *Nature*, *416*(6882), 703–709.

Zheng, N., Schulman, B. A., Song, L., Miller, J. J., Jeffrey, P. D., Wang, P., Chu, C., Koepp, D. M., Elledge, S. J., Pagano, M., Conaway, R. C., Conaway, J. W., Harper, J. W., & Pavletich, N. P. (2002b). Structure of the Cul1–Rbx1–Skp1–F boxSkp2 SCF ubiquitin ligase complex. *Nature 2002 416:6882*, *416*(6882), 703–709.

Zhou, Z., Song, X., Wavelet, C. M., & Wan, Y. (2020). Cullin 4-DCAF Proteins in Tumorigenesis. *Advances in Experimental Medicine and Biology*, *1217*, 241–259.

Study II

Publication

Ubiquitylation of the ER-Shaping Protein Lunapark via the $CRL3^{KLHL12}$ Ubiquitin Ligase Complex. Laurensia Yuniati, Angela Lauriola, Manouk Gerritsen, Susana Abreu, Eric Ni, Chiara Tesoriero, Jacob O. Onireti, Teck Yew Low, Albert J.R. Heck, Andrea Vettori, Timothy Cardozo, and Daniele Guardavaccaro. *Cell Reports.* **31**, 107664 (2020)

Cell Reports

Article

Ubiquitylation of the ER-Shaping Protein Lunapark via the CRL3^{KLHL12} Ubiquitin Ligase Complex

Graphical Abstract

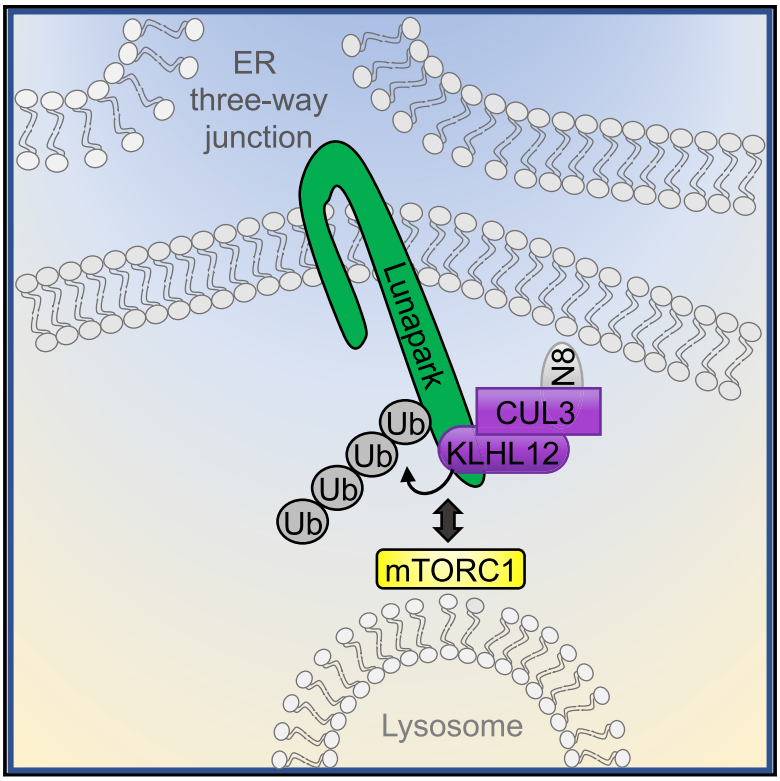

Authors

Laurensia Yuniati, Angela Lauriola, Manouk Gerritsen, ..., Andrea Vettori, Timothy Cardozo, Daniele Guardavaccaro

Correspondence

daniele.guardavaccaro@univr.it

In Brief

Yuniati et al. perform a proteomic screen to identify E3 substrates that are ubiquitylated at cellular membranes and find that the ER-shaping protein Lunapark is ubiquitylated by the CRL3^{KLHL12} ubiquitin ligase. They show that Lunapark binds mTORC1 and affects its activity, and defects in Lunapark ubiquitylation lead to neurodevelopmental defects.

Highlights

- A proteomic approach to identify CRL substrates ubiquitylated at cellular membranes
- The ER shaping protein Lunapark is ubiquitylated by the CRL3^{KLHL12} ubiquitin ligase
- Lunapark binds mTOR and its ubiquitylation affects lysosomal recruitment of mTORC1
- Inhibition of Lunapark ubiquitylation leads to neurodevelopmental defects

Yuniati et al., 2020, Cell Reports *31*, 107664
May 19, 2020
https://doi.org/10.1016/j.celrep.2020.107664

CellPress

Cell Reports

CellPress
OPEN ACCESS

Article

Ubiquitylation of the ER-Shaping Protein Lunapark via the CRL3^{KLHL12} Ubiquitin Ligase Complex

Laurensia Yuniati,[1,7] Angela Lauriola,[2,7] Manouk Gerritsen,[1] Susana Abreu,[1] Eric Ni,[3] Chiara Tesoriero,[2] Jacob O. Onireti,[2] Teck Yew Low,[4] Albert J.R. Heck,[5,6] Andrea Vettori,[2] Timothy Cardozo,[3] and Daniele Guardavaccaro[1,2,8,*]

[1]Hubrecht Institute-KNAW and University Medical Center Utrecht, 3584 CT Utrecht, the Netherlands
[2]Department of Biotechnology, University of Verona, 37134 Verona, Italy
[3]Department of Biochemistry and Molecular Pharmacology, New York University School of Medicine, NYU Langone Health, New York, NY 10016, USA
[4]UKM Medical Molecular Biology Institute (UMBI), Universiti Kebangsaan Malaysia, 56000 Kuala Lumpur, Malaysia
[5]Biomolecular Mass Spectrometry and Proteomics, Bijvoet Center for Biomolecular Research and Utrecht Institute for Pharmaceutical Sciences, Utrecht University, 3584 CH Utrecht, the Netherlands
[6]The Netherlands Proteomics Center, 3584 CH Utrecht, the Netherlands
[7]These authors contributed equally
[8]Lead Contact
*Correspondence: daniele.guardavaccaro@univr.it
https://doi.org/10.1016/j.celrep.2020.107664

SUMMARY

Cullin-RING ligases (CRLs) control key cellular processes by promoting ubiquitylation of a multitude of soluble cytosolic and nuclear proteins. Subsets of CRL complexes are recruited and activated locally at cellular membranes; however, few CRL functions and substrates at these distinct cellular compartments are known. Here, we use a proteomic screen to identify proteins that are ubiquitylated at cellular membranes and found that Lunapark, an endoplasmic reticulum (ER)-shaping protein localized to ER three-way junctions, is ubiquitylated by the CRL3^{KLHL12} ubiquitin ligase. We demonstrate that Lunapark interacts with mechanistic target of rapamycin complex-1 (mTORC1), a central cellular regulator that coordinates growth and metabolism with environmental conditions. We show that mTORC1 binds Lunapark specifically at three-way junctions, and lysosomes, where mTORC1 is activated, make contact with three-way junctions where Lunapark resides. Inhibition of Lunapark ubiquitylation results in neurodevelopmental defects indicating that KLHL12-dependent ubiquitylation of Lunapark is required for normal growth and development.

INTRODUCTION

Cullin-RING ligases (CRLs), the largest class of modular E3 ubiquitin ligases, control essential cellular processes by targeting protein substrates for ubiquitylation (Petroski and Deshaies, 2005). CRLs are composed of a cullin scaffold, a RING-finger protein (RBX1 or RBX2), an adaptor protein, and one of many substrate-receptor subunits. CRL activity is promoted by the reversible conjugation of the ubiquitin-like protein NEDD8 to the cullin subunit (Scott et al., 2014). Like ubiquitylation, neddylation of substrates is achieved by an enzymatic cascade. NEDD8 is first activated by specific E1 and E2 enzymes and then conjugated by E3 enzymes to a lysine residue of the cullin target through an isopeptide bond (Lydeard et al., 2013). A "dual E3" mechanism has been proposed for cullin neddylation, where one E3, RBX1, works as a typical E3 by recruiting both the cullin substrate and the E2-NEDD8 intermediate triggering NEDD8 ligation, and a second E3, termed co-E3, facilitates this process (Lydeard et al., 2013; Scott et al., 2010, 2011). This auxiliary scaffold-like co-E3 function is played by defective in Cul neddylation protein (DCN) in yeast and DCNL1 to DCNL5 in humans (DCN-like proteins). DCN and DCN-like proteins interact with the cullin subunit nearby its neddylation site as well as the acetylated N terminus of the E2 enzyme (UBC12) structurally constraining the RBX1-UBC12-NEDD8 complex to orientations that increase the kinetic efficiency of the NEDD8 conjugation to the right lysine residue (Kurz et al., 2005, 2008; Monda et al., 2013). Notably, one DCNL protein, DCNL3, has been shown to be localized to cellular membranes through an N-terminal lipid-modified motif (Keuss et al., 2016; Meyer-Schaller et al., 2009). Membrane-bound DCNL3 recruits CRLs to membranes where it contributes to their neddylation (Keuss et al., 2016; Meyer-Schaller et al., 2009).

The endoplasmic reticulum (ER), the largest membrane-bound organelle in eukaryotes, is a contiguous structure that extends from the nuclear envelope to the plasma membrane (Chen et al., 2013; Friedman and Voeltz, 2011; Phillips and Voeltz, 2016). The ER is composed of two main structural units, namely flat cisternal sheets and reticulated tubules. Whereas the cisternae are connected to the nuclear envelope and are localized mostly to the perinuclear region, the tubules form a polygonal network that extends throughout the cytoplasm. This polygonal array is highly dynamic as it undergoes rapid and constant reorganizations such as tubule extension and retraction, branching,

sliding, ring closure, and tubule-tubule fusion. Key elements of the ER tubule network are three-way junctions, mobile ER intersections generated by the fusion of one ER tubule tip with the side of another tubule. Lunapark, a recently identified factor implicated in ER morphology, is an evolutionarily conserved transmembrane protein that specifically localizes to ER three-way junctions. Although Lunapark is thought to stabilize these junctions and inhibit ring closure (Chen et al., 2012, 2015; Wang et al., 2016), its function and regulation are still poorly understood.

Mechanistic target of rapamycin complex 1 (mTORC1) is an evolutionarily conserved serine-threonine protein kinase complex that controls metabolic processes underlying the growth of cells, tissues, and organs (Saxton and Sabatini, 2017). In response to favorable internal and external cues, mTORC1 is activated to promote anabolic processes such as protein, lipid, and nucleotide synthesis, and inhibit catabolic processes like autophagy. Two independent conditions have to be achieved to activate mTORC1. First, mTORC1 has to transiently translocate to the lysosomal membrane in response to amino acids, a process promoted by the direct binding of activated Rag GTPases to Raptor, which forms a stoichiometric complex with mTOR and associates with the mTOR substrates eukaryotic initiation factor 4E-binding protein-1 and ribosomal protein S6 kinase (Kim et al., 2008; Manifava et al., 2016; Sancak et al., 2008; Sekiguchi et al., 2001). Second, lysosome-localized mTORC1 has to interact with Ras homolog enriched in brain (Rheb), a small GTPase that is activated in response to growth factors. Thus, the lysosome represents the cellular hub where the amino acid- and growth factor-sensing machineries intersect to activate mTORC1.

In this study, we have carried out a screen aimed at the identification of CRL substrates that are specifically ubiquitylated at cellular membranes. We specifically focused on CRL3 complexes, members of a subclass of Cullin-RING ubiquitin ligases composed of the cullin scaffold Cul3 and a broad-complex, tramtrack, and bric-a-brac (BTB) protein as a substrate receptor subunit. Using this screen, we identified the ER-shaping protein Lunapark as a substrate of $CRL3^{KLHL12}$, a ubiquitin ligase complex containing the BTB protein kelch like family member 12 (KLHL12) as substrate receptor (Angers et al., 2006; Jin et al., 2012; Rondou et al., 2008). To investigate the biological function of Lunapark ubiquitylation, we have expressed a ubiquitylation-resistant Lunapark mutant in cultured cells as well as in zebrafish embryos. The results of these studies are herein presented.

RESULTS

A Proteomic Approach for the Identification of CRL Substrates that Are Ubiquitylated at Cellular Membranes

To systematically identify targets of the CRL3 ubiquitin ligase complexes that are ubiquitylated locally at cellular membranes, we performed affinity-purification and mass spectrometry analysis of CUL3 variants bearing, at their N termini, the lipid-modified motif (N11) of DCNL3, a co-E3 that contributes to the neddylation of CRL complexes at membranes (Keuss et al., 2016; Kurz et al., 2005, 2008; Meyer-Schaller et al., 2009; Monda et al., 2013; Scott et al., 2010, 2011). A schematic representation of the experimental design is shown in Figure 1A. The presence of the lipid-modified motif of DCNL3 at the N terminus of CUL3 is sufficient to stably recruit CUL3 to the plasma membrane and endomembranes (Figures 1B and S1) (Meyer-Schaller et al., 2009). To increase the stability of the CUL3-BTB protein-substrate complexes, the lipid-modified motif (N11) of DCNL3 was fused to two CUL3 mutants encoding the first 199 or 225 N-terminal amino acid residues (CUL3-N199 and CUL3-N225, respectively), which are unable to interact with RBX1. We expressed FLAG-tagged N11-CUL3-N199 or N11-CUL3-N225 as well as FLAG-tagged CUL3-N199 or CUL3-N225 without the lipid-modified motif (N11) in HEK293T cells and purified CUL3 immunoprecipitates, which were then analyzed by mass spectrometry. In addition to 51 BTB proteins and the RING-finger protein RBX1 (Figure 1C), which are known to directly bind CUL3 within the CRL3 complex, and various components of the CSN complex that play a regulatory role (not shown), we recovered numerous CRL3 candidate substrates. At least three of them (i.e., GBB1, GBB2, and ACLY) are known CRL3 targets (Bertocci et al., 2017; Brockmann et al., 2017; Zhang et al., 2016). Among the top 21 hits that were enriched in the pull-down of membrane-bound CUL3 (Figure 1D), 19 proteins are (1) described multi-pass or single-pass membrane proteins, (2) reported to contain putative transmembrane domains, or (3) found associated to the plasma membrane or membranes of various cellular organelles (The UniProt Consortium, 2017).

Lunapark Is Ubiquitylated by the $CRL3^{KLHL12}$ Ubiquitin Ligase Complex

Among the proteins found enriched in the affinity purification of membrane-bound CUL3 mutants (N11-CUL3-N199 or N11-CUL3-N225), we recovered Lunapark (Figure 1D; Tables S1 and S2), an evolutionarily conserved integral membrane protein involved in network formation of the ER (Chen et al., 2012, 2015; Goyal and Blackstone, 2013; Moriya et al., 2013; Shemesh et al., 2014; Wang et al., 2016). The interaction between N11-CUL3-N225 and endogenous Lunapark was confirmed by immunoprecipitation followed by immunoblotting (Figure 2A).

If Lunapark is a substrate of a CRL3 ubiquitin ligase, a specific BTB protein is expected to bind it and recruit it to CUL3 and the rest of the CRL3 complex. To identify the BTB protein that interacts with Lunapark, we immunopurified FLAG-tagged Lunapark from HEK293T cells. Mass spectrometry analysis of immunoprecipitated Lunapark identified the BTB protein KLHL12 as well as the CRL subunits RBX1 and CUL3 (Figure 2B) (Angers et al., 2006; Jin et al., 2012; Rondou et al., 2008). KLHL12 was the only BTB protein (out of the 169 BTB proteins encoded by the human genome) recovered in the affinity purification of FLAG-tagged Lunapark. The KLHL12-Lunapark interaction was confirmed by immunoprecipitation followed by immunoblotting (Figure 2C). Other BTB proteins, namely KLHL18, KCTD11, and SPOP/BTBD32, did not coimmunoprecipitate with endogenous Lunapark (Figure 2D). A complex with endogenous Lunapark and KLHL12 was also observed (Figure 2E). These results suggest that the $CRL3^{KLHL12}$ ubiquitin ligase mediates Lunapark ubiquitylation. To test this hypothesis, we examined whether ectopic expression of KLHL12 stimulates Lunapark

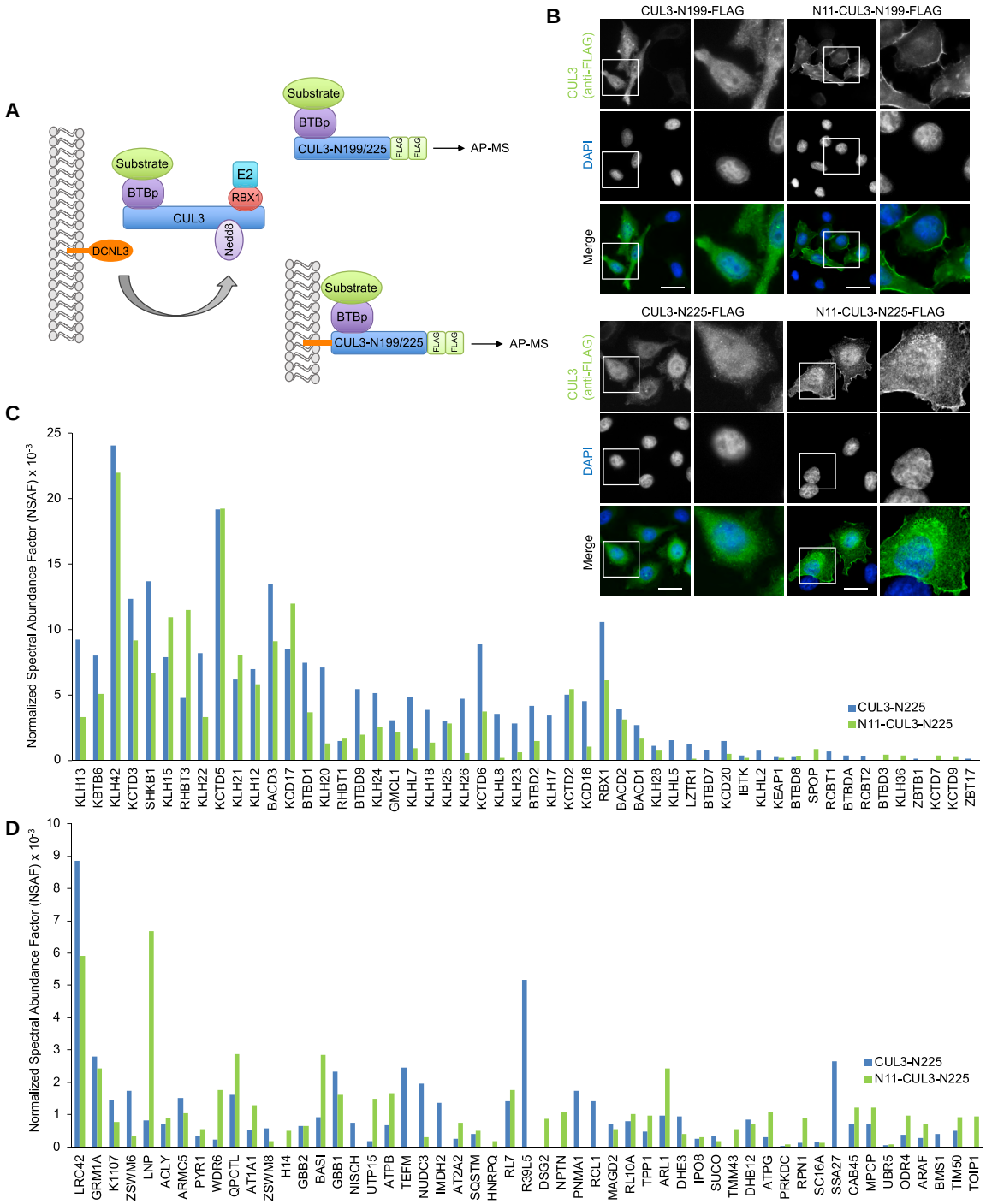

Figure 1. AP-MS-Based Screen to Identify CRL Substrates at Cellular Membranes

(A) Schematic representation of the experimental design aimed at identifying membrane associated CUL3 substrates.

(B) The indicated FLAG-tagged CUL3-N199 (top) and CUL3-N225 mutants (bottom) were expressed in HeLa cells. Cells were fixed and analyzed by immunofluorescence with an anti-FLAG antibody. DNA was stained with DAPI (blue). Bar indicates 20 μm.

(C and D) Graphical summary of CUL3 interactors, BTB proteins and RBX1 (C) and candidate substrates (D) that were recovered in the cytosolic/nuclear CUL3 pull-down (blue) or in the membrane-bound CUL3 pull-down (green). UniProt entry names are indicated on the X axes. Normalized spectral abundance factors (NSAFs) are shown on the Y axes.

See also Figure S1 and Tables S1 and S2.

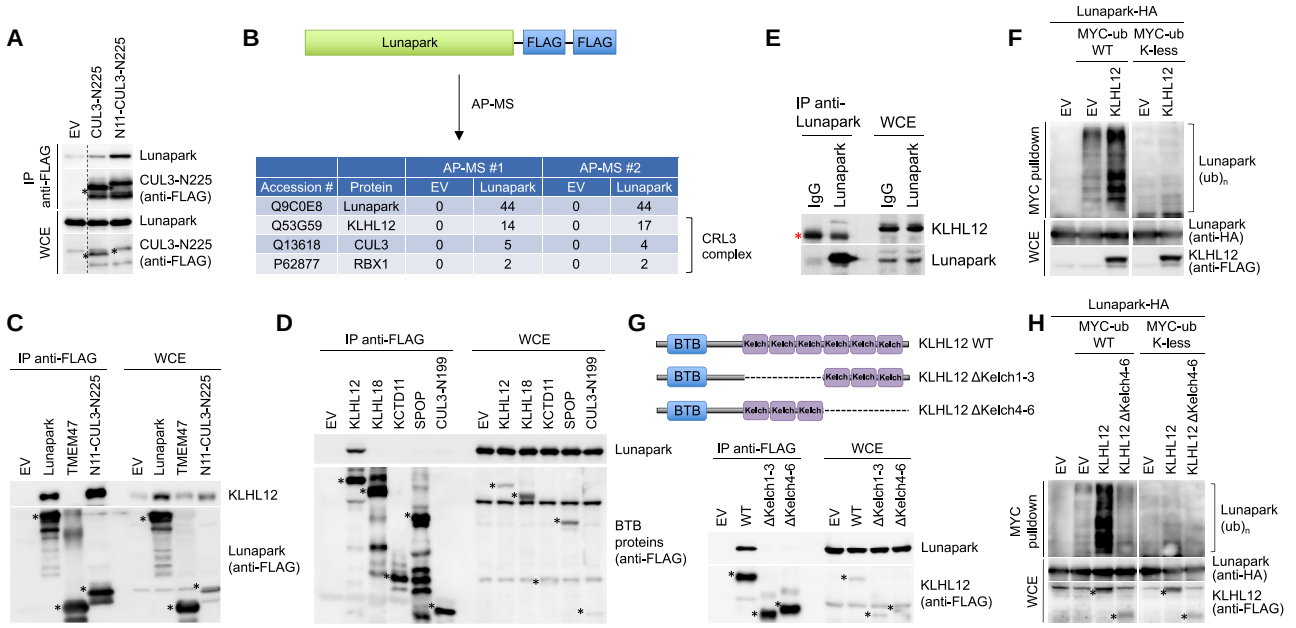

Figure 2. Lunapark Is a Substrate of the CRL3^{KLHL12} Ubiquitin Ligase

(A) HEK293T cells were transfected with an empty vector (EV) or the indicated FLAG-tagged CUL3 mutants. Whole-cell extracts (WCE) were immunoprecipitated (IP) with anti-FLAG resin and immunocomplexes were probed with antibodies to the indicated proteins. In all panels, black asterisks mark the FLAG-tagged proteins both in the IP and in the WCE.

(B) FLAG-tagged Lunapark was expressed in HEK293T cells. Cells were lysed and WCEs were subjected to immunoprecipitation using FLAG beads. Lunapark immunoprecipitates were then analyzed by mass spectrometry. The number of unique peptides identified by mass spectrometry in Lunapark and control immunopurifications is shown.

(C) HEK293T cells, transfected with FLAG-tagged Lunapark, the transmembrane protein TMEM47, and the membrane-bound N11-CUL3-N225 mutant, were lysed. WCE were immunoprecipitated (IP) with anti-FLAG resin and analyzed by immunoblotting.

(D) HEK293T cells, transfected with an EV or several FLAG-tagged BTB proteins, were lysed. WCE were used for FLAG immunoprecipitation and analyzed by immunoblotting. Note that the expressed CUL3 mutant does not contain the N-terminal lipid-modified motif and thus, as expected, does not interact with Lunapark.

(E) WCE from HEK293T cells were immunoprecipitated with an anti-Lunapark antibody. Lunapark immunocomplexes were then probed with antibodies to the indicated proteins. The red asterisk marks the IgG bands.

(F) HEK293T cells were transfected with HA-tagged Lunapark and MYC-tagged ubiquitin (wild-type [WT] or lysine-less [K-less]), with or without FLAG-tagged KLHL12. WCE were prepared in denaturing buffer and immunoprecipitated with an anti-MYC antibody. Immunoprecipitates were then immunoblotted to detect ubiquitylated Lunapark.

(G) Schematic representation of WT KLHL12 and two KLHL12 deletion mutants (top). HEK293T cells, transfected with an empty vector (EV), FLAG-tagged WT KLHL12 or the indicated KLHL12 mutants, were lysed. WCE were used for FLAG immunoprecipitations and probed for Lunapark binding by immunoblotting (bottom).

(H) As in (F), except that the KLHL12-ΔKelch4-6 mutant was also expressed.

See also Figure S2.

ubiquitylation in cultured cells. As shown in Figure 2F, Lunapark ubiquitylation is increased upon expression of KLHL12.

The BTB-Kelch proteins that form CRL3 ubiquitin ligase complexes contain an N-terminal BTB domain, which mediates their interaction with CUL3, and C-terminal Kelch repeats, which are required for substrate binding (Pintard et al., 2004). To test whether the Kelch repeats of KLHL12 are required for its interaction with Lunapark, we generated two KLHL12 mutants lacking either the first three or the last three Kelch repeats and assessed their ability to coimmunoprecipitate with endogenous Lunapark. As shown in Figure 2G, the two KLHL12-ΔKelch mutants do not interact with Lunapark further supporting a substrate-like interaction. Accordingly, the KLHL12-ΔKelch mutants are not able to stimulate Lunapark ubiquitylation in cells (Figures 2H and S2A). Taken together, these results suggest that Lunapark is a substrate of the CRL3^{KLHL12} ubiquitin ligase complex.

We then examined whether KLHL12-mediated ubiquitylation regulates Lunapark abundance. Treatment of cells with the NEDD8-activating enzyme inhibitor MLN4924, which blocks cullin neddylation and thus CRL activity, does not lead to Lunapark accumulation, but results in the accumulation of the CRL1 substrate β-catenin (Figure S2B). Likewise, proteasome inhibition by MG132 treatment does not have any effect on Lunapark abundance or turnover, whereas it leads to stabilization of the CRL1 substrates β-catenin and p27 (Figures S2B and S2C). Modulation of KLHL12 expression by RNA interference (Figure S2D) or overexpression (Figure S2E) does not result in any detectable change in the abundance of Lunapark. During

mitosis, Lunapark has been shown to be hyperphosphorylated (Wang et al., 2016). Because it has been suggested that phosphorylated Lunapark might be targeted for degradation in mitosis, we tested the effect of proteasome or CRL inhibition on the abundance of phosphorylated Lunapark. As shown in Figure S2F, Lunapark protein levels are not affected by either MG132 or MLN4924 treatment of mitotic cells. Taken together, these results demonstrate that Lunapark is ubiquitylated by the $CRL3^{KLHL12}$ ubiquitin ligase, and the $CRL3^{KLHL12}$-dependent ubiquitylation of Lunapark does not lead to its proteasomal degradation.

Analysis of the Minimal KLHL12-Binding Domain of Lunapark

Lunapark contains two N-terminal transmembrane domains (TMDs) that mediate its insertion into the outer leaflet of the ER membrane phospholipid bilayer, two TMD-flanking coiled coil regions, and a C-terminal zinc-finger motif (ZFM) that is essential for ER morphogenesis in yeast (Figure 3A). To map the KLHL12 binding motif in Lunapark, we generated multiple Lunapark deletion mutants and tested their interaction with endogenous KLHL12. We found that a proline-rich middle region (M, amino acids 138–246) in Lunapark is required for its binding to KLHL12 (Figure 3B). To narrow down the KLHL12 binding motif in Lunapark, we aligned the M region in different Lunapark vertebrate orthologs and identified three evolutionarily conserved regions, which we termed M1, M2, and M3 (Figure 3A). A series of pull-down experiments, in which the Lunapark ΔM1, ΔM2, and ΔM3 mutants were expressed in HEK293T cells and immunoprecipitated, narrowed the KLHL12 binding motif down to the M2 region of Lunapark (amino acids 202–210: SAPGGPPER) (Figure 3C). Accordingly, the KLHL12-mediated ubiquitylation of the Lunapark ΔM2 mutant was decreased when compared to the one of wild-type Lunapark (Figure 3D).

Further characterization of this 9-amino acid region by alanine-scanning mutagenesis demonstrated that mutation of the tri-amino-acid stretch SAP to AAA or GGP to AAA completely abolished Lunapark binding to KLHL12 (Figure 3E). Each of these tri-amino-acid stretches contains a proline forming a PXXP core, which is known to mediate the interaction to various domains that recognize proline-rich motifs (Kaneko et al., 2008). Therefore, we mutated both proline residues (i.e., Pro204 and Pro207) to alanine and determined the ability of the Lunapark(P204A/P207A) mutant to interact with KLHL12. As shown in Figure 3F, mutations of Pro204 and Pro207 rendered Lunapark unable to interact with KLHL12. Accordingly, Lunapark(P204A/P207A) is not ubiquitylated via KLHL12 in cultured cells (Figure 3G). Altogether, these data show that a Lunapark proline-rich domain centered on Pro204 and Pro207 mediates the binding of Lunapark to KLHL12 and its ubiquitylation.

As an additional approach to characterize the Lunapark-KLHL12 interaction, we employed immobilized synthetic peptides comprising the KLHL12-binding domain of Lunapark (aa 200–213). A Lunapark peptide containing Pro204 and Pro207 interacted with *in vitro* translated KLHL12, but not with a different BTB-Kelch protein (KLHL18), whereas the same peptide in which Pro204 and Pro207 were replaced by alanine did not associate at all, suggesting that Pro204 and Pro207 directly mediate the binding to KLHL12 (Figure 3H).

These results were further supported by computational molecular docking (Bordner and Abagyan, 2006; Lee et al., 2016; Neves et al., 2012). The peptide comprising the KLHL12-binding domain of Lunapark (aa 200–213) docks preferentially (large energy gap between lowest and next lowest conformation) to a groove on the molecular surface of KLHL12 with Pro204 and Pro207 forming the central loop of its interaction surface contacting the Kelch repeats of KLHL12 and Arg210 stabilizing the loop conformation intramolecularly (Figures 3I–3K). Replacing Pro204 and Pro207 with Ala and re-docking resulted in displacement of the peptide to a different, predicted conformation and location on the complex (Figure 3L) and a large reduction in the calculated energy of binding and the energy gap, indicating a more transient interaction (Figure 3M).

Lunapark Ubiquitylation Does Not Regulate ER Architecture and Dynamics

Next, we investigated the biological role of the KLHL12-dependent ubiquitylation of Lunapark. Because Lunapark is involved in the maintenance of the ER tubular network in mammalian cells (Chen et al., 2015), we examined whether inhibition of Lunapark ubiquitylation affects the architecture of the ER network and, in particular, the relative abundance of its two main morphological domains (i.e., ER sheets and tubules). To that end, we carried out live cell imaging analysis in U2OS cells expressing moderate levels of either GFP-tagged wild-type Lunapark or Lunapark(P204A/P207A) as well as the ER marker Sec61β fused to mCherry. As shown in Figures S3A and S3B, expression of the ubiquitylation-resistant Lunapark mutant did not affect the abundance of ER sheets and tubules. To further investigate a possible role of Lunapark ubiquitylation in the regulation of ER architecture, we generated Lunapark knockout U2OS cells by CRISPR-Cas9 genome editing. We then re-expressed in these cells moderate levels of either GFP-tagged wild-type Lunapark or Lunapark(P204A/P207A) (Figures S3C and S3D) as well as the ER marker Sec61β (fused to mCherry). Cells expressing GFP-tagged Lunapark(P204A/P207A) did not display any detectable change in ER architecture when compared to cells expressing wild-type Lunapark (Figures S3E and S3F). Moreover, both wild-type Lunapark and Lunapark(P204A/P207A) were detected as puncta with a diameter of 0.5–1 μm at three-way junctions (Figures S3 and S4) suggesting that the KLHL12-dependent ubiquitylation of Lunapark is not required for its localization to the ER three-way junctions. The same results were observed when the expression of KLHL12 was silenced by RNAi (not shown). We then analyzed the mobility of these junctions by marking the original position of Lunapark puncta and measuring the time it takes for each Lunapark puncta to move out of the circle. As shown in Figure S4, junctions with Lunapark(P204A/P207A) were as stable as junctions with wild-type Lunapark. Similarly, we did not observe differences in the percentage of merging and splitting junctions between cells containing Lunapark(P204A/P207A) and the ones containing wild-type Lunapark (Figure S4). Finally, inhibition of the KLHL12-dependent ubiquitylation of Lunapark does not affect Lunapark ability to form oligomers (Figure S5).

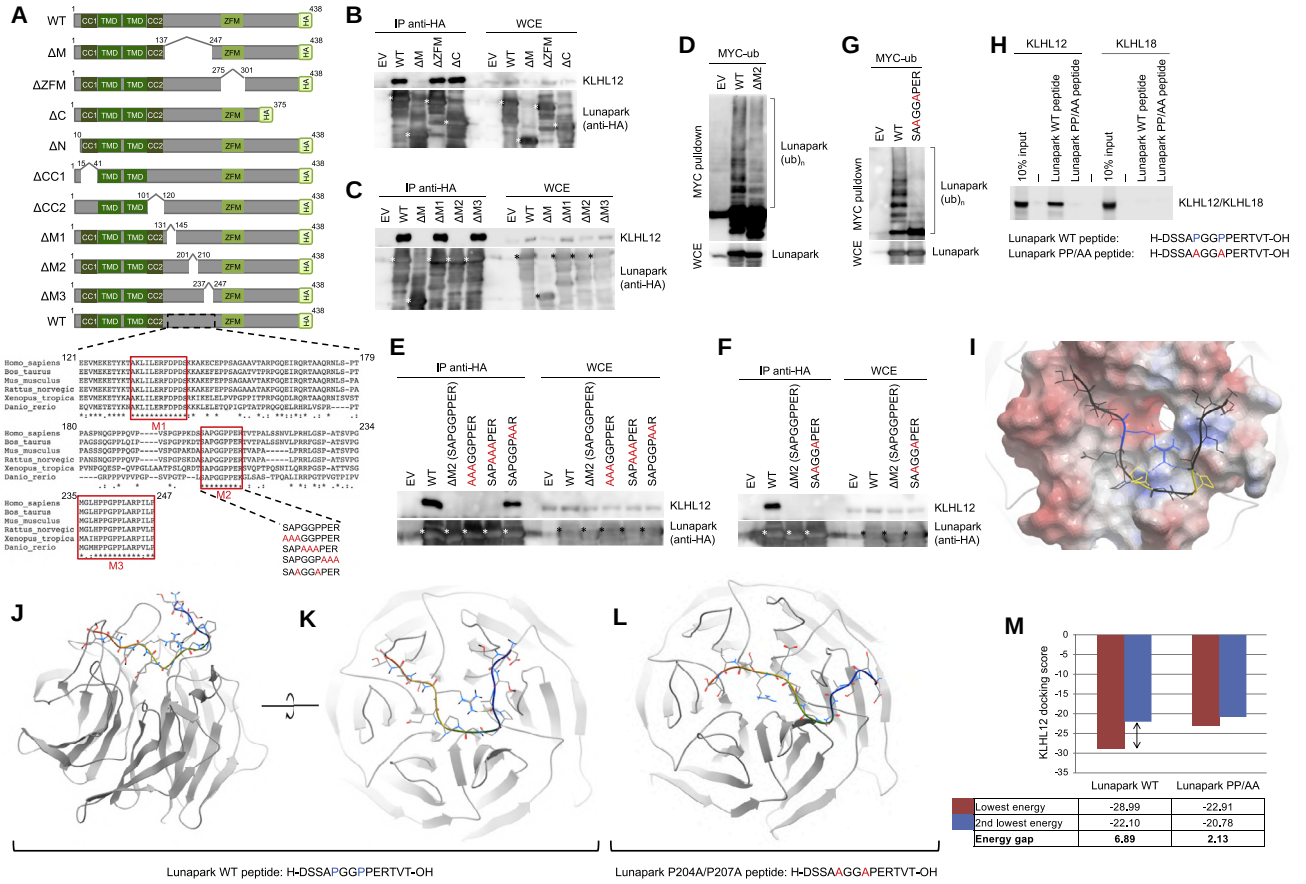

Figure 3. Identification of the KLHL12 Binding Site in Lunapark

(A) Top: schematic representation of WT Lunapark and the deletion mutants generated (TMD, transmembrane domain; CC, coiled-coil; ZFM, zinc-finger motif). Bottom: alignment of the Lunapark M (middle) region in vertebrate species. The evolutionarily conserved regions M1, M2, and M3 are boxed in red. Point mutants generated for alanine-scanning analysis are shown.

(B and C) HEK293T cells were transfected with an EV, HA-tagged WT Lunapark, or the indicated Lunapark mutants. WCEs were IP with anti-HA resin, and immunocomplexes were probed with antibodies to the indicated proteins. In all immunoblot panels, white and black asterisks mark the HA-tagged proteins in the IP and in the WCE.

(D) Ubiquitylation of Lunapark by KLHL12. HEK293T cells were transfected with HA-tagged Lunapark (WT or ΔM2 mutant), FLAG-tagged KLHL12, and MYC-tagged ubiquitin. WCE were prepared in denaturing buffer and identical aliquots were immunoprecipitated with antibodies directed against MYC. Immunoprecipitates were then immunoblotted to detect ubiquitylated Lunapark.

(E and F) As in (B) and (C).

(G) As in (D), except that the indicated Lunapark mutant was transfected instead of Lunapark ΔM2.

(H) *In vitro* binding between KLHL12 and a Lunapark peptide spanning Pro204 and Pro207. ^{35}S-KLHL12 and KLHL18 were transcribed/translated *in vitro* and incubated with beads coupled to a peptide spanning Pro204 and Pro207 or the same peptide in which Pro204 and Pro207 were replaced by alanine.

(I) Electrostatic surface rendering of KLHL12 with Lunapark WT peptide (black) with key residues highlighted: prolines whose substitution with alanines abrogates binding (yellow); arginine forming intramolecular bridge (blue).

(J) Ribbon representation of the Kelch domain of crystallized KLHL12 (PDB: 2VPJ; blue, N terminus; red, C terminus) and the predicted binding conformation of the Lunapark peptide.

(K and L) 90° anterior rotation of KLHL12 docking with Lunapark WT (K) or Lunapark(P204A/P207A) (L) peptide.

(M) Histogram of lowest energy conformation docking scores and energy gaps (Grigoryan et al., 2012) for Lunapark WT and the Lunapark(P204A/P207A) mutant peptides.

Lunapark Binds mTORC1 at ER Three-Way Junctions

The mass spectrometry analysis of endogenous proteins that copurified with FLAG-tagged Lunapark revealed the presence of peptides of mechanistic target of rapamycin (mTOR) and its cofactor mLST8 (Figure 4A). We confirmed the binding of ectopically expressed Lunapark to endogenous mTOR and mLST8 by coimmunoprecipitation (Figure 4B). A complex with endogenous Lunapark and mTOR was also detected by either immunoprecipitating Lunapark (Figure 4C) or mTOR (Figure 4D). However, neither Raptor nor Rictor, complex-specific subunits of mTORC1 and mTORC2 respectively, were detected by immunoblotting or mass spectrometry in the Lunapark

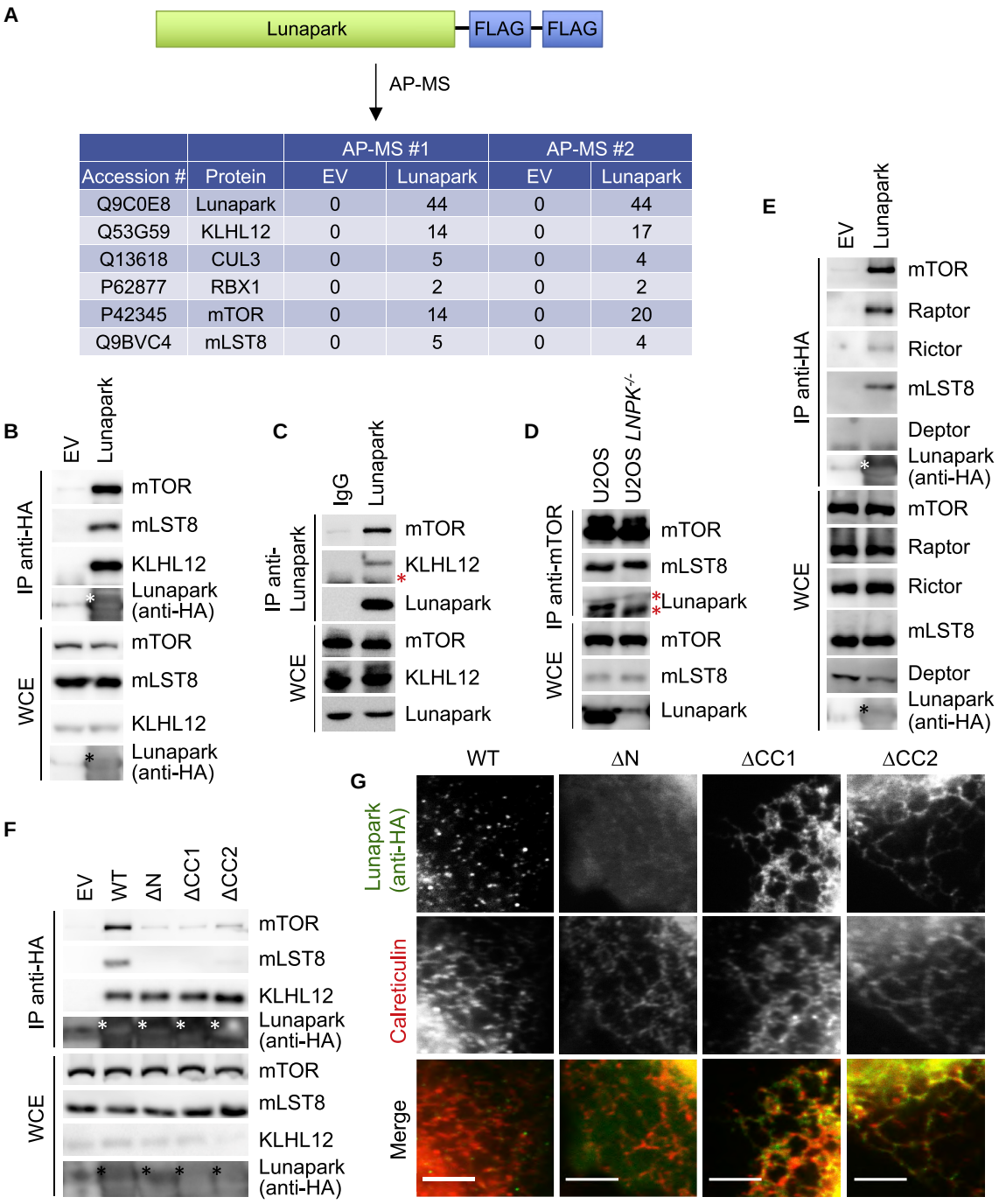

		AP-MS #1		AP-MS #2	
Accession #	Protein	EV	Lunapark	EV	Lunapark
Q9C0E8	Lunapark	0	44	0	44
Q53G59	KLHL12	0	14	0	17
Q13618	CUL3	0	5	0	4
P62877	RBX1	0	2	0	2
P42345	mTOR	0	14	0	20
Q9BVC4	mLST8	0	5	0	4

Figure 4. Lunapark Binds mTORC1 at ER Three-Way Junctions

(A) FLAG-tagged Lunapark was expressed in HEK293T cells and immunoprecipitated. Immunocomplexes were then analyzed by mass spectrometry. The number of unique peptides identified by mass spectrometry in Lunapark and control immunopurifications is shown.

(B) HEK293T cells were transfected with an EV or HA-tagged Lunapark. WCEs were IP with anti-HA resin, and immunocomplexes were probed with antibodies to the indicated proteins. In all immunoblot panels, white and black asterisks mark the HA-tagged proteins in the IP and in the WCE.

(C) WCE from HEK293T cells were immunoprecipitated with an anti-Lunapark antibody. Lunapark immunocomplexes were then probed with antibodies to the indicated proteins. The red asterisk marks unspecific bands.

(D) WCE from parental or *LNPK*$^{-/-}$ U2OS cells were immunoprecipitated with an anti-mTOR antibody. mTOR immunocomplexes were then probed with antibodies to the indicated proteins. The red asterisks mark unspecific bands.

(legend continued on next page)

immunoprecipitation. As NP40 (used in the affinity purification-mass spectrometry [AP-MS] shown in Figure 4A) and Triton X-100 (used in the pull-down shown in Figures 4B–4D) are known to disrupt the Raptor-mTOR and Rictor-mTOR interactions (Hara et al., 2002; Kim et al., 2002; Sarbassov et al., 2004), we immunoprecipitated Lunapark in the presence of the reversible crosslinker dithiobis(succinimidyl propionate) (DSP) which was shown to preserve both the Raptor-mTOR and Rictor-mTOR interactions (Hara et al., 2002; Kim et al., 2002; Sarbassov et al., 2004). Using these experimental conditions, we found that Raptor is also part of the Lunapark-mTOR-mLST8 complex that was pulled down from cell lysates (Figure 4E).

Next, we examined the ability of various Lunapark mutants to coimmunoprecipitate with endogenous mTOR and mLST8. Two Lunapark mutants that are still localized to the ER but do not concentrate at the ER three-way junctions due to the deletion of either of the two coiled-coil regions (CC1 or CC2) adjacent to the transmembrane motifs (Figure 3A) (Wang et al., 2016; Zhao et al., 2016) do not interact with mTOR and mLST8 (Figure 4F and 4G). Similarly, a Lunapark mutant that lacks the N-terminal myristoylated Gly2, and consequently is not localized to the ER, is unable to coimmunoprecipitate with mTOR and mLST8 (Figures 3A, 4F, and 4G). Taken together, these results indicate that the localization of Lunapark to ER three-way junctions is required for its binding to mTORC1.

mTORC1-Positive Lysosomes and Late Endosomes Form Contact Sites with Lunapark-Containing Three-Way Junctions

We then characterized the Lunapark-mTOR interaction in cultured cells. First, we detected, by *in situ* proximity ligation assay (PLA), the interaction between endogenous mTOR and Lunapark stably re-expressed (at physiological levels) in *LNPK*$^{-/-}$ U2OS cells generated by CRISPR-Cas9 technology (Figures 5A–5C and S3C). No signal was observed when only one antibody was used in these cells or when both antibodies were used in *LNPK*$^{-/-}$ U2OS cells. Notably, *in situ* PLA carried out in cells expressing GFP-Sec61β showed PLA puncta (marking the mTOR/Lunapark interaction) at ER three-way junctions (Figure 5D). Second, we examined the localization of Raptor, the complex-specific subunit of mTORC1, and Lunapark by live confocal fluorescence microscopy. U2OS cells were transfected with mCherry-Raptor and GFP-Lunapark and imaged by live confocal fluorescence microscopy. As shown in Figure 5E, Raptor-positive puncta were detected adjacent to Lunapark-positive puncta at the cell periphery where both signals can be well resolved.

The recruitment of mTORC1 to the membrane of lysosomes and late endosomes (LyLEs) via the Rag guanosine triphosphatases (GTPases) in response to amino acids is an obligate step in the activation of mTORC1 (Saxton and Sabatini, 2017). Once at the LyLE surface, mTORC1 interacts with GTP-bound Rheb, which unlocks the kinase activity of mTORC1 triggering phosphorylation of its substrates. Because active mTORC1 is localized to the LyLE membrane, we tested whether ER three-way junctions (where Lunapark resides) and LyLEs (where mTORC1 is recruited and activated) make contact. To visualize the ER and LyLEs, U2OS cells were co-transfected with mCherry-Sec61β (an ER marker) and GFP-LAMP1 (a LyLE marker). ER and LyLEs were then imaged by live confocal fluorescence microscopy at the cell periphery where both organelles can be well resolved (Figure 5F). LyLEs were found to be in close proximity to, or in contact with, tubular regions of the ER and associated with ER three-way junctions. This association was dynamic and variable as LyLEs transiently made contact and overlap with ER three-way junctions and tubules before dissociating and contacting the ER elsewhere. Examples of LyLE-ER contacts are shown in Figure 5F. We could distinguish between LAMP1-positive structures that overlap with ER three-way junctions (top), are in apposition with three-way junctions (middle), or partly overlap (bottom). Accordingly, when we imaged cells expressing mCherry-LAMP1 and GFP-Lunapark, we observed Lunapark-positive puncta contacting LAMP1-positive structures (Figures 5G and 5H). Finally, live cell imaging analysis of triple-labeled U2OS cells expressing GFP-Lunapark, BFP-KDEL (ER marker), and mCherry-LAMP1 (lysosome marker) confirmed that Lunapark-positive ER three-way junctions and LyLEs make contact (Figure S6). Of note, we observed LyLEs associating with ER regions that contain Lunapark (mostly at the ER three-way junctions) as well as LyLEs associating with ER regions that do not contain Lunapark (not at ER three-way junctions) in agreement with previous studies (Rowland et al., 2014).

Inhibition of Lunapark Ubiquitylation Affects Lysosomal Recruitment of mTORC1

Next, we assessed whether the KLHL12-dependent ubiquitylation of Lunapark affects mTORC1 translocation to the lysosomal membrane. We employed Lunapark-knockout U2OS cells (generated by CRISPR-Cas9 technology) transduced with lentiviruses expressing physiological levels of either HA-tagged wild-type Lunapark or the Lunapark(P204A/P207A) mutant that is unable to interact with KLHL12 and be ubiquitylated (Figures 6A and S3D). These cells were stimulated with amino acids and immunostained for endogenous mTOR and the lysosome marker LAMP2 (Sancak et al., 2010). In cells expressing wild-type Lunapark, mTOR colocalized with LAMP2 in the presence, but not in the absence of amino acids where mTOR was dispersed throughout the cytoplasm (Figure 6B-C). Cells expressing Lunapark(P204A/P207A) displayed increased amino acid-induced colocalization of mTOR with the lysosomal surface (LAMP2) when compared with control cells.

As the translocation of mTORC1 to the lysosomal membrane triggers its activation, we analyzed whether the KLHL12-mediated ubiquitylation of Lunapark affects mTORC1 signaling activity. Compared to nutrient-stimulated cells expressing wild-type

(E) As in (B) except that the reversible crosslinker dithiobis(succinimidyl propionate) (DSP) was used.
(F) As in (B) except that the indicated Lunapark mutants (described in Figure 3A) were also expressed.
(G) U2OS cells expressing HA-tagged WT Lunapark or the indicated Lunapark mutants (as in E) were fixed and immunostained for HA (green) and the ER marker calreticulin (red). Scale bar indicates 5 μm.

CellPress
OPEN ACCESS

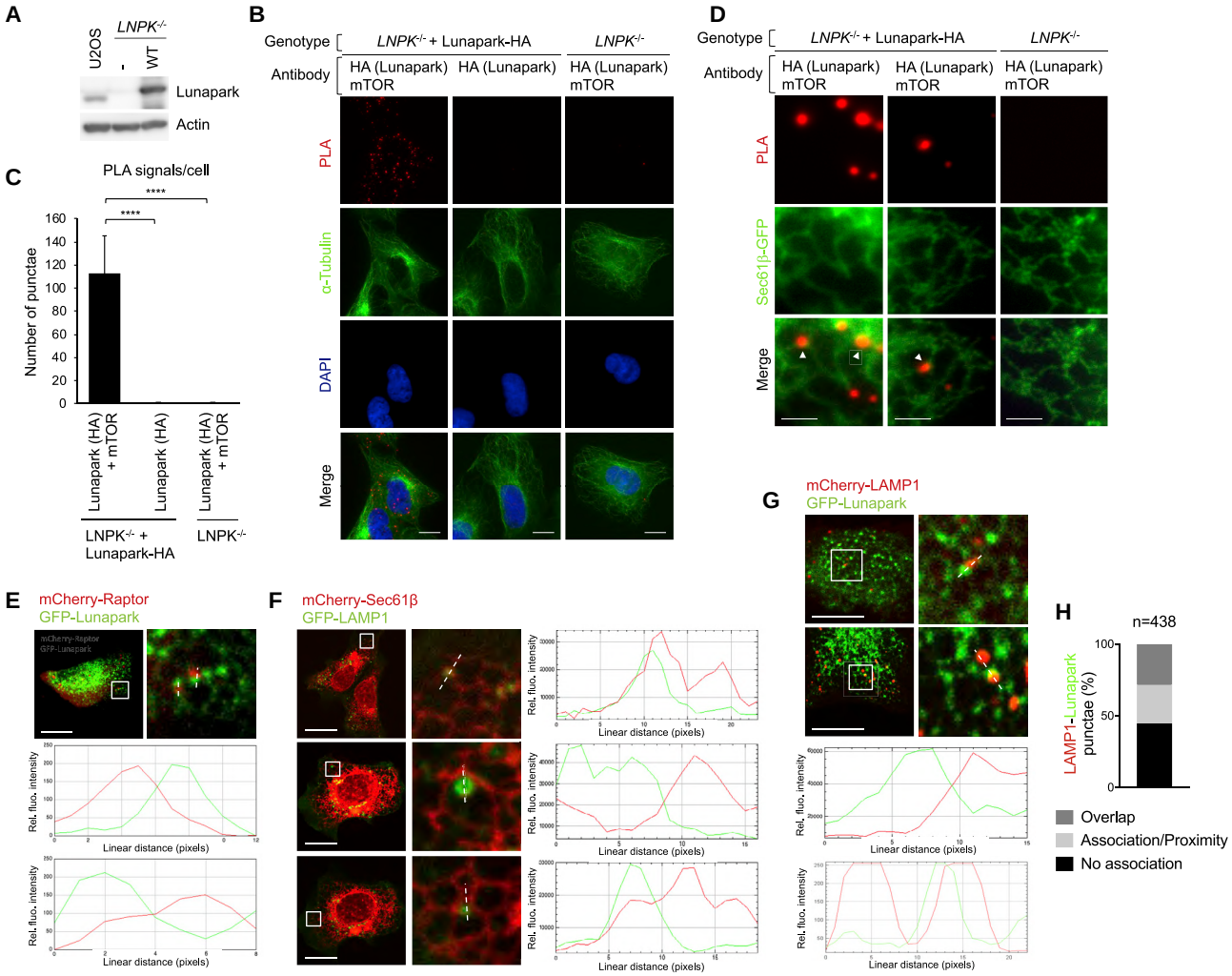

Figure 5. mTORC1-Positive LyLEs Form Contact Sites with Lunapark-Containing Three-Way Junctions

(A) Parental, *LNPK*$^{-/-}$, or *LNPK*$^{-/-}$ U2OS cells re-expressing HA-tagged WT Lunapark were lysed. Whole cell extracts were analyzed by immunoblotting with antibodies specific for the indicated proteins.

(B) *In situ* PLA of *LNPK*$^{-/-}$ U2OS cells or *LNPK*$^{-/-}$ U2OS cells re-expressing HA-tagged Lunapark probed with the indicated antibodies. Cells were counterstained with an anti-α-tubulin-FITC-conjugated antibody. The cell genotypes and the antibodies utilized are indicated on top. Scale bar indicates 10 μm.

(C) Quantification of (B). p values <0.0001 are indicated with four asterisks.

(D) As in (B), except that cells were transfected with GFP-Sec61β to visualize the ER network and not counterstained. Left and middle panels show two *LNPK*$^{-/-}$ + Lunapark-HA cells with PLA puncta localized to three-way junctions (pointed by white triangles, both anti-mTOR and anti-HA antibodies are employed). The right panels show a *LNPK*$^{-/-}$ cell stained with both antibodies (anti-mTOR and anti-HA). Scale bar indicates 2 μm.

(E) Live cell epifluorescence images and relative magnification insets of U2OS cells expressing mCherry-Raptor and GFP-Lunapark. Scale bar indicates 10 μm. Corresponding line-scan graphs of the relative fluorescence intensities of GFP and mCherry along the line indicated in the images are shown (bottom). The top line-scan graph corresponds to the left dotted line whereas the bottom line-scan graph corresponds to the right dotted line.

(F) As in (E), except that U2OS cells express mCherry-Sec61β and GFP-LAMP1. LAMP1 positive structures that overlap with ER three-way junctions (top), are in apposition with three-way junctions (middle) or partly overlap (bottom) are shown.

(G) As in (E), except that U2OS cells express mCherry-LAMP1 and GFP-Lunapark.

(H) Percentage of mCherry-LAMP1 puncta that show overlap, association/proximity, or no association with GFP-Lunapark (n = 438).

See also Figures S3 and S6

Lunapark, nutrient-stimulated cells expressing Lunapark(P204A/P207A) displayed increased degree and duration of mTORC1 activation as measured by phosphorylation of the mTORC1 substrate S6-kinase (Figures 6D and 6E). Of note, the pattern of S6K phosphorylation looks alike in parental U2OS cells and LNPK$^{-/-}$ U2OS cells reexpressing wild-type Lunapark indicating that the increased mTORC1 activity observed in LNPK$^{-/-}$ U2OS cells re-expressing Lunapark(P204A/P207A) is not due to its overexpression. To rule out that the observed phenotype may result from the expression of a non-functional Lunapark protein caused by the Pro204/207 substitution that could impair protein structure and function, we prevented Lunapark ubiquitylation in U2OS cells

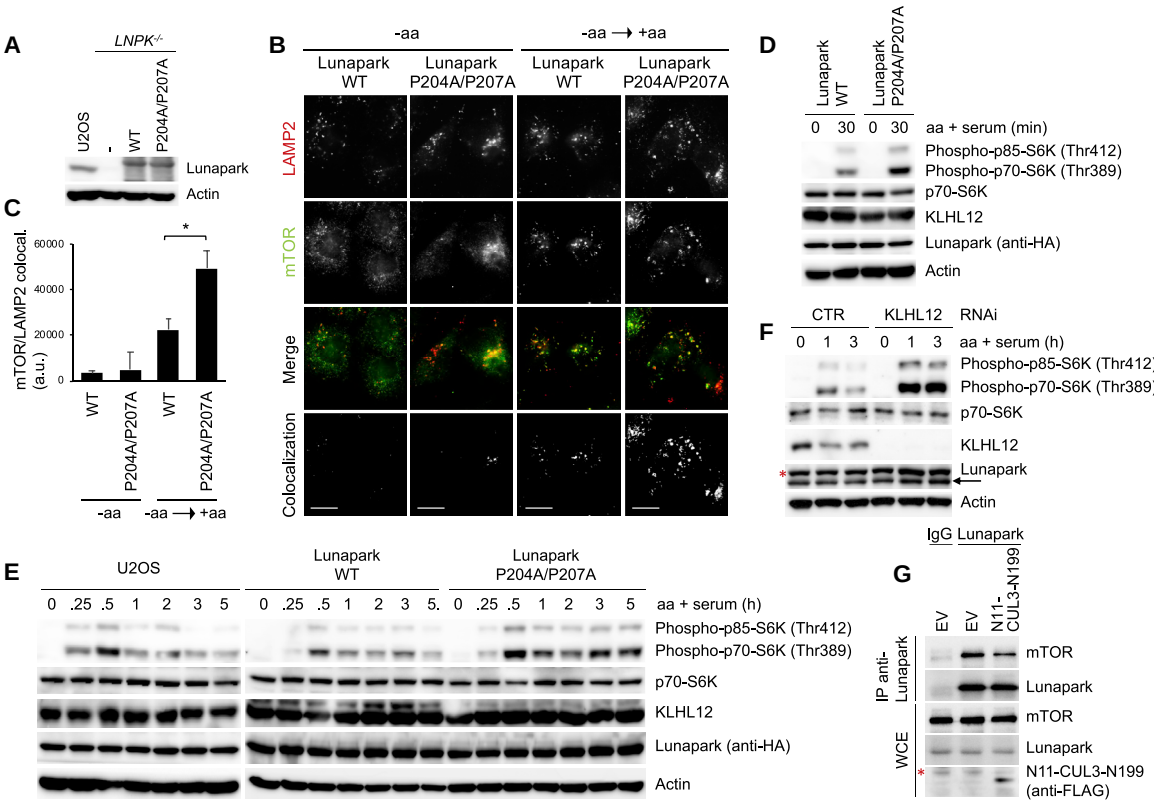

Figure 6. KLHL12-Dependent Ubiquitylation of Lunapark Limits mTOR Targeting to the Lysosomes and mTORC1 Activation

(A) Parental, *LNPK*$^{-/-}$, or *LNPK*$^{-/-}$ U2OS cells re-expressing WT Lunapark or Lunapark(P204A/P207A) were lysed. WCEs were then analyzed by immunoblotting.

(B) *LNPK*$^{-/-}$ or *LNPK*$^{-/-}$ U2OS cells re-expressing (by lentiviral transduction) either WT Lunapark or Lunapark(P204A/P207A) were starved of amino acids for 50 min and then re-stimulated for 10 min. Cells were then fixed and immunostained for endogenous mTOR (green) and the lysosomal marker protein LAMP2 (red). Colocalization panels show overlapping LAMP2 and mTOR signals. Scale bar indicates 10 μm.

(C) Quantification of mTOR/LAMP2 colocalization shown in (B). Three independent experiments were performed (n = 100 for each condition). Mean ± SD. *$p \leq 0.01$.

(D) *LNPK*$^{-/-}$ cells re-expressing WT Lunapark or Lunapark(P204A/P207A) were starved of amino acids for 50 min and then re-stimulated for the indicated times. Cells were collected, lysed, and analyzed by immunoblotting.

(E) As in (D), except that also parental U2OS cells were also analyzed.

(F) U2OS cells were transfected with either an siRNA targeting KLHL12 or a control siRNA and then treated as in (D). The red asterisk marks an unspecific band.

(G) HEK293T cells were transfected with an EV or N11-CUL3-N199 and lysed. WCE were used for Lunapark immunoprecipitation (employing an anti-Lunapark antibody) and analyzed by immunoblotting. As additional negative control, cells transfected with an EV were mocked immunoprecipitated using control IgGs. The red asterisk marks an unspecific band.

See also Figures S3, S4, S5, S6, and S7.

by silencing KLHL12 expression. The phosphorylation of S6-kinase was increased in KLHL12 knockdown cells when compared with the one in cells transfected with control small interfering RNA (siRNA) (Figure 6F) indicating that mTORC1 hyperactivation results from inhibition of the KLHL12-dependent ubiquitylation of Lunapark. Moreover, the KLHL12-mediated ubiquitylation of Lunapark limits mTORC1 activation also in non-transformed cells. Indeed, as shown in Figures S7A and S7B, the knockdown of KLHL12 as well as the expression of the ubiquitylation-resistant Lunapark mutant in hTERT-RPE cells results in increased degree and duration of mTORC1 activation.

We then tested the effect of blocking Lunapark ubiquitylation in response to amino acid deprivation. The rationale behind this experiment was to examine whether cells in which the KLHL12-mediated ubiquitylation of Lunapark is blocked are insensitive to stimuli or conditions that inactivate mTORC1. As shown in Figures S7C and S7D, cells expressing Lunapark(P204A/P207A) display the same kinetics of mTOR inactivation when compared to cells expressing wild-type Lunapark as judged by S6K dephosphorylation in response to nutrient withdrawal. The same results were obtained when we blocked the activity of mTORC1 by treating cells with rapamycin (Figure S7E).

Inhibition of Lunapark Ubiquitylation Results in Neurodevelopmental Defects

To investigate the role of the KLHL12-dependent ubiquitylation of Lunapark in normal growth and development, one-cell stage zebrafish embryos were microinjected with mRNA encoding

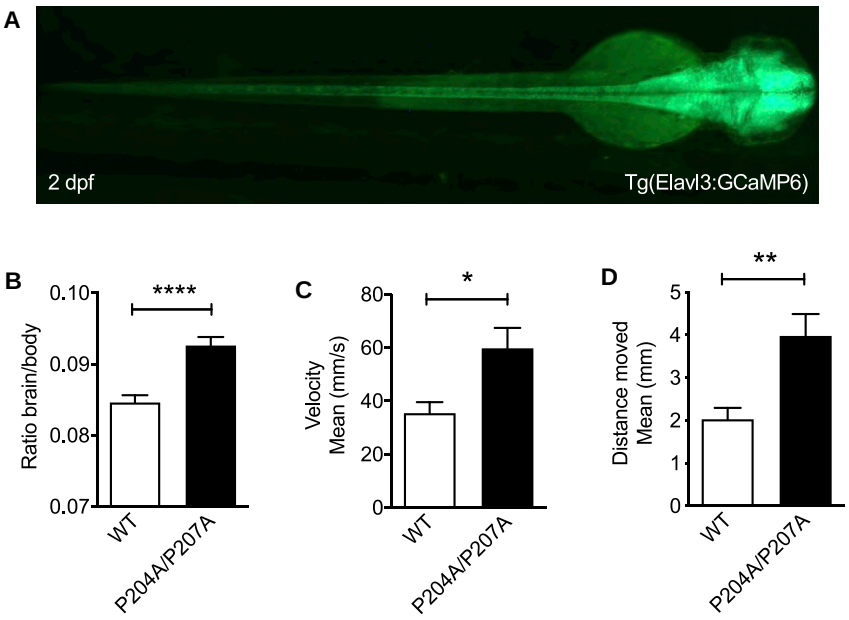

Figure 7. Expression of the Ubiquitylation-Resistant Lunapark Mutant in Zebrafish Results in Megalencephaly and Sensitizes Zebrafish to Pentylenetetrazole (PTZ) Treatment

(A) Dorsal view of a 2 dpf Tg(Elavl3:GCaMP6) embryo employed for the phenotypic analysis described in (B).

(B) Tg(Elavl3:GCaMP6) zebrafish embryos were injected with mRNA encoding WT Lunapark or Lunapark(P204A/P207A). The brain size of 2 dpf microinjected embryos was measured and normalized against the body length. Mean ± SEM. ****$p < 0.0001$ (Student's t test).

(C and D) Zebrafish embryos were injected as in (B). Four dpf injected larvae were placed in wells of a flat-bottom plate. Locomotion analysis was carried out as described in the STAR Methods. The graphs show velocity (C) and distance covered (D) by the injected larvae. Mean ± SEM. *$p < 0.05$, **$p < 0.01$ (Student's t test).

wild-type Lunapark or Lunapark(P204A/P207A). No significant phenotypic alterations in the head, heart, swim bladder, eye, tail, and fin were identified in injected zebrafish until 5 days post-fertilization (dpf). However, larvae expressing Lunapark(P204A/P207A) displayed larger brains when compared to sibling larvae expressing wild-type Lunapark (Figures 7A and 7B). Interestingly, mTOR signaling has been shown to be critical in brain development. Loss of function mutations in the tuberous sclerosis complex TSC1 or TSC2 genes, which lead to dysregulated mTOR activity, are associated with brain lesions, epilepsy, cognitive impairment, and autism (Luarte et al., 2018; Switon et al., 2017). Moreover, mTOR hyperactivation resulting from inhibition of TSC2 or Depdc5 expression in zebrafish has been associated with altered locomotion activity (de Calbiac et al., 2018; Scheldeman et al., 2017). Therefore, we tested whether blocking Lunapark ubiquitylation affects locomotion activity in zebrafish. Four dpf larvae injected with wild-type Lunapark or Lunapark(P204A/P207A) mRNAs were placed into individual wells of a 24-well plate and acclimated to a recording chamber. Locomotor analysis performed in basal condition did not revealed significant differences in activity between the two samples (data not shown). However, Lunapark(P204A/P207A)-expressing larvae treated with low doses of the CNS proconvulsant pentylenetetrazole (PTZ) displayed increased locomotor activity when compared to larvae injected with wild-type Lunapark (Figures 7C and 7D). Taken together, our results show that inhibition of Lunapark ubiquitylation in zebrafish results in megalencephaly and increased sensitivity to chemical compounds that induce epilepsy.

DISCUSSION

Our biochemical data indicate that the interaction of Lunapark with KLHL12 is mediated by the Kelch repeats of KLHL12 and a Lunapark proline-rich domain centered on Pro204 and Pro207. These results are supported by computational molecular docking, which indicates that the peptide containing Pro204 and Pro207 is also structurally and energetically complementary to the KLHL12 binding groove and is displaced by mutation of the prolines. Currently we do not know how the KLHL12-Lunapark interaction is regulated, however, we believe that proline hydroxylation might control Lunapark binding to KLHL12. Indeed, we retrieved Lunapark peptides harboring hydroxylated Pro204 in our mass spectrometry data and found that Pro204, which is essential for Lunapark binding to KLHL12, lies within a region matching the canonical X-Pro-Gly recognition sequence of prolyl 4-hydroxylases (P4Hs), enzymes that catalyze proline hydroxylation, yielding (2S,4R)-4-hydroxyproline (Hyp) (Gorres and Raines, 2010; Qi et al., 2008). P4Hs are $\alpha 2\beta 2$ tetramers in which the α-subunits contain enzymatic activity and a substrate-binding domain, while the β-subunits function as a protein disulfide isomerase (PDI) that anchors the enzyme to the ER. For the prolyl hydroxylation reaction P4Hs require α-ketoglutarate (αKG), which acts as the rate limiting electron donor under normoxic conditions (Gorres and Raines, 2010; Qi et al., 2008). αKG is the product of the deamination of glutamine, a potent mTORC1 activator. Indeed during glutaminolysis, glutaminases catalyze the conversion of glutamine into glutamate, which is then deamined to αKG (Durán et al., 2013; Jewell et al., 2015; Villar et al., 2015). The conversion of glutamate to αKG depends on the allosteric activation of glutamate dehydrogenase (GDH) by leucine and the metabolism of other amino acids, such as arginine, proline, and histidine, also results in αKG production. Thus, the KLHL12-mediated ubiquitylation of Lunapark might be part of a feedback mechanism in which amino acid abundance increases αKG production thus promoting the P4H-dependent hydroxylation of Lunapark. In turn, hydroxylation of Pro204 would stimulate Lunapark interaction with KLHL12 and

Lunapark ubiquitylation, preventing nutrient-stimulated hyper-accumulation of mTORC1 on the lysosomal membrane and de-regulated mTORC1 signaling.

How the KLHL12-dependent ubiquitylation of Lunapark limits the activation of mTORC1 in response to amino acids is not known. Our results show that inhibition of Lunapark ubiquitylation decreases its interaction with mTOR (Figure 6G). Interestingly, it has been recently shown that when amino acids are abundant, mTORC1 is only transiently associated with the lysosomal membrane as it undergoes dynamic binding and release cycles at the lysosomal surface (Lawrence et al., 2018). This mechanism prevents mTORC1 hyperactivation by reducing the amount of time during which mTORC1 is in direct contact with its activator Rheb at the lysosomal membrane. One possibility that needs to be tested is that Lunapark ubiquitylation mediated by KLHL12 could regulate the accumulation of mTORC1 to the lysosomal membrane by affecting its spatial cycling.

Our data demonstrate that inhibition of Lunapark ubiquitylation results in neurodevelopmental defects in *D. rerio*. Although Lunapark is ubiquitously expressed, it is present at high levels in the CNS of mice and chickens during embryo development and is involved in synaptic vesicle transport in *C. elegans* neuronal structures (Ghila and Gomez, 2008). Furthermore, Lunapark expression was observed throughout brain development in both mice and humans as well as in differentiating neural precursor cells (Breuss et al., 2018). Recently, homozygous mutations in the gene encoding Lunapark have been described in three children with a recessive neurodevelopmental syndrome characterized by intellectual disability, psychomotor developmental delay, defects in social interactions, hyperactivity, inattention, and epilepsy (Breuss et al., 2018). Interestingly, hyperactivation of mTORC1 signaling observed in tuberous sclerosis complex patients results in epilepsy, neurodevelopmental delays, behavioral problems including attention deficit hyperactivity disorder, and autism spectrum disorder (Luarte et al., 2018; Switon et al., 2017). Moreover, mutations in any of the three components (DEPDC5, NPRL2, and NPRL3) of the GATOR1 complex, which inhibits mTORC1 signaling by acting as a GAP for RagA/B, results in epilepsy (Marsan and Baulac, 2018).

Although proper ER morphology is key in many cellular processes and tissues, axons that require a highly elongated ER polygonal network are more sensitive to perturbations of the ER architecture (Luarte et al., 2018). Indeed, the axonal ER network is essential for vesicular transport from the soma to the axon growth cone, lipid, and cholesterol synthesis as well as their trafficking to the synapses, and it is crucial for axonal Ca^{2+} dynamics. Accordingly, mTOR has been shown to be essential for neuron development, specifically dendritogenesis, neuronal physiology, axon guidance, and axonogenesis. An assessment of the role of Lunapark ubiquitylation in neurons and its potential implication in neurodegeneration should be warranted.

STAR★METHODS

Detailed methods are provided in the online version of this paper and include the following:

SUPPLEMENTAL INFORMATION

Supplemental Information can be found online at https://doi.org/10.1016/j.celrep.2020.107664.

ACKNOWLEDGMENTS

The authors thank M. Rossi, C. Rabouille, and M. Perduca for helpful comments and discussion, the aquarium team of the Interdepartmental Centre for Experimental Research (C.I.R.S.A.L.) (University of Verona) for zebrafish husbandry, L. Di Marcotullio for reagents, and L.M. Young, C. Valdes Quezada, Z. Lei, R. Magliozzi, M. Marogna, and E. Cadoria for contributions. This work was funded by grants from the Dutch Cancer Society (KWF) and Fondazione Cariverona to D.G.

AUTHOR CONTRIBUTIONS

Conceptualization, L.Y., A.L., A.V., T.C., and D.G.; Methodology, L.Y., A.L., M.G., S.A., E.N., C.T., J.O.O., and T.Y.L.; Investigation, L.Y., A.L., M.G., S.A., E.N., C.T., J.O.O., and T.Y.L.; Writing, D.G.; Funding Acquisition, D.G.; Resources, A.V., T.C., A.J.R.H., and D.G.; Supervision, D.G.

DECLARATION OF INTERESTS

The authors declare no competing interests.

Received: March 12, 2019
Revised: January 16, 2020
Accepted: April 28, 2020
Published: May 19, 2020

REFERENCES

Angers, S., Thorpe, C.J., Biechele, T.L., Goldenberg, S.J., Zheng, N., MacCoss, M.J., and Moon, R.T. (2006). The KLHL12-Cullin-3 ubiquitin ligase negatively regulates the Wnt-beta-catenin pathway by targeting Dishevelled for degradation. Nat. Cell Biol. *8*, 348–357.

Astone, M., Lai, J.K.H., Dupont, S., Stainier, D.Y.R., Argenton, F., and Vettori, A. (2018). Zebrafish mutants and TEAD reporters reveal essential functions for Yap and Taz in posterior cardinal vein development. Sci. Rep. *8*, 10189.

Bertocci, B., Lecoeuche, D., Sterlin, D., Kühn, J., Gaillard, B., De Smet, A., Lembo, F., Bole-Feysot, C., Cagnard, N., Fadeev, T., et al. (2017). Klhl6 Deficiency Impairs Transitional B Cell Survival and Differentiation. J. Immunol. *199*, 2408–2420.

Bordner, A.J., and Abagyan, R. (2006). Ab initio prediction of peptide-MHC binding geometry for diverse class I MHC allotypes. Proteins *63*, 512–526.

Breuss, M.W., Nguyen, A., Song, Q., Nguyen, T., Stanley, V., James, K.N., Musaev, D., Chai, G., Wirth, S.A., Anzenberg, P., et al. (2018). Mutations in LNPK, Encoding the Endoplasmic Reticulum Junction Stabilizer Lunapark, Cause a Recessive Neurodevelopmental Syndrome. Am. J. Hum. Genet. *103*, 296–304.

Brockmann, M., Blomen, V.A., Nieuwenhuis, J., Stickel, E., Raaben, M., Bleijerveld, O.B., Altelaar, A.F.M., Jae, L.T., and Brummelkamp, T.R. (2017). Genetic wiring maps of single-cell protein states reveal an off-switch for GPCR signalling. Nature *546*, 307–311.

Canning, P., Cooper, C.D., Krojer, T., Murray, J.W., Pike, A.C., Chaikuad, A., Keates, T., Thangaratnarajah, C., Hojzan, V., Ayinampudi, V., et al. (2013). Structural basis for Cul3 protein assembly with the BTB-Kelch family of E3 ubiquitin ligases. J. Biol. Chem. *288*, 7803–7814.

Chen, S., Novick, P., and Ferro-Novick, S. (2012). ER network formation requires a balance of the dynamin-like GTPase Sey1p and the Lunapark family member Lnp1p. Nat. Cell Biol. *14*, 707–716.

Chen, S., Novick, P., and Ferro-Novick, S. (2013). ER structure and function. Curr. Opin. Cell Biol. *25*, 428–433.

Chen, S., Desai, T., McNew, J.A., Gerard, P., Novick, P.J., and Ferro-Novick, S. (2015). Lunapark stabilizes nascent three-way junctions in the endoplasmic reticulum. Proc. Natl. Acad. Sci. USA *112*, 418–423.

de Calbiac, H., Dabacan, A., Marsan, E., Tostivint, H., Devienne, G., Ishida, S., Leguern, E., Baulac, S., Muresan, R.C., Kabashi, E., and Ciura, S. (2018). Depdc5 knockdown causes mTOR-dependent motor hyperactivity in zebrafish. Ann. Clin. Transl. Neurol. *5*, 510–523.

Durán, R.V., MacKenzie, E.D., Boulahbel, H., Frezza, C., Heiserich, L., Tardito, S., Bussolati, O., Rocha, S., Hall, M.N., and Gottlieb, E. (2013). HIF-independent role of prolyl hydroxylases in the cellular response to amino acids. Oncogene *32*, 4549–4556.

Friedman, J.R., and Voeltz, G.K. (2011). The ER in 3D: a multifunctional dynamic membrane network. Trends Cell Biol. *21*, 709–717.

Ghila, L., and Gomez, M. (2008). The evolutionarily conserved gene LNP-1 is required for synaptic vesicle trafficking and synaptic transmission. Eur. J. Neurosci. *27*, 621–630.

Gorres, K.L., and Raines, R.T. (2010). Prolyl 4-Hydroxylase. Crit. Rev. Biochem. Mol. Biol. *45*, 106–124.

Goyal, U., and Blackstone, C. (2013). Untangling the web: mechanisms underlying ER network formation. Biochim. Biophys. Acta *1833*, 2492–2498.

Grigoryan, A.V., Wang, H., and Cardozo, T.J. (2012). Can the energy gap in the protein-ligand binding energy landscape be used as a descriptor in virtual ligand screening? PLoS ONE *7*, e46532.

Hara, K., Maruki, Y., Long, X., Yoshino, K., Oshiro, N., Hidayat, S., Tokunaga, C., Avruch, J., and Yonezawa, K. (2002). Raptor, a binding partner of target of rapamycin (TOR), mediates TOR action. Cell *110*, 177–189.

Jewell, J.L., Kim, Y.C., Russell, R.C., Yu, F.-X., Park, H.W., Plouffe, S.W., Tagliabracci, V.S., and Guan, K.-L. (2015). Metabolism. Differential regulation of mTORC1 by leucine and glutamine. Science *347*, 194–198.

Jin, L., Pahuja, K.B., Wickliffe, K.E., Gorur, A., Baumgärtel, C., Schekman, R., and Rape, M. (2012). Ubiquitin-dependent regulation of COPII coat size and function. Nature *482*, 495–500.

Kaneko, T., Li, L., and Li, S.S. (2008). The SH3 domain–a family of versatile peptide- and protein-recognition module. Front. Biosci. *13*, 4938–4952.

Keuss, M.J., Thomas, Y., Mcarthur, R., Wood, N.T., Knebel, A., and Kurz, T. (2016). Characterization of the mammalian family of DCN-type NEDD8 E3 ligases. J. Cell Sci. *129*, 1441–1454.

Kim, D.-H., Sarbassov, D.D., Ali, S.M., King, J.E., Latek, R.R., Erdjument-Bromage, H., Tempst, P., and Sabatini, D.M. (2002). mTOR interacts with raptor to form a nutrient-sensitive complex that signals to the cell growth machinery. Cell *110*, 163–175.

Kim, E., Goraksha-Hicks, P., Li, L., Neufeld, T.P., and Guan, K.L. (2008). Regulation of TORC1 by Rag GTPases in nutrient response. Nat. Cell Biol. *10*, 935–945.

Kurz, T., Ozlü, N., Rudolf, F., O'Rourke, S.M., Luke, B., Hofmann, K., Hyman, A.A., Bowerman, B., and Peter, M. (2005). The conserved protein DCN-1/Dcn1p is required for cullin neddylation in C. elegans and S. cerevisiae. Nature *435*, 1257–1261.

Kurz, T., Chou, Y.C., Willems, A.R., Meyer-Schaller, N., Hecht, M.L., Tyers, M., Peter, M., and Sicheri, F. (2008). Dcn1 functions as a scaffold-type E3 ligase for cullin neddylation. Mol. Cell *29*, 23–35.

Lawrence, R.E., Cho, K.F., Rappold, R., Thrun, A., Tofaute, M., Kim, D.J., Moldavski, O., Hurley, J.H., and Zoncu, R. (2018). A nutrient-induced affinity switch controls mTORC1 activation by its Rag GTPase-Ragulator lysosomal scaffold. Nat. Cell Biol. *20*, 1052–1063.

Lee, S.B., Frattini, V., Bansal, M., Castano, A.M., Sherman, D., Hutchinson, K., Bruce, J.N., Califano, A., Liu, G., Cardozo, T., et al. (2016). An ID2-dependent mechanism for VHL inactivation in cancer. Nature *529*, 172–177.

Low, T.Y., Peng, M., Magliozzi, R., Mohammed, S., Guardavaccaro, D., and Heck, A.J. (2014). A systems-wide screen identifies substrates of the SCFβTrCP ubiquitin ligase. Sci. Signal. *7*, rs8.

Luarte, A., Cornejo, V.H., Bertin, F., Gallardo, J., and Couve, A. (2018). The axonal endoplasmic reticulum: One organelle-many functions in development, maintenance, and plasticity. Dev. Neurobiol. *78*, 181–208.

Lydeard, J.R., Schulman, B.A., and Harper, J.W. (2013). Building and remodelling Cullin-RING E3 ubiquitin ligases. EMBO Rep. *14*, 1050–1061.

Manifava, M., Smith, M., Rotondo, S., Walker, S., Niewczas, I., Zoncu, R., Clark, J., and Ktistakis, N.T. (2016). Dynamics of mTORC1 activation in response to amino acids. eLife *5*, 1–21.

Marsan, E., and Baulac, S. (2018). Review: Mechanistic target of rapamycin (mTOR) pathway, focal cortical dysplasia and epilepsy. Neuropathol. Appl. Neurobiol. *44*, 6–17.

Meyer-Schaller, N., Chou, Y.C., Sumara, I., Martin, D.D., Kurz, T., Katheder, N., Hofmann, K., Berthiaume, L.G., Sicheri, F., and Peter, M. (2009). The human Dcn1-like protein DCNL3 promotes Cul3 neddylation at membranes. Proc. Natl. Acad. Sci. USA *106*, 12365–12370.

Monda, J.K., Scott, D.C., Miller, D.J., Lydeard, J., King, D., Harper, J.W., Bennett, E.J., and Schulman, B.A. (2013). Structural conservation of distinctive N-terminal acetylation-dependent interactions across a family of mammalian NEDD8 ligation enzymes. Structure *21*, 42–53.

Moriya, K., Nagatoshi, K., Noriyasu, Y., Okamura, T., Takamitsu, E., Suzuki, T., and Utsumi, T. (2013). Protein N-myristoylation plays a critical role in the endoplasmic reticulum morphological change induced by overexpression of protein Lunapark, an integral membrane protein of the endoplasmic reticulum. PLoS ONE *8*, e78235.

Neves, M.A., Totrov, M., and Abagyan, R. (2012). Docking and scoring with ICM: the benchmarking results and strategies for improvement. J. Comput. Aided Mol. Des. *26*, 675–686.

Petroski, M.D., and Deshaies, R.J. (2005). Function and regulation of cullin-RING ubiquitin ligases. Nat. Rev. Mol. Cell Biol. *6*, 9–20.

Phillips, M.J., and Voeltz, G.K. (2016). Structure and function of ER membrane contact sites with other organelles. Nat. Rev. Mol. Cell Biol. *17*, 69–82.

Pintard, L., Willems, A., and Peter, M. (2004). Cullin-based ubiquitin ligases: Cul3-BTB complexes join the family. EMBO J. *23*, 1681–1687.

Qi, H.H., Ongusaha, P.P., Myllyharju, J., Cheng, D., Pakkanen, O., Shi, Y., Lee, S.W., Peng, J., and Shi, Y. (2008). Prolyl 4-hydroxylation regulates Argonaute 2 stability. Nature *455*, 421–424.

Rondou, P., Haegeman, G., Vanhoenacker, P., and Van Craenenbroeck, K. (2008). BTB Protein KLHL12 targets the dopamine D4 receptor for ubiquitination by a Cul3-based E3 ligase. J. Biol. Chem. *283*, 11083–11096.

Rowland, A.A., Chitwood, P.J., Phillips, M.J., and Voeltz, G.K. (2014). ER contact sites define the position and timing of endosome fission. Cell *159*, 1027–1041.

Sancak, Y., Peterson, T.R., Shaul, Y.D., Lindquist, R.A., Thoreen, C.C., Bar-Peled, L., and Sabatini, D.M. (2008). The Rag GTPases bind raptor and mediate amino acid signaling to mTORC1. Science *320*, 1496–1501.

Sancak, Y., Bar-Peled, L., Zoncu, R., Markhard, A.L., Nada, S., and Sabatini, D.M. (2010). Ragulator-Rag complex targets mTORC1 to the lysosomal surface and is necessary for its activation by amino acids. Cell *141*, 290–303.

Sarbassov, D.D., Ali, S.M., Kim, D.H., Guertin, D.A., Latek, R.R., Erdjument-Bromage, H., Tempst, P., and Sabatini, D.M. (2004). Rictor, a novel binding partner of mTOR, defines a rapamycin-insensitive and raptor-independent pathway that regulates the cytoskeleton. Curr. Biol. *14*, 1296–1302.

Saxton, R.A., and Sabatini, D.M. (2017). mTOR Signaling in Growth, Metabolism, and Disease. Cell *168*, 960–976.

Scheldeman, C., Mills, J.D., Siekierska, A., Serra, I., Copmans, D., Iyer, A.M., Whalley, B.J., Maes, J., Jansen, A.C., Lagae, L., et al. (2017). mTOR-related neuropathology in mutant tsc2 zebrafish: Phenotypic, transcriptomic and pharmacological analysis. Neurobiol. Dis. *108*, 225–237.

Scott, D.C., Monda, J.K., Grace, C.R., Duda, D.M., Kriwacki, R.W., Kurz, T., and Schulman, B.A. (2010). A dual E3 mechanism for Rub1 ligation to Cdc53. Mol. Cell *39*, 784–796.

Scott, D.C., Monda, J.K., Bennett, E.J., Harper, J.W., and Schulman, B.A. (2011). N-terminal acetylation acts as an avidity enhancer within an interconnected multiprotein complex. Science *334*, 674–678.

Scott, D.C., Sviderskiy, V.O., Monda, J.K., Lydeard, J.R., Cho, S.E., Harper, J.W., and Schulman, B.A. (2014). Structure of a RING E3 trapped in action reveals ligation mechanism for the ubiquitin-like protein NEDD8. Cell *157*, 1671–1684.

Sekiguchi, T., Hirose, E., Nakashima, N., Ii, M., and Nishimoto, T. (2001). Novel G proteins, Rag C and Rag D, interact with GTP-binding proteins, Rag A and Rag B. J. Biol. Chem. *276*, 7246–7257.

Shemesh, T., Klemm, R.W., Romano, F.B., Wang, S., Vaughan, J., Zhuang, X., Tukachinsky, H., Kozlov, M.M., and Rapoport, T.A. (2014). A model for the generation and interconversion of ER morphologies. Proc. Natl. Acad. Sci. USA *111*, E5243–E5251.

Switon, K., Kotulska, K., Janusz-Kaminska, A., Zmorzynska, J., and Jaworski, J. (2017). Molecular neurobiology of mTOR. Neuroscience *341*, 112–153.

The UniProt Consortium (2017). UniProt: the universal protein knowledgebase. Nucleic Acids Res. *45* (*D1*), D158–D169.

Turrini, L., Fornetto, C., Marchetto, G., Müllenbroich, M.C., Tiso, N., Vettori, A., Resta, F., Masi, A., Mannaioni, G., Pavone, F.S., and Vanzi, F. (2017). Optical mapping of neuronal activity during seizures in zebrafish. Sci. Rep. *7*, 3025.

Villar, V.H., Merhi, F., Djavaheri-Mergny, M., and Durán, R.V. (2015). Glutaminolysis and autophagy in cancer. Autophagy *11*, 1198–1208.

Wang, S., Tukachinsky, H., Romano, F.B., and Rapoport, T.A. (2016). Cooperation of the ER-shaping proteins atlastin, lunapark, and reticulons to generate a tubular membrane network. eLife *5*, e18605.

Wilson, A.A., Kwok, L.W., Hovav, A.H., Ohle, S.J., Little, F.F., Fine, A., and Kotton, D.N. (2008). Sustained expression of alpha1-antitrypsin after transplantation of manipulated hematopoietic stem cells. Am. J. Respir. Cell Mol. Biol. *39*, 133–141.

Zhang, C., Liu, J., Huang, G., Zhao, Y., Yue, X., Wu, H., Li, J., Zhu, J., Shen, Z., Haffty, B.G., et al. (2016). Cullin3-KLHL25 ubiquitin ligase targets ACLY for degradation to inhibit lipid synthesis and tumor progression. Genes Dev. *30*, 1956–1970.

Zhao, Y., Zhang, T., Huo, H., Ye, Y., and Liu, Y. (2016). Lunapark Is a Component of a Ubiquitin Ligase Complex Localized to the Endoplasmic Reticulum Three-way Junctions. J. Biol. Chem. *291*, 18252–18262.

STAR★METHODS

KEY RESOURCES TABLE

REAGENT or RESOURCE	SOURCE	IDENTIFIER
Antibodies		
Rabbit polyclonal anti-Lunapark	Sigma-Aldrich	Cat# HPA014205; RRID:AB_2234186
Mouse monoclonal anti-KLHL12	Cell Signaling Technology	Cat# 9406; RRID:AB_2797699
Mouse monoclonal anti-FLAG	Sigma-Aldrich	Cat# F3165; RRID:AB_259529
Mouse Monoclonal anti-HA	Biolegend	Cat# 901514; RRID:AB_2565336
Rabbit polyclonal anti-GFP	Torrey Pines Biolabs	Cat# TP401; RRID:AB_10013661
Rabbit polyclonal anti-GβL(mLST8)	Cell Signaling Technology	Cat# 3274; RRID:AB_823685
Rabbit polyclonal anti-FLAG	Sigma-Aldrich	Cat# F7425; RRID:AB_439687
Rabbit polyclonal anti-βActin	Santa Cruz	Cat# sc69879; RRID:AB_1119529
Rabbit polyclonal anti-AKT	Bethyl Laboratories	Cat# A302-065A; RRID:AB_1604215
Rabbit polyclonal anti-HA	Cell Signaling Technology	Cat# 3724; RRID:AB_1549585
Rabbit polyclonal anti-phospho-p70-S6K (Thr389)	Cell Signaling Technology	Cat# 9234; RRID:AB_2269803
Rabbit polyclonal anti-p70-S6K	Bethyl Laboratories	Cat# A300-510A; RRID:AB_2182248
Rabbit polyclonal anti-Raptor	Bethyl Laboratories	Cat# A300-553A; RRID:AB_2130793
Rabbit monoclonal anti-Rictor	Cell Signaling Technology	Cat# 2114; RRID:AB_2179963
Rabbit monoclonal anti-Deptor/DEPDC6	Cell Signaling Technology	Cat# 11816; RRID:AB_2750575
Rabbit monoclonal anti-mTOR	Cell Signaling Technology	Cat# 2983; RRID:AB_2105622
Mouse monoclonal anti-mTOR	Merck-Millipore	Cat# 05-1592; RRID:AB_1977357
Mouse monoclonal anti-LAMP2/CD107b	Novus Biologicals	Cat# NBP2-22217SS; RRID:AB_2722697
Rabbit polyclonal anti-Calreticulin	Abcam	Cat# ab2907; RRID:AB_303402
Mouse IgG, HRP-linked whole Ab (from sheep)	GE Healthcare	Cat# NA931; RRID:AB_772210
Rabbit IgG, HRP-linked whole Ab (from donkey)	GE Healthcare	Cat# NA934; RRID:AB_772206
Mouse monoclonal anti-Myc	Sigma-Aldrich	Cat# M5546; RRID:AB_260581
Chemicals, Peptides, and Recombinant Proteins		
Proteasome Inhibitor MG132	Peptide Institute	Cat# 3175-V
Lipofectamine RNAiMAX	Thermo Fisher Scientific	Cat# 13778075
MLN-4924	Active Biochem	Cat# 1139
Cycloheximide	Sigma Aldrich	Cat# C104450
Experimental Models: Cell Lines		
Human U2OS	ATCC	Cat# HTB-96; RRID:CVCL_0042
Human HEK293T	ATCC	Cat# CRL-11268; RRID:CVCL_1926
Human HeLa	ATCC	Cat# CCL-2; RRID:CVCL_0030
Oligonucleotides		
Human KLHL12 siRNA targeting sequence	Dharmacon	Cat# 2958852
Recombinant DNA		
mCherry-Sec61β	Addgene plasmids	Cat# 49155; RRID:Addgene_49155
Rtn4a-GFP	Addgene plasmids	Cat# 61807; RRID:Addgene_61807
LAMP1-GFP	Addgene plasmids	Cat# 34831; RRID:Addgene_34831
LAMP1-mCherry	Addgene plasmids	Cat# 45147; RRID:Addgene_45147
pAc-GFPC1-Sec61β	Addgene plasmids	Cat# 15108; RRID:Addgene_15108
pRK5-HA-mCherry-RAPTOR	Addgene plasmids	Cat# 73386; RRID:Addgene_73386
pcDNA3-FLAG-FLAG-HA-HA-Lunapark	This paper	N/A
pHAGE2-EF1α-IRES-Lunapark	This paper	N/A
pcDNA3-2xFLAG-CUL3-N225	This paper	N/A
pcDNA3-2xFLAG-CUL3-N225-MB	This paper	N/A

(*Continued on next page*)

Continued

REAGENT or RESOURCE	SOURCE	IDENTIFIER
pcDNA3-FLAG-CUL3-N199-MB	This paper	N/A
pcDNA3-FLAG-CUL3-N199	This paper	N/A
pWC7-His-MYC-ubiquitin	This paper	N/A
pcDNA3-Lunapark-HA	This paper	N/A
pcDNA-FLAG-KLHL12	This paper	N/A
Critical Commercial Assays		
QuickChange Site-Directed Mutagenesis Kit	Stratagene	Cat# 200518
Software and Algorithms		
ImageJ	https://imagej.nih.gov/ij/	https://imagej.nih.gov/ij/ ; RRID:SCR_003070

RESOURCE AVAILABILITY

Lead Contact

Further information and requests for resources and reagents should be directed to and will be fulfilled by the Lead Contact, Daniele Guardavaccaro. (daniele.guardavaccaro@univr.it).

Materials Availability

All unique/stable reagents generated in this study are available from the Lead Contact with a completed Materials Transfer Agreement. Commercially available reagents are indicated in the Key Resources Table.

Data and Code Availability

This article includes all datasets/code generated or analyzed during this study (Tables S1 and S2).

EXPERIMENTAL MODEL AND SUBJECT DETAILS

Human cells, transfection and drug treatment

HEK293T, HeLa, U2OS and hTERT-RPE cells were maintained in Dulbecco's modified Eagle's medium (DMEM; Thermo Fisher Scientific) containing 10% fetal calf serum, 100 U/ml penicillin, and 100 μg/ml streptomycin. Cells were transfected by the polyethylenimine (PEI) method. siRNA oligonucleotide against human KLHL12 was purchased from Dharmacon (Clone ID: 2958852) and transfected into cells using Lipofectamine RNAiMAX (Thermo Fisher Scientific) according to manufacturer's protocol. The following drugs were used: MG132 (Peptide Institute, 10 μM), MLN4924 (Active Biochemicals, 0.5 μM), and cycloheximide (Sigma-Aldrich, 100 μM).

Zebrafish embryo injections and analysis

Wild-type and transgenic [Tg(Elavl3:GCaMP6)] zebrafish lines were maintained under standard husbandry conditions and mated according to standard procedures at the Interdepartmental Centre for Experimental Research (CIRSAL) of the University of Verona. mRNAs for injection were transcribed using the mMESSAGE mMACHINE SP6 Transcription Kit (ThermoFisher Scientific-Ambion) using linearized pCS2+ constructs as template. One-cell stage zebrafish embryos were injected with 2.5 pg of mRNA [wild-type Lunapark or Lunapark(P204A/P207A)] as previously described (Astone et al., 2018). Injected fish were screened to detect the presence of phenotypic alterations including evident morphological distortion, cardiac edema, abnormalities of head, eye, tail and fin by visual assessment.

For brain analysis, the Tg(Elavl3:GCaMP6) transgenic reporter line, which displays robust transgene expression in the brain at 2 dpf, was employed (Turrini et al., 2017). Two dpf injected embryos were positioned dorsally in 3% methylcellulose on a microscope slide. Images were taken using a LEICA MZ16F fluorescence microscope and the Leica Application Suite V4.12 software. The brain size was measured using the Fiji-ImageJ software and normalized against the body length. GraphPad Prism was used to conduct statistical analysis (Student's t test). For locomotion analysis, 4 dpf injected larvae were placed individually in wells of a 24-well flat-bottomed culture dish. Locomotion was tracked for 30 minutes in basal condition followed by 45 minutes of recording after administration of 1.25 mM pentylenetetrazole (PTZ) at 28.5°C using a DanioVision system (Noldus) consisting of an isolated chamber with an infrared camera. Both the distance traveled and the velocity of swimming were analyzed using the EthoVision XT-15 locomotion tracking software. GraphPad Prism was used for statistical analysis (Student's t test). Differences were considered significant if $p < 0.05$. All experiments were carried in accordance to the Italian law on animal experimentation (D.L. 4 March 2014, n.26), under authorization n°186474 (27/05/2019).

METHOD DETAILS

Plasmids, cloning and lentivirus production

The Cullin-3 deletion mutants CUL3-N199 and CUL3-N225 carrying one or two C-terminal FLAG tags, respectively, were generated by PCR and subcloned into the pcDNA3 vector. The membrane-targeted Cullin-3 mutants (CUL3-N199-MB and CUL3-N225-MB) were constructed by fusing the first 11 amino acids of DCNL3 (Meyer-Schaller et al., 2009) to the N-terminal of the CUL3 deletion mutants by PCR. Human Lunapark and KLHL12 cDNAs were obtained from GE Healthcare. Lunapark carrying C-terminal 2xFLAG-2xHA or a single HA and KLHL12 carrying an N-terminal FLAG were subcloned into pcDNA3. Deletion mutants of Lunapark (ΔMs, ΔZFM, ΔC) and KLHL12 (ΔKelch1-3, ΔKelch4-6) were generated by PCR and subcloned into pcDNA3. The HA-tagged Lunapark(P204A/P207A) was generated by site-directed mutagenesis (Stratagene). Lunapark WT, ΔM2 and P204A/P207A were also subcloned into pEGFP-N1. mCherry-Sec61β (Addgene plasmids # 49155) and Rtn4a-GFP (Addgene plasmids # 61807) were gifts from Gia Voeltz, LAMP1-GFP (Addgene plasmids # 34831) was a gift from Esteban Dell'Angelica, LAMP1-mCherry (Addgene plasmids # 45147) was a gift from Amy Palmer, pAc-GFPC1-Sec61β (Addgene plasmids # 15108) was a gift from Tom Rapoport, pRK5-HA-mCherry-RAPTOR (Addgene plasmids # 73386) was a gift from Jie Chen and Taekjip Ha. For lentiviral transduction, wild-type Lunapark and mutants were subcloned into pHAGE2-EF1α-IRES-puromycin vectors (Wilson et al., 2008). For lentiviral transduction, HEK293T cells were transfected by the polyethylenimine (PEI) method with the pHAGE2 vector together with packaging vectors encoding Gag-Pol, Rev, Tat, and the G protein of the vesicular stomatitis virus (VSV). Supernatants were collected every 48 hours on two consecutive days starting 24 hours after transfection, filtered and transferred to cells in the presence of polybrene (4 μg/ml).

Identification of CUL3 and Lunapark interactors

HEK293T cells were transfected with pcDNA3-FLAG-CUL3-N199, pcDNA3-2xFLAG-CUL3-N225, pcDNA3-FLAG-CUL3-N199-MB, pcDNA3-2xFLAG-CUL3-N225-MB or pcDNA3-Lunapark-2xFLAG-2xHA. Cells were harvested and subsequently lysed in lysis buffer [50 mM Tris-HCl (pH 7.5), 150 mM NaCl, 1 mM EDTA, and 0.5% NP-40 plus protease and phosphatase inhibitors]. CUL3 and Lunapark were immunopurified with anti-FLAG agarose resin (Sigma-Aldrich). The beads were washed and proteins were eluted using RapiGest SF (Waters). Eluents were subsequently treated with reduction buffer (1 μg/μl dithiothreitol) for 30 minutes and alkylation buffer (5 μg/μl iodoacetamide) for 20 minutes, followed by Lys-C for 4 hours. Trypsin was then added at the 1:50 ratio and mixture was incubated overnight at 37°C. Trypsin was quenched by adding trifluoroacetic acid (TFA). The mixture was then subjected to C18 SEP-PAK desalting.

For MS analysis, peptides were first separated with a C18 column (Zorbax) and introduced by nanoelectrospray into the LTQ Orbitrap Elite (Thermo Fisher) and MS/MS in data-dependent decision tree mode (collision-induced dissociation/electron transfer dissociation) as described previously (Low et al., 2014). Raw files were converted to MGF files using Proteome Discoverer version 1.4 (Thermo Fisher). The non-fragment filter was used to simplify ETD spectra and the Top N filter (6 highest peaks admitted per 100 Da) for the CID spectra. All MGF files were submitted to Mascot search engine (version 3.0) via Proteome Discoverer version 1.4. The spectra were searched against the UniProt Human database (version 2013-07, 20,277 entries). Trypsin/P was chosen as the protease with 2 missed cleavages, cysteine carbamidomethylation was set as fixed modification; and oxidation of methionine and acetylation of the N terminus of the protein were set as variable modifications. Peptide tolerance was set to 15 ppm and MS/MS tolerance set to 0.5 dalton. All peptide-spectrum matches (PSMs) were filtered at a Mascot score cutoff at 30. Only PSMs with a minimum length of 7 amino acids were kept. To normalize spectral count data, we exported the full list with Normalized Spectral Abundance Factors (NSAF). NSAF is calculated as the number of spectral counts (SpC) identifying a protein, divided by the protein's length (L), in turn divided by the sum of SpC/L for all proteins in the experiment.

CRISPR genome editing

To generate *LNPK*$^{-/-}$ cell lines, two optimal gRNA target sequences targeting both exon 1 and exon 13 (genomic deletion) were designed using the Benchling CRISPR Genome Engineering tool and cloned into pSpCas9(BB)-2A-GFP (PX458). U2OS cells were seeded into 10-cm dishes at approximately 70% confluency and transfected with 2.5 μg of both gRNA-containing PX458 plasmids using the polyethylenimine (PEI) method. Two days after transfection, GFP-positive cells were sorted using the BD FACSJazz™ cell sorter, and 20 cells/well were plated in a 96-well plate. One to two weeks later, single cell clones were picked, trypsinized in 0.25% Trypsin-EDTA for 5 minutes, and plated into individual wells of a 96-well plate for genotyping. Genomic DNA was collected using DNA lysis buffer (100 mM Tris-HCl pH 8.0, 200 mM NaCl, 5 mM EDTA pH 8.0, 0.2% SDS) supplemented with 10 μg/μl proteinase K. Genotyping PCRs were performed with GoTaq G2 Flexi DNA Polymerase (Promega), using primers surrounding the genomic target sites. Positive clones were sequenced to determine the presence of deletion event (*LNPK* knockout). To further validate the mutational status of candidate clones, single clones were screened for Lunapark expression by immunoblotting.

Biochemical methods

For preparation of cell extracts, cells were washed and collected in ice-cold PBS and lysed in Triton-X lysis buffer (50 mM Tris pH 7.5, 250 mM NaCl, 0.1% Triton X-100, 1 mM EDTA, 50 mM NaF and protease and phosphatase inhibitors) for 30 minutes on ice, followed by centrifugation for 20 minutes at 4°C. Cell extracts were then submitted to either immunoblotting or immunoprecipitation followed by immunoblotting. For immunoprecipitation, cell extracts were first precleared by incubation with protein G- or protein A-Sepharose

beads (Thermo Fisher Scientific) for 45 minutes at 4°C. Precleared extracts were incubated with the indicated antibody for 3 hours at 4°C followed by protein G- or protein A-Sepharose beads for 45 minutes. Beads were washed 4 times with lysis buffer and proteins were eluted in 5x Laemmli sample buffer [50mM Tris-HCl, pH 6,8, 2% (w/v) SDS, 5% (v/v), β-mercaptoethanol, 0,1% (w/v) bromophenol blue and 1% (v/v) glycerol]. The immunoprecipitation in the presence of the crosslinking agent dithiobis (succinimidyl propionate)(DSP) (Thermo Fisher Scientific PG82081) was performed as previously described (Kim et al., 2002). For immunoblotting, proteins were separated by SDS-polyacrylamide gel electrophoresis (SDS-PAGE), transferred onto PVDF membranes (Merck-Millipore), and incubated with the indicated antibodies. For ubiquitylation assay in cultured cells, HEK293T cells were transfected with pcDNA3-Lunapark-HA (WT or mutants), pcDNA-FLAG-KLHL12 (WT or ΔKelch4-6), or pWC7-His-MYC-ubiquitin (WT or K-less), as indicated. Forty-eight hours later, cells were treated with MG132 for 4 hours before harvesting. Cells were lysed in RIPA buffer (25 mM Tris pH 7.5, 150 mM NaCl, 1% NP40, 1% sodium deoxycholate, 0.1% SDS and protease and phosphatase inhibitors) and subjected to immunoprecipitation using c-Myc antibody. Ubiquitylated Lunapark was detected by immunoblotting using an anti-Lunapark antibody.

Antibodies

The following antibodies were used in this study: anti-Lunapark, rabbit polyclonal (Sigma-Aldrich, HPA014205), anti-KLHL12, mouse monoclonal (Cell Signaling Technology, 9406), anti-FLAG, rabbit polyclonal (Sigma-Aldrich, F7425), anti-FLAG, mouse monoclonal (Sigma-Aldrich, F7425), anti-HA, mouse monoclonal (Biolegend, 901514), anti-HA, rabbit monoclonal (Cell Signaling Technology, 3724), anti-β-actin, mouse monoclonal (Santa Cruz, sc-69879), anti-Myc, mouse monoclonal (Sigma-Aldrich, M5546), anti-GFP, rabbit polyclonal (Torrey Pines Biolabs, TP401), anti-GβL(mLST8), rabbit monoclonal (Cell Signaling Technology, 3274), anti-AKT, rabbit polyclonal (Bethyl Laboratories, A302-065A), anti-phospho-p70-S6K (Thr389), rabbit monoclonal (Cell Signaling Technology, 9234), anti-p70-S6K, rabbit polyclonal (Bethyl Laboratories, A300-510A), anti-Raptor, rabbit polyclonal (Bethyl Laboratories, A300-553A), anti-Rictor, rabbit monoclonal (Cell Signaling Technology, 2114), anti-Deptor/DEPDC6, rabbit monoclonal (Cell Signaling Technology, 11816). Anti-mouse IgG (NA931) and anti-rabbit IgG (NA934) horseradish peroxidase (HRP) conjugated secondary antibodies were from GE Healthcare. The following primary antibodies were used for immunofluorescence and proximity ligation assays: anti-HA, mouse monoclonal (Biolegend, 901514), anti-mTOR, rabbit monoclonal (Cell Signaling Technology, 2983), anti-mTOR, mouse monoclonal (Merck-Millipore, 05-1592), anti-LAMP2/CD107b, mouse monoclonal (Novus Biologicals, NBP2-22217SS) and anti-Calreticulin, rabbit polyclonal (Abcam, ab2907). Alexa Fluor 488-, Alexa Fluor 568- or Alexa Fluor 594-conjugated secondary antibodies were from Thermo Fisher Scientific.

Immunofluorescence

Cells were seeded on polylysine-L (Sigma-Aldrich) treated glass coverslips and, when specified, transfected with the indicated plasmids. One day after transfection, cells were fixed with 4% paraformaldehyde (PFA), permeabilized with 0.1% Triton X-100 in PBS and incubated with primary antibodies for 1.5 hours at room temperature. Cells were washed three times using 0.5% Tween-20 in PBS (PBS-T) and incubated with Alexa Fluor 488-, Alexa Fluor 568- or Alexa Fluor 594-conjugated secondary antibodies (Thermo Fisher Scientific) for 1 hour at room temperature. Cells were washed three times with PBS-T and slides were mounted using the Vectashield antifade mounting medium (Vector Laboratories). Fluorescence images were acquired on a Leica DM6000 fluorescence microscope and analyzed using the ImageJ (NIH) software. The colocalization plugin in ImageJ was used to visualize co-localization between two channels (thresholds were set equal for all images analyzed).

In situ proximity ligation assay (PLA)

Cells were seeded on glass coverslips treated with polylysine-L (Sigma-Aldrich). After 24 hours, cells were fixed with 4% paraformaldehyde (PFA) and permeabilized with 0,1% Triton X-100 in PBS. The PLA assay was performed according to the manufacturer's protocol (Duolink *In situ* Red, Sigma-Aldrich DUO92101-1KT). Briefly, following permeabilization, the coverslips were subjected to blocking, incubation with primary antibodies for 1.5 hours at room temperature, hybridization with PLA probes, ligation, amplification and counterstaining with mouse monoclonal anti-α-tubulin antibody-FITC (Sigma-Aldrich F2168) before mounting. Fluorescent images were acquired on a Leica DM6000 fluorescence microscope and analyzed using the ImageJ software (NIH). The number of PLA punctae, indicative of a direct interaction between Lunapark and mTOR, were counted for all three conditions ($n < 20$ cells). P values were determined by unpaired, two-tailed Student's t test using Graphpad Prism 7. P values < 0.05 are indicated with one asterisk, < 0.01 with two asterisks, < 0.001 with three asterisks and < 0.0001 with four asterisks, respectively.

Live cell imaging by spinning disc confocal microscopy

U2OS cells were grown in glass bottom dishes and transfected with mCherry-Sec61β, Lunapark-GFP (WT or mutants), mCherry-Raptor, mCherry-LAMP1 or GFP-LAMP1. One day after transfection, cells were imaged using a Nikon-SD spinning disk confocal microscope. The movies were generated using the ImageJ software (NIH). The multichannel plot profile function in ImageJ was used to obtain line-scan graphs representing the relative fluorescence intensity of the mCherry and GFP channels along the length (linear distance in pixels) of a line drawn in ImageJ. For triple-labeled live cell imaging, U2OS cells were transfected with Lunapark-GFP, BFP-KDEL (ER marker) and mCherry-LAMP1 (lysosome marker). One day after transfection, cells were imaged using a Leica TCS SP5 AOBS (Acousto-Optical Beam Splitter) confocal microscope and analyzed using the ImageJ (NIH) software.

In vitro binding assay

In vitro translated ^{35}S-labeled KLHL12 or KLHL18 were incubated with protein G-Sepharose beads precoupled with the following Lunapark synthetic peptides: H-DSSAPGGPPERTVT-OH, or H-DSSAAGGAPERTVT-OH for 2 hours at 4°C. Beads were washed four times with lysis buffer (50 mM Tris-HCl, pH 7.4, 1 mM EDTA, 250 mM NaCl, 0.1% Triton X-100, 50 mM NaF, 1 mM DTT, 0.1 mM Na_3VO_4). Proteins were then eluted with Laemmli buffer for 3 minutes at 95°C and subjected to SDS-PAGE followed by autoradiography.

Computational molecular docking of Lunapark peptide to KLHL12

A highly accurate, flexible peptide docking method (ICM-Pro, Molsoft LLC, La Jolla CA) was used as previously described (Bordner and Abagyan, 2006; Lee et al., 2016) to dock Lunapark peptides to KLHL12. Full atom models of Lunapark peptides were docked to grid potential maps generated from the atomic coordinates of the Kelch repeats of KLHL12 reported in the crystallographic structure of KLHL12 (Canning et al., 2013). The all-atom model of the peptide was docked into the grid potentials using stochastic global optimization in internal coordinates with pseudo-Brownian and collective 'probability-biased' random moves as implemented in the ICM-Pro program. For the grids, five types of potentials for the peptide-receptor interaction energy - hydrogen van der Waals, non-hydrogen van der Waals, hydrogen bonding, hydrophobicity and electrostatics - were precomputed on a rectilinear grid with 0.5 Å spacing that fills a 34 Å × 34 Å × 25 Å box containing KLHL12, to which the peptide was docked by searching its full conformational space within the space of the grid potentials. The preferred docking conformation was identified by the lowest energy conformation in the search.

QUANTIFICATION AND STATISTICAL ANALYSIS

GraphPad Prism was used for statistical analysis (Student's t test). Sample sizes and *p* values are indicated in STAR Methods, figures or figure legends. All images are representative of at least three biological replicates, except where specified in the figure legends.

Cell Reports, Volume *31*

Supplemental Information

Ubiquitylation of the ER-Shaping Protein Lunapark via the CRL3^{KLHL12} Ubiquitin Ligase Complex

Laurensia Yuniati, Angela Lauriola, Manouk Gerritsen, Susana Abreu, Eric Ni, Chiara Tesoriero, Jacob O. Onireti, Teck Yew Low, Albert J.R. Heck, Andrea Vettori, Timothy Cardozo, and Daniele Guardavaccaro

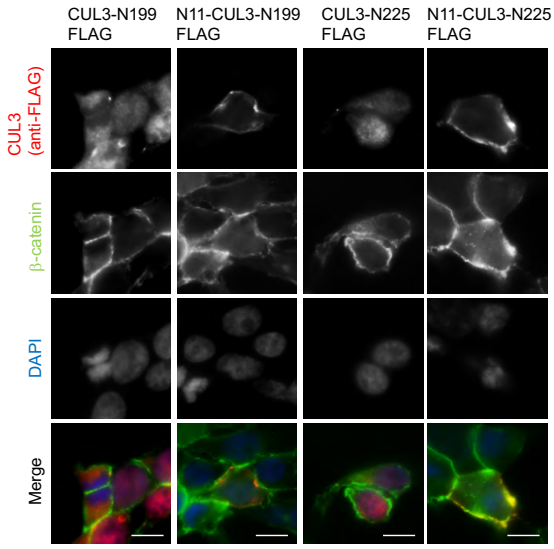

Figure S1. Subcellular localization of CUL3 mutants. Related to Figure 1.
The indicated FLAG-epitope tagged CUL3 mutants were expressed in HEK293T cells. Cells were fixed and analyzed by indirect immunofluorescence with the indicated antibody. DNA was stained with DAPI (blue). Scale bar indicates 10 μm.

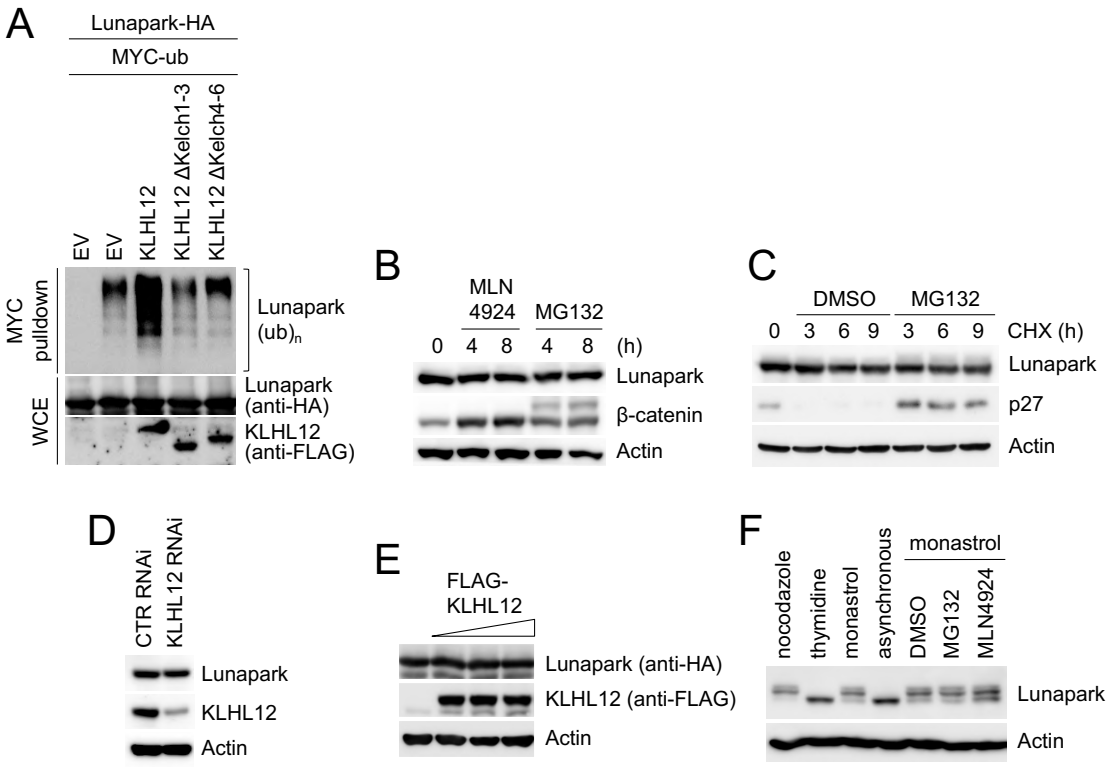

Figure S2. Ubiquitylation of Lunapark does not targeted it for proteasomal degradation. Related to Figure 2.

(A) HEK293T cells were transfected with HA-tagged Lunapark, MYC-tagged ubiquitin with or without the indicated FLAG-tagged KLHL12 constructs. Lysates were prepared in denaturing buffer and immunoprecipitated with an anti-MYC antibody. Immunoprecipitates were then immunoblotted to detect ubiquitylated Lunapark. Whole-cell extracts (WCE).

(B) HEK293T cells were treated with the NEDD8-activating enzyme (NAE) inhibitor MLN4924 or the proteasome inhibitor MG132. Cells were then collected at the indicated times and lysed for immunoblotting.

(C) HEK293T cells were treated with cycloheximide (CHX) and either the proteasome inhibitor MG132 or DMSO. Cells were then collected at the indicated times and lysed for immunoblotting.

(D) COS7 cells were transfected with either a control (CTR) siRNA or siRNA to KLHL12. Forty-eight hours after transfection, cells were collected and lysed for immunoblotting.

(E) HEK293T cells were transfected with HA-tagged Lunapark and increasing amount of FLAG-tagged KLHL12. Forty-eight hours after transfection, cells were collected and lysed. Total extracts were then probed with the indicated antibodies.

(F) Hela cells were treated with nocodazole (16 h), thymidine (24 h), or monastrol (16 h). Cells treated with monastrol were then incubated with MG132, MLN4924 or DMSO. Cells were then collected and lysed for immunoblotting.

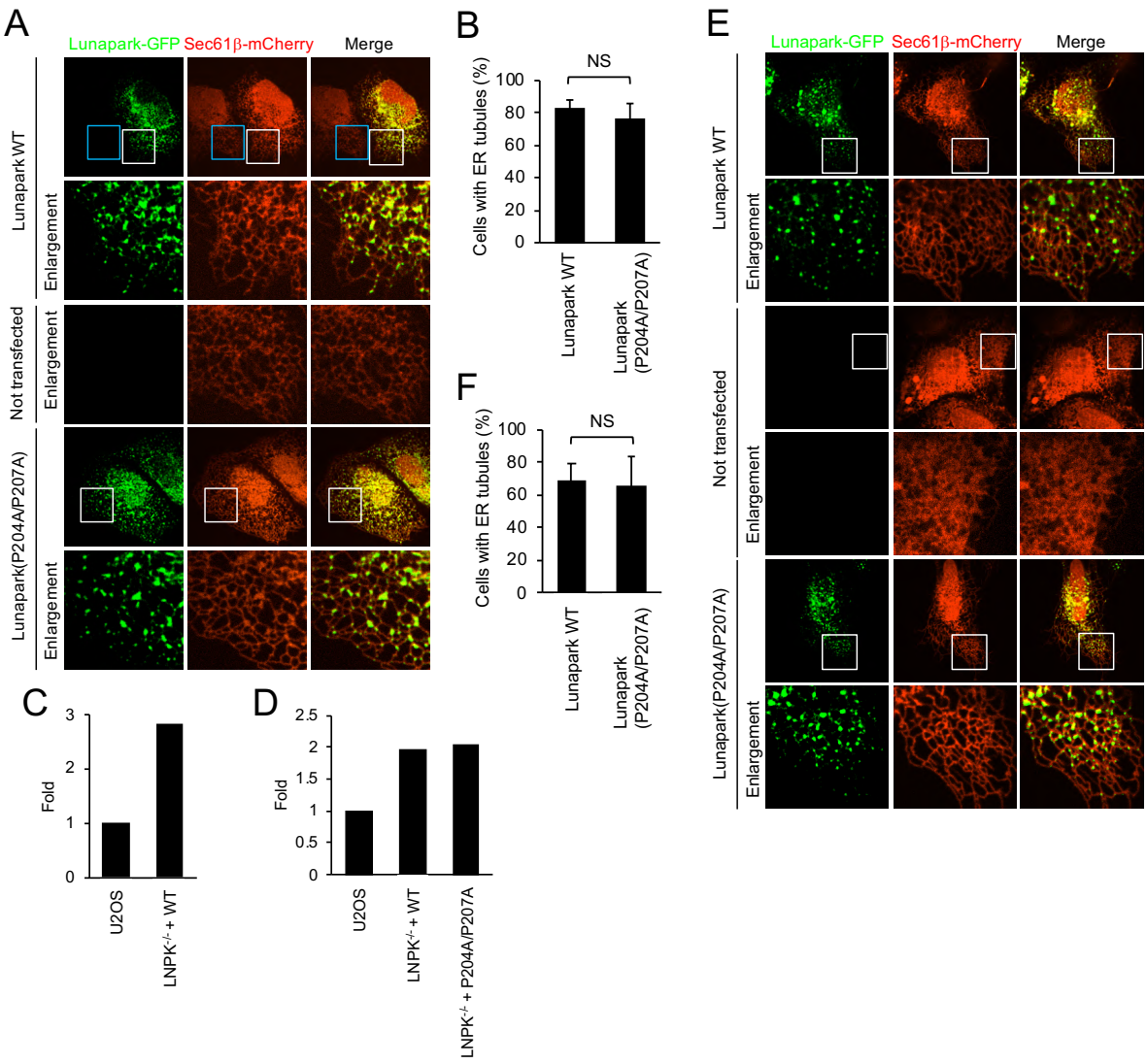

Figure S3. KLHL12-dependent ubiquitylation of Lunapark does not control ER morphology. Related to Figures 5 and 6.

(A) U2OS cells were transfected with the ER marker Sec61β-mCherry and either wild type Lunapark-GFP or Lunapark(P204A/P207A)-GFP and then analyzed by live cell imaging.

(B) Quantification of cells with tubular ER morphology shown in A. Mean ± s.d. NS, not significant (Student's t-test).

(C-D) Quantification of the immunoblots shown in Figures 5A (C) and 6A (D).

(E) LNPK$^{-/-}$ U2OS cells were transfected with the ER marker Sec61β-mCherry and either wild type Lunapark-GFP or Lunapark(P204A/P207A)-GFP and then analyzed by live cell imaging.

(F) Quantification of cells with tubular ER morphology shown in A. Mean ± s.d. NS, not significant (Student's t-test).

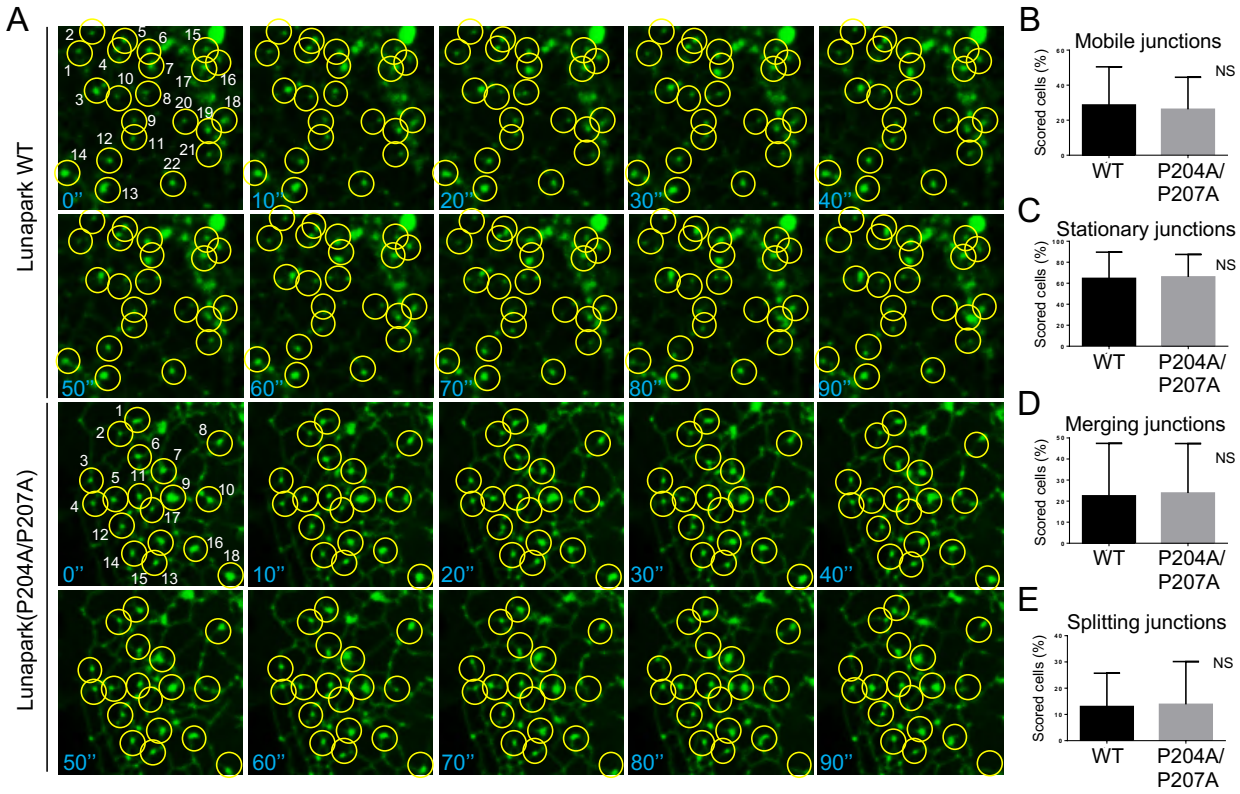

Figure S4. KLHL12-dependent ubiquitylation of Lunapark is not involved in three-way junction mobility. Related to Figure 6.

(A) The mobility of Lunapark-containing three-way junctions were analyzed by live cell imaging in U2OS cells expressing Sec61β-mCherry and either wild type Lunapark-GFP or Lunapark(P204A/P207A)-GFP. For the sake of clarity only the green channel (GFP) is shown. Solid circles indicate the Lunapark-GFP-containing junctions that were tracked during a 90-second period.

(B-E) Quantification of three-way junction mobility. Percentage of: (B) mobile junctions (Lunapark-positive junctions move at least once out of the circle); (C) stationary junctions (Lunapark-positive junctions stay within the circle; (D) merging junctions (Lunapark-positive junctions fuse with other Lunapark-positive junctions; (E) splitting junctions (Lunapark-positive junctions split into two new Lunapark-positive junctions). Wild type Lunapark-GFP-containing junctions: n = 161; Lunapark(P204A/P207A)-GFP-containing junctions: n = 224. Parametric and unpaired t-test with Welch’s correction. NS, not significant.

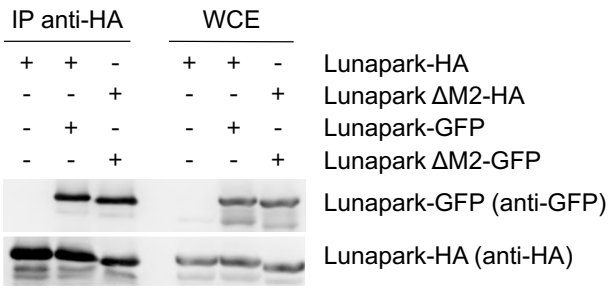

Figure S5. Lunapark ubiquitylation does not control its oligomerization.
Related to Figure 6.
HEK293T cells were transfected with HA-tagged Lunapark (WT or the ΔM2 mutant) and GFP-tagged Lunapark (WT or the ΔM2 mutant) as indicated. HA-Lunapark complexes were immunoprecipitated with anti-HA beads and analyzed by immunoblotting with the indicated antibodies.

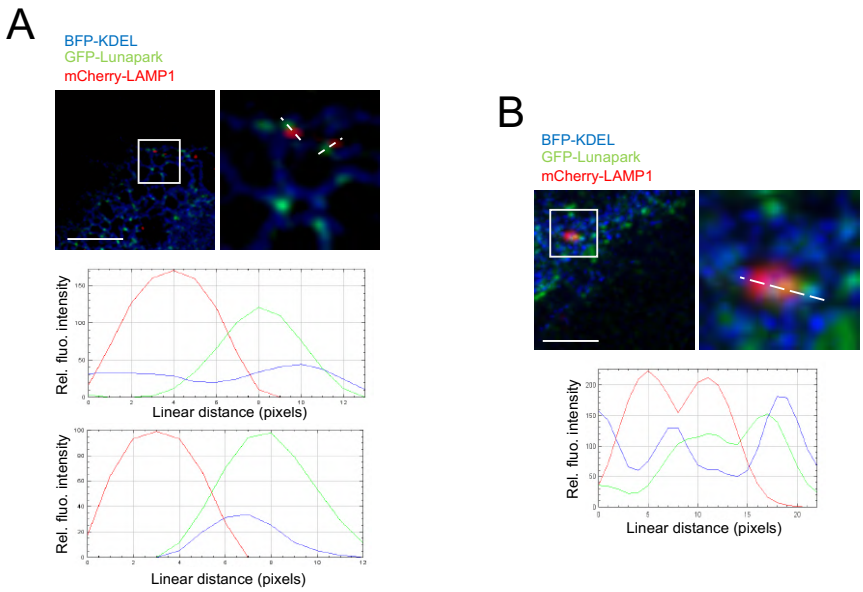

Figure S6. LyLEs form contact sites with Lunapark-containing three-way junctions. Related to Figure 5.

(A, B) Live cell epifluorescence images and relative magnification insets of U2OS cells expressing GFP-Lunapark, BFP-KDEL (ER marker) and mCherry-LAMP1 (lysosome marker). Representative confocal images in which Lunapark is adjacent to LAMP1 (A) or in which Lunapark partly overlap with LAMP1 (B) are shown. Scale bar indicates 5 µm. Corresponding line-scan graphs of the relative fluorescence intensities of GFP, mCherry, and BFP along the lines indicated in the images are shown. In (A), the top line-scan graph corresponds to the left dotted line whereas the bottom line-scan graph corresponds to the right dotted line.

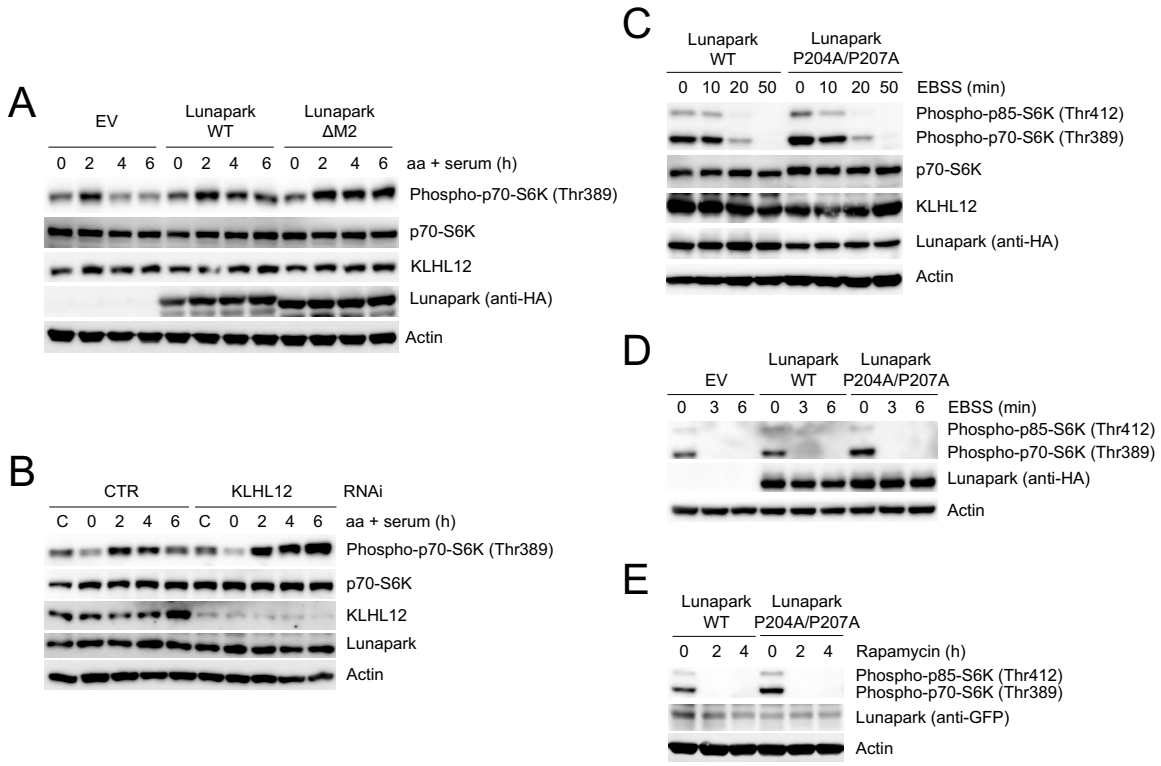

Figure S7. KLHL12-dependent ubiquitylation of Lunapark limits mTORC1 activation in non-transformed cells. Related to Figure 6.

(A) hTERT-RPE cells either transduced with an empty lentivirus (EV) or lentiviruses expressing HA-tagged wild type Lunapark or the Lunapark(P204A/P207A) mutant were starved of amino acids for 50 minutes and then re-stimulated for the indicated times. Cells were collected and lysed. Cell lysates were analyzed by immunoblotting with the indicated antibodies.

(B) hTERT-RPE cells were transfected with either an siRNA targeting KLHL12 or a control siRNA and then treated as in (A). C: exponentially growing control cells.

(C-D) U2OS (C) or hTERT-RPE cells (D) expressing either HA-tagged wild type Lunapark or the Lunapark(P204A/P207A) mutant were starved of amino acids for the indicated times. Cells were collected and lysed. Cell lysates were analyzed by immunoblotting with the indicated antibodies. EV: empty vector.

(E) U2OS cells expressing either GFP-tagged wild type Lunapark or the Lunapark(P204A/P207A) mutant were treated with the mTOR inhibitor rapamycin for the indicated times. Cell lysates were analyzed by immunoblotting with the indicated antibodies.